

**LEVEL II**

MRDC41082.4AR

Copy No. 10

12

AD A109738

# RESEARCH ON SAW SENSOR BIAS STABILITY

ANNUAL TECHNICAL REPORT FOR THE PERIOD  
October 1, 1980 through October 1, 1981

ARPA ORDER NO. 4061  
CONTRACT NO. MDA903-81-C-0081

Prepared for

Defense Supply Service  
Department of Army  
Washington, D.C. 20310

SDTIC  
ELECTE  
JAN 20 1982  
E

E.J. Staples  
& A.P. Andrews  
Principal Investigators

The views and conclusions contained in this document are those of the authors and should not be interpreted as necessarily representing the official policies, either expressed or implied, of the Defense Advanced Research Projects Agency or the U.S. Government.

DTIC FULL COPY



**Rockwell International**

Microelectronics Research  
and Development Center

This document has been approved  
for public release and sale; its  
distribution is unlimited.

01 18 82 083

UNCLASSIFIED

SECURITY CLASSIFICATION OF THIS PAGE (When Data Entered)

REPORT DOCUMENTATION PAGE		READ INSTRUCTIONS BEFORE COMPLETING FORM
1. REPORT NUMBER	2. GOVT ACCESSION NO. AD-A109 738	3. RECIPIENT'S CATALOG NUMBER
4. TITLE (and Subtitle) RESEARCH ON SAW SENSOR BIAS STABILITY		5. TYPE OF REPORT & PERIOD COVERED Annual Technical Report 10/1/80 through 10/1/81
		6. PERFORMING ORG. REPORT NUMBER MRDC41082.4AR
7. AUTHOR(s) E.J. Staples A.P. Andrews		8. CONTRACT OR GRANT NUMBER(s) MDA903-81-C-0081
9. PERFORMING ORGANIZATION NAME AND ADDRESS Rockwell International Science Center 1049 Camino Dos Rios Thousand Oaks, CA 91360		10. PROGRAM ELEMENT, PROJECT, TASK AREA & WORK UNIT NUMBERS ARPA Order No. 4061
11. CONTROLLING OFFICE NAME AND ADDRESS Defense Supply Service Department of Army Washington, D.C. 20310		12. REPORT DATE October 1981
14. MONITORING AGENCY NAME & ADDRESS (if different from Controlling Office) Director, Advanced Research Projects Agency 1400 Wilson Boulevard Arlington, VA 22209		13. NUMBER OF PAGES 85
		15. SECURITY CLASS. (of this report) UNCLASSIFIED
16. DISTRIBUTION STATEMENT (of this Report) Approved for public release; distribution unlimited.		15a. DECLASSIFICATION/DOWNGRADING SCHEDULE
17. DISTRIBUTION STATEMENT (of the abstract entered in Block 20, if different from Report)		
18. SUPPLEMENTARY NOTES		
19. KEY WORDS (Continue on reverse side if necessary and identify by block number) Surface Acoustic Wave (SAW) Accelerometer, Bias Stability . . . Frequency Stability, Inertial Navigation . . . . Crystal Resonator Aging, Crystal Controlled Oscillator, Chemisorption and Oxidation in Crystal Resonators.		
20. ABSTRACT (Continue on reverse side if necessary and identify by block number) The results of measurements of absolute and differential bias stability in surface acoustic wave (SAW) accelerometers is reported. The objective is to develop SAW accelerometers with improved bias stability characteristics for moderately accurate inertial navigation. A method of determining pre-aging and long term stability in large numbers of dual-resonator structures using only a single frequency standard as reference is discussed. The results of stability measurements were combined with a study of the surface		

DD FORM 1 JAN 73 1473 A EDITION OF 1 NOV 65 IS OBSOLETE

UNCLASSIFIED

SECURITY CLASSIFICATION OF THIS PAGE (When Data Entered)

412310

(cont)

UNCLASSIFIED

SECURITY CLASSIFICATION OF THIS PAGE(When Data Entered)

chemistry of electroded SAW crystals. Chemisorption and electrode oxidation were found to increase instability in these crystals. Careful control of the composition of electrode materials was found necessary in order to obtain low aging SAW resonators.

Preliminary studies of bias stability with respect to inertial navigation using SAW accelerometers indicates cumulative displacement errors less than 20 meters/hour can be achieved over time periods up to one hour. Applications for SAW accelerometers as tactical inertial sensors are discussed in this report.

Accession For	
NTIS GRA&I	<input checked="" type="checkbox"/>
DTIC TAB	<input type="checkbox"/>
Unannounced	<input type="checkbox"/>
Justification	
By	
Distribution/	
Availability Codes	
Dist	Avail and/or Special
A	

UNCLASSIFIED

SECURITY CLASSIFICATION OF THIS PAGE(When Data Entered)



TABLE OF CONTENTS

	<u>Page</u>
LIST OF FIGURES.....	iii
APPENDICES LIST OF FIGURES.....	v
1.0 PROGRESS AND TECHNICAL REPORT SUMMARY.....	1
2.0 TECHNICAL PROBLEM.....	2
3.0 TECHNICAL RESULTS.....	4
3.1 SAW Resonator Fabrication.....	5
3.2 Surface Acoustic Wave Resonator Aging Measurements.....	9
3.3 Surface Chemistry Related to SAW Resonator Aging.....	16
3.4 Absolute and Differential Aging in SAW Resonators.....	19
3.5 SAW Sensor Electronics and Inertial Errors.....	27
4.0 FUTURE PLANS.....	35
5.0 PUBLICATIONS AND PRESENTATIONS.....	37
6.0 REFERENCES.....	38
7.0 APPENDICES.....	39
7.1 Appendix I - Automatic Aging Measurement Software.....	39
7.2 Appendix II - Impedance Characterization.....	50
7.3 Appendix III - Absolute Aging Results.....	54
7.4 Appendix IV - Differential Aging Results.....	61
7.5 Appendix V - Preprints of Publications.....	68



LIST OF FIGURES

<u>Figure</u>		<u>Page</u>
1.	Photomicrographs of SAW resonator structure used in absolute and differential aging study.....	6
2.	Surface wave resonator fabrication process used in study of absolute and differential aging.....	7
3.	Photographs of resonator calibration system used to place SAW resonators on frequency. This system used a parallel plate plasma discharge in freon and oxygen.....	10
4.	Photographs of testing oven containing the RF coaxial switching matrix. In these photographs 18 TO-5 enclosures containing 18 dual resonators are shown loaded into the test circuit board.....	13
5.	Block diagram of automatic aging system and RF coaxial switching matrix. The system is controlled by signals passed over the IEEE-488 data buss from the desktop computer.....	14
6.	Aging data representative of one group of 36 resonator crystals. In Fig. 6a the absolute aging is plotted vs linear time and in Fig. 6b the same data is shown vs logarithmic time.....	15
7.	Profile showing chemical composition of resonator electrodes as determined by SIMS analysis. In this case chrome is seen to migrate both into the top aluminum as well as the underlying quartz substrate.....	18
8.	Theoretically plotted frequency changes based on the logarithmic rate law plotted as a function of (a) linear time and (b) logarithmic time with the constant A as a parameter.....	21
9.	(a) Typical absolute aging data vs linear time for a SAW resonator. The same data is plotted (b) vs logarithmic time and compared to rate-law models with different A parameters.....	22
10.	Theoretical behavior of resonator aging using logarithmic rate law with different A constants but identical B constants plotted vs linear time.....	25
11.	Theoretical behavior of resonator aging using logarithmic rate law with different B constants but identical A constants plotted vs linear time.....	26



LIST OF FIGURES (continued)

<u>Figure</u>		<u>Page</u>
12.	Theoretical behavior of resonator aging using logarithmic rate law with different B constants but identical A constants plotted vs logarithmic time.....	28
13.	A SAW acceleration sensor using dual resonator crystal in conjunction with difference frequency measurement system.....	29
14.	Allan variance as measured on a typical SAW dual crystal oscillator.....	31
15.	Measured count output of a SAW dual crystal sensor vs time. Total time was approximately 18 minutes with a 1 second gate time. Also shown is the computed velocity from integrating once as well as the displacement as a result of integrating the counter output twice.....	32
16.	Measured count output of a SAW dual crystal sensor vs time. Total time was approximately 3 minutes with a 10 msec gate time. Also shown is the computed velocity from integrating once as well as the displacement as a result of integrating the counter output twice.....	34



APPENDICES LIST OF FIGURES

<u>Figure</u>		<u>Page</u>
AII-1	Complex input scattering parameters for crystals #1 through #12.....	51
AII-2	Complex input scattering parameters for crystals #13 through #24.....	52
AII-3	Complex input scattering parameters for crystals #25 through #36.....	53
AIII-1	Absolute aging plotted vs linear time for crystals #1 through #12.....	55
AIII-2	Absolute aging plotted vs linear time for crystals #13 through #24.....	56
AIII-3	Absolute aging plotted vs linear time for crystal #25 through #36.....	57
AIII-4	Absolute aging plotted vs logarithmic time for crystals #1 through #12.....	58
AIII-5	Absolute aging plotted vs logarithmic time for crystals #13 through #24.....	59
AIII-6	Absolute aging plotted vs logarithmic time for crystals #25 through #36.....	60
AIV-1	Differential aging plotted vs linear time for crystals #1 through #12.....	62
AIV-2	Differential aging plotted vs linear time for Crystals #13 through #24.....	63
AIV-3	Differential aging plotted vs linear time for crystals #25 through #36.....	64
AIV-4	Differential aging plotted vs logarithmic time for crystals #1 through #12.....	65
AIV-5	Differential aging plotted vs logarithmic time for crystals #13 through #24.....	66
AIV-6	Differential aging plotted vs logarithmic time for crystals #25 through #36.....	67



## 1.0 PROGRESS AND TECHNICAL REPORT SUMMARY

The objective of this program is to perform fundamental studies on SAW resonators leading to improved bias stability characteristics for acceleration sensors. The end goal is to develop small, low cost and moderately accurate accelerometers for tactical guidance systems.

During the first year progress has been made in several areas which are discussed in this report. A method of fabricating dual-resonator crystals with absolute and differential aging characteristics has been developed. Using a unique method of measuring process dependent shifts in resonator frequency with time, both absolute and differential bias stability has been studied. In conjunction with a study of crystal processing methods a study of the surface chemistry of electroded quartz resonators using such techniques as Auger, ESCA, and mass spectroscopy was carried out. The quantitative results of these studies have been combined with frequency stability measurement data to arrive at a mathematical model which explains long term frequency shifts in terms of logarithmic rate laws associated with chemisorption, oxidation and stress relief in surface wave resonators.

Hybrid RF circuitry for prototype dual resonator accelerometers has been developed. Preliminary results using dual resonator crystals show extremely good stability, typically less than  $10^{-10}$  for 1 second averaging times. Noise levels due to electronic circuitry are consistent with a SAW sensor dynamic range of  $1 \times 10^6$ . Tests were also performed on integrated noise levels for simulated guidance system mission times. For a mission time of 3 min the cumulative displacement error rate was typically less than 1 meter/hour and for simulated mission times of 20 min the cumulative displacement error rate was less than 20 meters/hour. This data is to be compared to a typical error rate for a moderately accurate accelerometer of 1 nautical mile per hour or 1851 meters/hour. These results are encouraging and during the second year further studies of SAW accelerometers will be performed.



## 2.0 TECHNICAL PROBLEM

Accelerometers are transducers which convert sensed acceleration into analog or digital signals. They are used in a wide variety of applications, such as in sensing seismic and vibrational motions; but the most stringent requirements for these devices occur in their applications for guided missiles.

The development of guided missiles in the 1940's required the development of accurate accelerometers for steering and stability. This led to the development of accelerometers for autonomous inertial navigation of missiles, aircraft and ships. They are also used for autopilots and smoothing for navigational mechanizations using satellite data.

The technological approaches for accelerometers of the 1940's are still in use today. These include integrating gyroscopic accelerometers of the type used on the German V-2 rockets (R-1). Refinements to these approaches have improved these instruments in many respects, but they have not made them less expensive. They require precision machining and assembly of many mechanical parts, which cannot be accomplished at low cost. Typical unit costs for accelerometers used in inertial navigation range from a few thousand dollars to tens of thousands of dollars.

There is a constant need for less costly accelerometers, especially for applications such as cruise missiles and tactical missiles, for which large numbers of accelerometers are required. Many technological approaches have been proposed for meeting this need. These include vibrating string (R-2), laser (R-3), piezoresistive (R-4), piezoelectric (R-5), and acoustic (R-6,7) accelerometers. All of these approaches use a 'proof mass' which is connected to the host vehicle by means of a stress sensor. The stress sensor measures the force applied to the proof mass, which is proportional to the sensed acceleration of the host vehicle. These are 'open loop' sensors, because the force is not applied by a precision servo loop, as in the case of the gyroscopic and pendulous accelerometers.



The surface acoustic wave (SAW) resonator transforms strain input to frequency output (R-8,10). When used as an open-loop accelerometer without a rebalance servo loop, the SAW oscillator functions as a solid-state digital accelerometer with the desirable characteristics of low power consumption, low weight, small size, and potentially very low cost. In order to meet performance requirements for moderately accurate inertial navigation systems, the frequency stability must be high. Because SAW resonators operate well into the UHF range, SAW sensors are normally configured as dual resonator controlled oscillators and one resonator acts as a frequency reference or standard. In this case the differential frequency stability determines the noise level of the accelerometer output.

The objective of this program is to perform fundamental studies on SAW resonator processing methods that yield stability characteristics which successfully meet the bias stability requirements of inertial navigation accelerometers. The technical problems involved are SAW resonator fabrication methodology, surface chemistry of electroded single crystal quartz, absolute and differential aging measurements, design and characterization of high frequency oscillator circuitry, and common mode noise rejection including temperature effects. During the first phase mathematical models for predicting and explaining frequency shifts in SAW resonators configured as acceleration sensors were compared with experimental data. Statistically valid measurement methods were developed in conjunction with improved SAW sensor crystal fabrication methods.



### 3.0 TECHNICAL RESULTS

During the first year of this program, the specific technical tasks were the following:

1. To develop methods for experimentally evaluating single and differential bias stability in two-resonator crystals. This problem involved the use of automatic data-acquisition hardware and software for measuring long term frequency shifts.
2. To develop mathematical models for predicting frequency shifts in SAW resonators based upon the known behavior of physical processes. This model was used to interpret the experimentally measured aging data.
3. To perform studies of the chemical interactions which take place within and on surface wave structures when sealed under specified environmental conditions. The problem is to explain the kinematics of chemical interactions in sealed crystal packages and relate these effects to the surface chemistry of the quartz crystal and metallic surface wave electrode structure.
4. To design and construct hybrid rf circuitry for prototype SAW accelerometers. The circuitry must be low in cost and power, and provide long term stability. The technical problem was to operate two oscillators from a single crystal, without experiencing lock-up of the oscillators to a common frequency.
5. To assess the inertial errors of prototype SAW acceleration sensors in terms of the integrated velocity and displacement errors. This required integration of the SAW sensor digital output twice, once to derive velocity and once to derive displacement from velocity. The inertial errors were studied as a function of mission time at constant temperature.



### 3.1 SAW Resonator Fabrication

The surface acoustic wave resonator is a planar electrode structure photolithographically defined on a suitable piezoelectric material. The SAW resonator functions in much the same manner as a conventional quartz oscillator crystal. Acoustic waves are confined within a cavity whose boundaries are accurately maintained. The Q of the cavity is determined by the material losses and cavity leakage. The same excellent frequency control properties of bulk wave quartz resonators is also achieved by the SAW resonators provided the fabrication techniques are closely controlled.

The planar electrode pattern of a SAW resonator contains an interdigital transducer which provides electrical-to-mechanical as well as mechanical-to-electrical signal transduction. Shown in Fig. 1 is a photograph of the resonator geometry used in this study. The interdigital transducer contained 40 electrode finger-pairs with a periodicity of 8.3 microns. On either side of the input/output transducer are two gratings which contain 400 reflecting stripes with a periodicity slightly less than in the transducer. The gratings act as mirrors when the acoustic wavelength is approximately equal to twice the grating periodicity. In this frequency range all of the surface acoustic wave energy is confined within the cavity formed by the two gratings.

The complete SAW resonator fabrication process used in this study is shown in Fig. 2. The starting material is Y-cut single crystal quartz purchased from Valpey-Fisher with an ultrafine polish on one surface. Typically the rms surface roughness is less than 50 angstroms. The first row of Fig. 2 represents the photolithographic process used to define the SAW electrode pattern of Fig. 1. A photomask with over 100 resonators covering a two inch square area is used to define and etch the electrode pattern in a vacuum deposited aluminum film. In our work three types of metalization systems were used, (1) electron-beam evaporation of chrome (50 Å) and aluminum (1000 Å), (2) sputter deposited pure aluminum (1000 Å), and (3) sputter deposited copper-doped (4%) aluminum (1000 Å).



MRDC81-15712

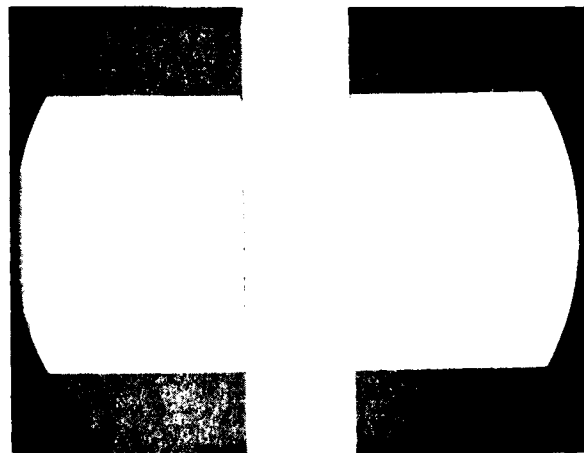
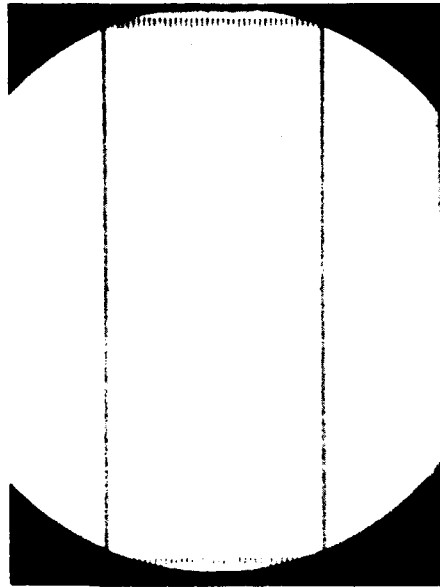


Fig. 1 Photomicrographs of SAW resonator structure used in absolute and differential aging study.

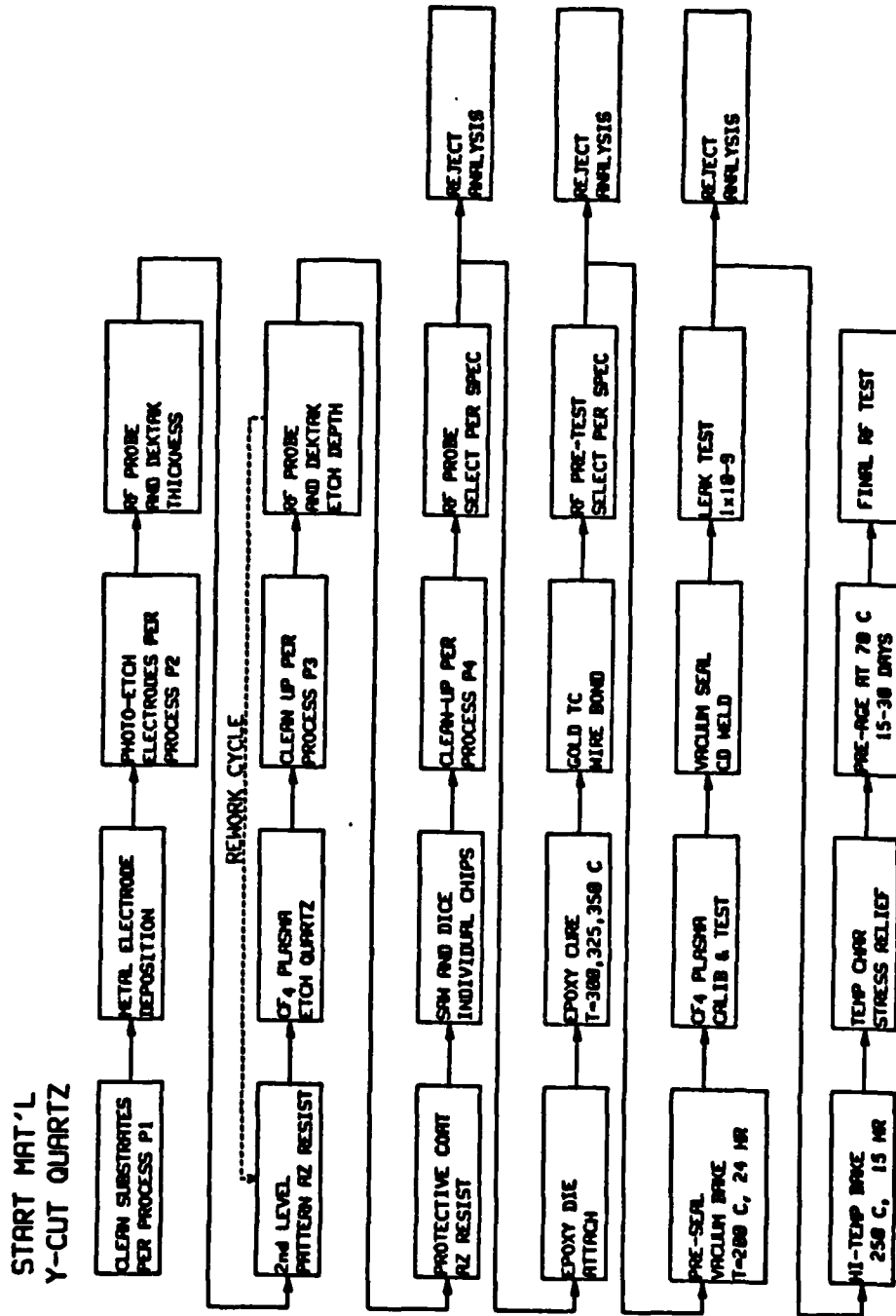


Fig. 2 Surface wave resonator fabrication process used in study of absolute and differential aging.



After the metal electrode pattern has been delineated the metal thickness is evaluated for the desired value as well as a check of metal thickness uniformity. Uniformity of the deposited metal was important to achieving resonators closely matched in frequency. An rf probing technique was used to measure the resonator frequencies prior to any other processing of the wafers. The frequency sensitivity of aluminum electrode thickness was typically 1.67 kHz/Å at nominally 375 MHz. In the early fabrication runs the frequency variation was typically 1000 ppm. It was necessary to maintain a deposition uniformity of less than 5% in order to achieve runs with less than 200 ppm frequency variation.

In order to achieve high Q in SAW resonators efficient surface wave reflection in the grating regions of the resonator must occur. This is accomplished in the next step (second line in Fig. 2). A photoresist (AZ1350) is spun onto the wafers and patterned such that windows are opened in the reflecting grating regions of the resonator. Following this a freon ( $CF_4$ ) reactive ion etch of the quartz substrate material was performed. The photoresist prevented any etching of the transducer regions and the aluminum in the grating regions acted as an etch mask allowing only the quartz between the gratings to be etched. This produced grooves between these electrodes which enhanced the surface wave reflection at the groove edges and also lowered the resonant frequency of the gratings to coincide with the transducer frequency. This dispersion was accounted for by designing the photomask with different periodicity in the gratings and transducer. After plasma etching the resist was removed and the resonators again rf probed. A rework cycle was used to place the resonators within a prescribed frequency range. Typically the total frequency change due to plasma etching was 1% and resonator Q's were nominally 10-15,000 at 375 MHz.

After plasma etching the wafers were diced and probed. The dicing procedure was designed to yield chips with two resonators on the same chip. This structure was termed the 'dual crystal' resonator and was used extensively in our testing of stability and aging. After dicing the chips were



mounted using a polyimide epoxy which was cured at 350°C. Following mounting, typically to a T0-5 header, the individual resonators were wire bonded and a pre-test of the resonator characteristics was performed. Pre-testing of the resonators yielded device frequency, Q, and resistance before sealing.

Sealing was performed in a controlled glove box environment. The controls included an automatic pressure controller and a gaseous dri-train system for removal of all water vapor and oxygen from the glove box enclosure. A capacitance-discharge resistance weld was used to seal the T0-5 crystal enclosures. Input and output vacuum load-looks were used to transport the resonators through the sealing system. The input load-look chamber was also a vacuum oven and a 24 hour pre-seal bake at 200°C was routinely performed. After this vacuum bake but prior to actual sealing, each crystal was calibrated to a desired frequency using a short plasma etch in freon. The calibration system was installed inside the glove box and is shown in Fig. 3. The etching geometry is of the parallel-plate type with the SAW resonator attached to the anode and rf power applied to the cathode. Provisions for monitoring the resonator frequency were made using rf feed-throughs to the vacuum chamber. The SAW resonators could be tuned by as much as 1000 ppm without degradation and could be placed to within  $\pm 10$  ppm of the desired frequency.

The sealing operation itself was carried out under a vacuum of  $10^{-7}$  torr. After sealing the devices were bombed with helium and leak checked with a mass spectrometer. Those devices which showed no leakage were then put through a series of tests to determine their long term frequency stability under various environmental conditions.

### 3.2 Surface Acoustic Wave Resonator Aging Measurements

The quantitative determination of resonator aging was a major task of this study. The amount by which a quartz resonator, bulk or SAW, changes with time is very small. Measurement accuracies of 0.1 ppm or less are required



MRDC81-15711

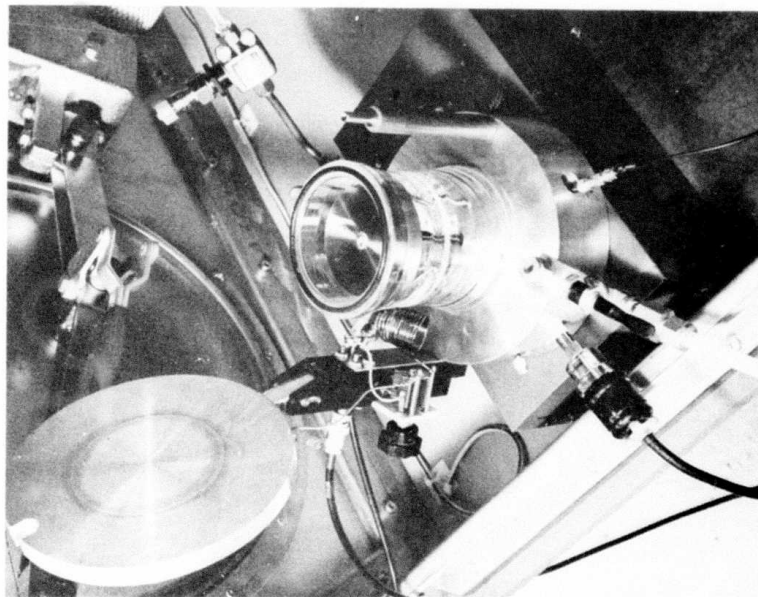
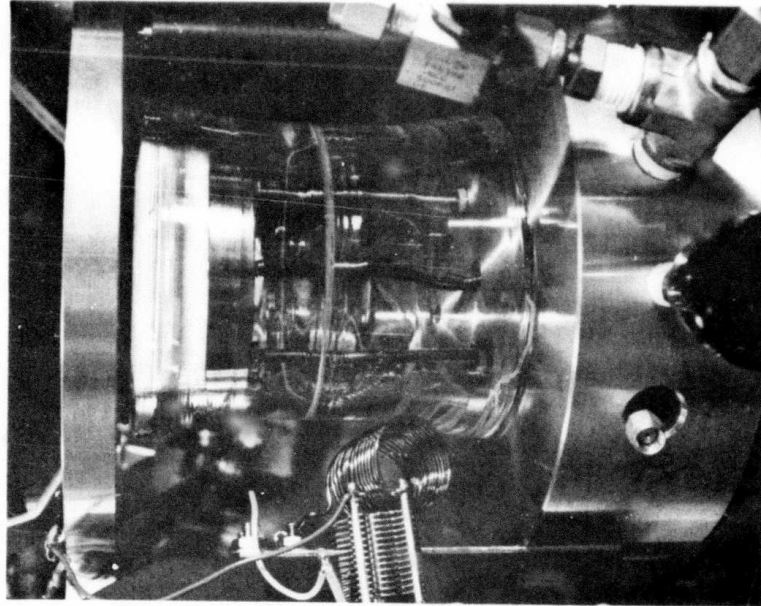


Fig. 3 Photographs of resonator calibration system used to place SAW resonators on frequency. This system used a parallel plate plasma discharge in freon and oxygen.



over time periods ranging up to one year. Because the resonator is a passive device the conventional method is to build oscillator circuitry with the resonator as the frequency feedback element. However, when considering the large numbers of resonators to be tested this approach was not practical. Instead, a method of determining the individual resonator series resonant frequency periodically with an automated network analyzer system was developed. In this technique absolute frequency accuracy was obtained by phase locking the network analyzer to an external frequency standard, such as a frequency synthesizer locked to a rubidium clock. In practice the rubidium standard was not needed for time periods less than 1 year.

The system which was first built, successfully monitored the frequency stability of 12 resonators in two ovens. Each oven was fitted with a single pole, 6-throw, coaxial switch which selected which resonator was to be tested. The coaxial switches were driven by an HP3495A scanner digitally programmed by an HP9825A desktop calculator. The coaxial switch outputs were connected to the A and B ports of an HP 8505A, 0.1-1300 MHz, network analyzer, also controlled by the desktop calculator via an IEEE-488 data bus. The network analyzer was phase locked to an HP8660C frequency synthesizer which acted as the system frequency standard as well as the primary scanning frequency source for the network analyzer. The crystal ovens were controlled at a temperature of 85°C,  $\pm 0.1^\circ\text{C}$ . All of the aging data taken in the first two quarters of this study was obtained using this prototype measurement system.

Software for the aging measurements was designed to control the system hardware and take measurements periodically. This was accomplished by using a real time clock within the desktop computer. Resonator aging data was not continuously taken, but rather a system of interrupts was used. Whenever the real time clock generated an interrupt, the controller automatically directed the scanner to step through the crystals and the network analyzer to determine the scattering parameters of each crystal. Impedance characteristics and series resonant frequencies were then derived in software and stored on magnetic tape.



Extensive testing showed that this method of measuring resonator aging was satisfactory and a larger oven with an integral rf switching matrix was designed for monitoring the aging of 36 crystals simultaneously. By using interchangeable PC boards, the aging of either 18 T0-5 packages with resonator pairs, or 36 packages containing single resonators, could be monitored. Resonator groups of six were connected to a single-pole six-throw (SP6T) coaxial switch. The six switches were connected to a seventh in a switching matrix arrangement. Figure 4 shows a photograph of the oven containing the PC board into which the T0-5 packages were inserted and the coaxial switching matrix.

The resonators were periodically interrogated through the switches by a network analyzer, frequency synthesizer and counter, all of which were controlled by a desktop computer as shown in Fig. 5. The resonant frequencies were sequentially measured, the oven temperature recorded, and the time logged from the computer's real time clock. In this manner, the frequency/temperature drift was tracked with time. Software computed the differential drift between packaged pairs of SAW resonators.

Experimental data taken with the 36 crystal switching oven is shown in Fig. 6. The plotting of experimental data was controlled by interactive software which could be directed to simultaneously plot the frequency changed (ppm) of all 36 crystals as a function of linear time, Fig. 6a, or as logarithmic time ( $\log[T+1]$ ), Fig. 6b. Examination of such data clearly indicates the anomalous behavior of some crystals and more importantly shows the overall or average aging characteristics of the entire group. Knowledge of the latter was invaluable in obtaining a better understanding of the functional dependence fabrication methods play in SAW resonator aging.

Breaks in the aging data curves represent times when the measurement system was interrupted for other types of measurements or tests. Overall stability and repeatability was excellent. Even through the interrupt time was several days in some cases, the curves continue without any apparent discrepancies in aging trends. Individual or paired plots of crystal aging or

MRDC81-15713

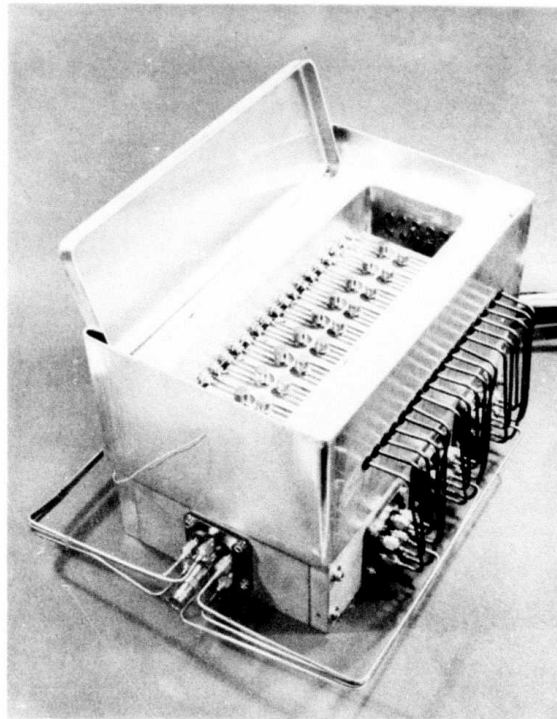
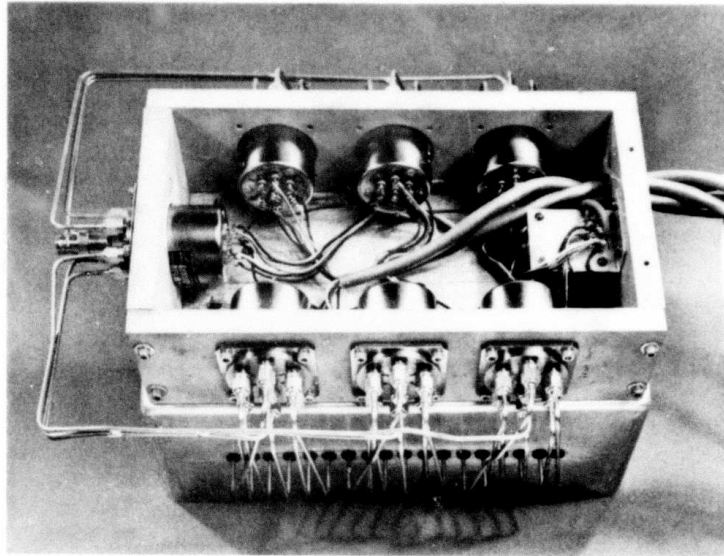


Fig. 4 Photographs of testing oven containing the RF coaxial switching matrix. In these photographs 18 T0-5 enclosures containing 18 dual resonators are shown loaded into the test circuit board.

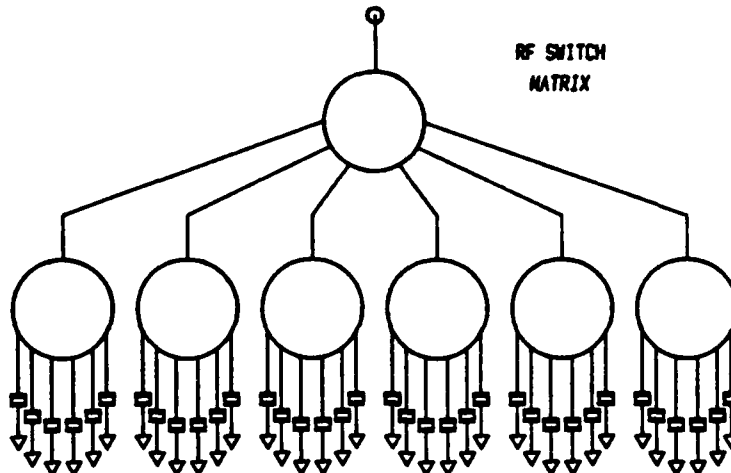
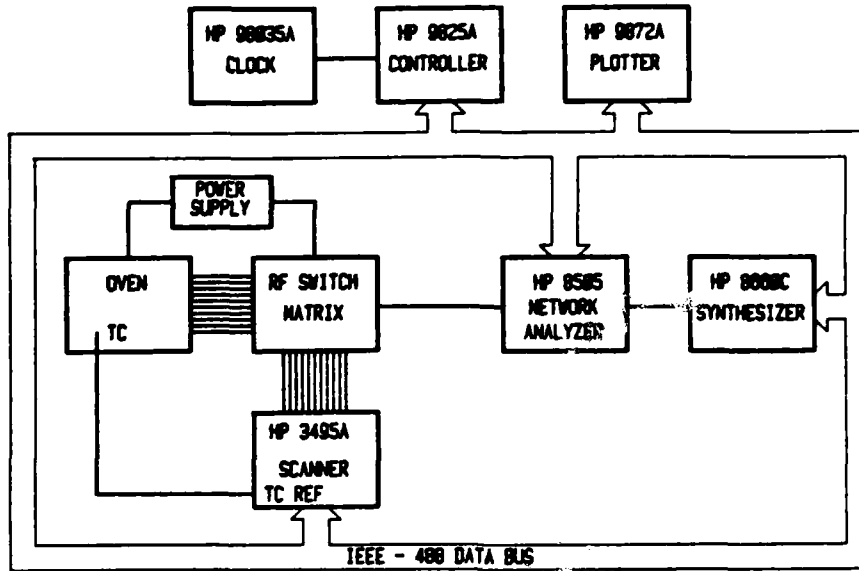


Fig. 5. Block diagram of automatic aging system and RF coaxial switching matrix. The system is controlled by signals passed over the IEEE-488 data buss from the desktop computer.

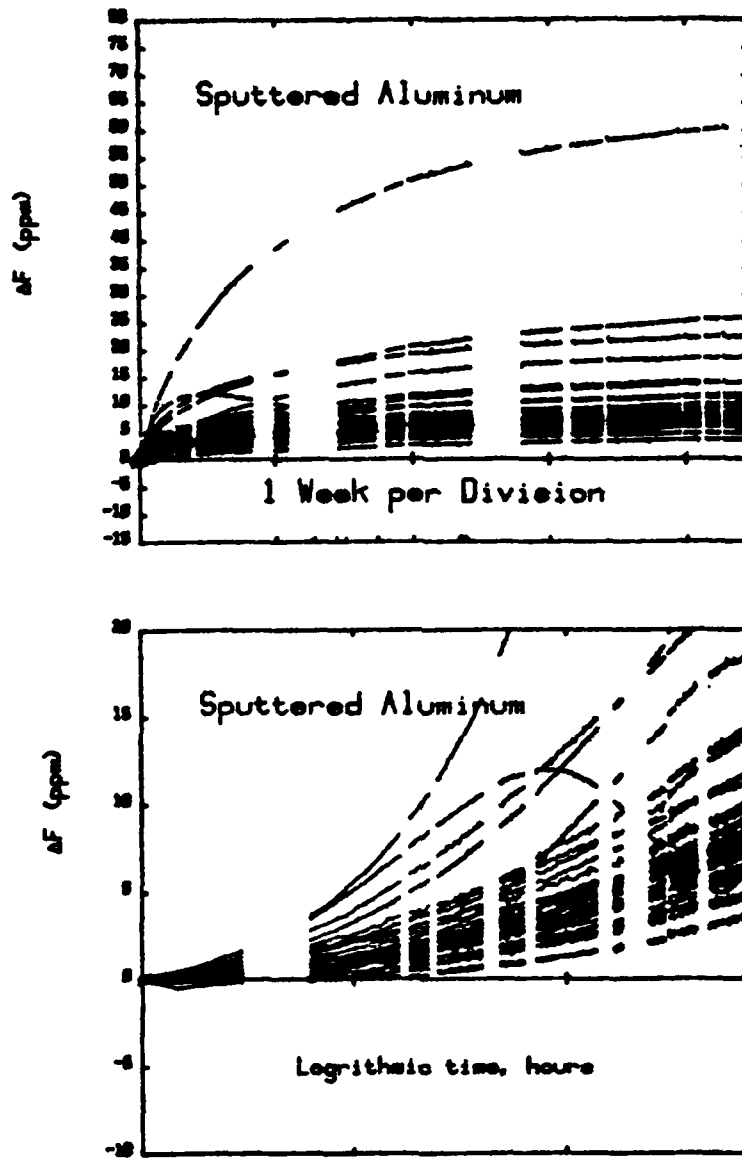


Fig. 6. Aging data representative of one group of 36 resonator crystals. In Fig. 6a the absolute aging is plotted vs linear time and in Fig. 6b the same data is shown vs logarithmic time.



scattering parameters could easily be obtained for more detailed study. Examples of these types of plots as well as measurement system software are discussed in Appendices I-IV of this report.

### 3.3 Surface Chemistry Related to SAW Resonator Aging

A series of ultra-high vacuum, surface analysis experiments were carried out on the bulk materials of the SAW oscillators to evaluate the effects of the processing steps upon the aging characteristics of the devices. In one series of experiments the individual processing steps were investigated to establish the level of impurities which they contribute in resonator materials. In the second series of experiments the device materials were depth profiled by secondary ion mass spectroscopy (SIMS) to establish the extent of diffusion of the aluminum and chromium reflector material layers into the quartz substrate and each other.

The investigation of the contamination levels associated with the bulk materials and the processing steps were carried out using the techniques of x-ray photoelectron spectroscopy (XPS) and SIMS. The XPS analysis of the surface of the quartz substrate material generally showed little chemical reactivity of the quartz with atmospheric gases; however, the SIMS analysis identified a significant involvement of water in the top 20Å of the surface with the  $\text{SiOH}^+$  being generated as a secondary ion under argon ion bombardment. In addition to the presence of hydroxide groups on the quartz surface, hydrocarbons at the level of 0.5 atom % were also found to be present at the quartz metal interface.

Samples of the substrate material upon which a thin layer (40 Å) of chromium followed by aluminum had been deposited, were also examined for incorporation of contaminants. XPS and SIMS analysis showed that the layers were free from any major contaminants with only potassium and water being observed at a level of about 0.1 atom %. These levels of contamination were compared against those observed in single crystal aluminum samples exposed to air and were found to be the same magnitude.



MRDC41082.4AR

Depth profiling of the deposited layers of Cr-Al upon the quartz-substrate substrate were carried out again using XPS as well as SIMS. The profiling studies showed the layered structure to be composed of six distinct regions as shown in Fig. 7. The upper layer of aluminum showed no major impurities; however, the chromium substrate layer had diffused into aluminum to a distance of approximately 100 to 300 Å. The chromium layer itself was not pure metal, containing a significant fraction of oxide. At the quartz-chromium interface the SIMS analysis clearly identified the presence of hydroxides, both the presence of the  $\text{SiOH}^+$  ion and a marked increase in the amplitude of the  $\text{Cr}^+$  ion intensity, at the interface which is normally associated with the presence of oxygen. The impurity layer, however, was again clearly defined and quite thin, covering only about 10 to 20 Å at the interface. The chromium was found to have diffused into the quartz substrate to a distance of 300 to 600 Å, showing an exponential decrease in concentration with sputtering time into the quartz.

This marked diffusion of chromium into the Al layer and the quartz lead to the investigation of an improved reflector material made of layers of Al containing about 4% Cu. This material was investigated on samples which had been specifically designed for SIMS analysis and which had been exposed to all the device processing steps. The quartz substrates were cleaned and metalized with the Al/Cu material. Then a photoresist was laid down, developed, and acid-etched to leave a pattern of Al/Cu rectangles on the exposed quartz substrate. The samples were then acetone-rinsed, A-40 stripped, and nitric acid cleaned. Some of the samples were then exposed to plasma etching in freon gas ( $\text{CF}_4 + 4\% \text{O}_2$ ).

SIMS analysis of the metalized areas clearly showed the presence of the Cu impurity in the Al; however, no evidence was found for any residual Cu in the exposed quartz after the etching and cleaning process. The Al surface before the plasma etch showed a clear  $\text{AlO}_x$  oxide film on the surface. This oxide layer was quite thin (10-20 Å) and the bulk elemental Al could be clearly distinguished under the oxide by XPS, which observes only the top 30 to 50 Å of the surface.

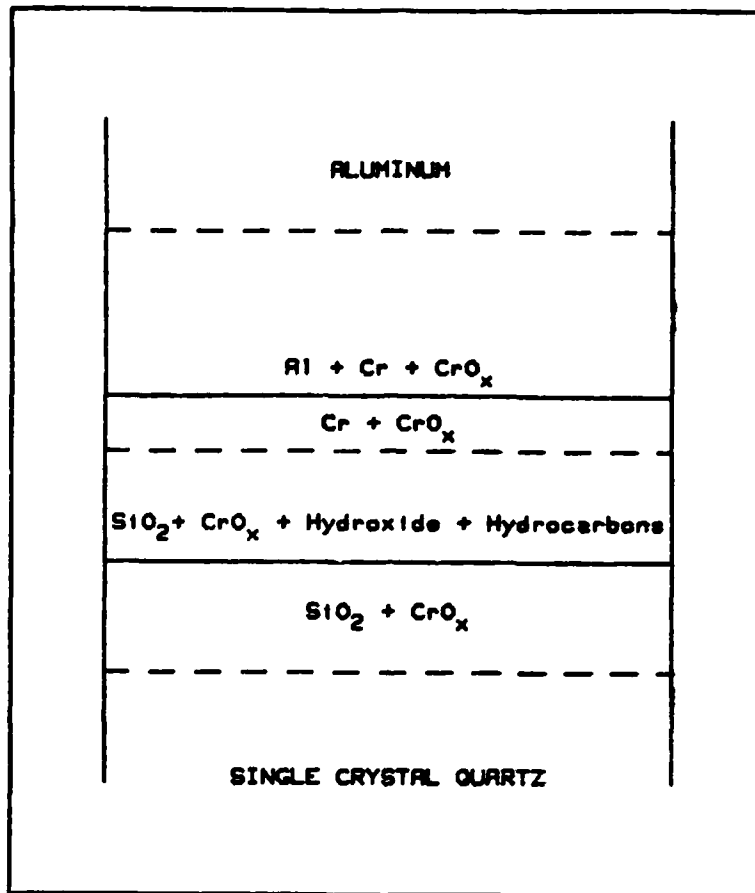


Fig.7. Profile showing chemical composition of resonator electrodes as determined by SIMS analysis. In this case chrome is seen to migrate both into the top aluminum as well as the underlying quartz substrate.



Exposure of the device surface to the  $CF_4 + O_2$  plasma etch clearly formed a surface layer of  $CF_x$ . The layer was approximately 20 to 30 Å thick and had a fluorine-to-carbon ratio of 3 to 3.4. A marked shift in the Al XPS lines toward higher binding energies indicated  $CF_x$  was associating with the Al, possibly as  $AlO_xCF_3$ . Samples of the plasma treated devices were heated to 350°C in  $N_2$  and showed no marked decrease in the intensity of the XPS signals from the fluorocarbon surface layer, demonstrating the layer to be chemically bound and quite stable rather than simply adsorbed gas. Heating the samples in air or oxygen as an annealing process, however, removed 80 to 90% of the fluorocarbon; returning the surface to a dominantly  $AlO_x$  layer. The residual oxide layer still contained a small quantity of the  $AlO_xCF_3$  type structure and was overall slightly thicker than the original oxide film prior to the plasma etching and annealing procedure.

Studies of the surface chemistry of electroded quartz resonators using techniques such as SIMS, Auger, and mass spectroscopy have clearly indicated that chemisorption and oxidation are taking place and that interfacial and/diffusion layers do form in these electrodes. This information was supported by actual SAW resonator isothermal aging data. In the case of chrome, the aging with time was 2-5 times the rate with pure aluminum electrodes. The aging rate was even lower when copper doped aluminum was used. In addition, degradation under high rf power levels was less, indicating mass transport was less. These studies have contributed greatly to our understanding of SAW resonator long term aging.

### 3.4 Absolute and Differential Aging in SAW Resonators

An important objective of this study was to develop mathematical models for predicting frequency shifts in SAW resonators based upon the known behavior of physical processes. Three types of aging models were postulated for these processes,



$$\frac{\Delta F}{F} = A \log (BT + 1)$$

$$\frac{\Delta F}{F} = A(1 - e^{-BT})$$

$$\frac{\Delta F}{F} = A(T)^B$$

The first model is applicable to chemisorption, oxidation, and stress-relief (R-11,R-12). The second applies to first order chemical reactions or adsorption/desorption of physisorbed monolayers upon the substrate. The final model has been identified with diffusion processes when B is near 1/2.

In virtually every experimental SAW resonator which had been sealed under vacuum without significant leakage, the aging data was always of the form predicted by the first model. This result strongly suggested that the aging of SAW resonators was dominated by either chemisorption, oxidation, stress-relief, or a mixture of all three. Physically these types of processes are expected and were clearly detected during our work on electroded quartz surface chemistry. Oxidation of the aluminum electrodes was unavoidable. Stress induced by crystal mounting as well as electrode formation during evaporation or sputtering was also present. Chemisorption was not easily detected, however diffusion of metal ions, particularly when chromium was used, was confirmed by XPS and SIMS spectroscopy.

Theoretically plotted logarithmic frequency changes based on the first model are shown in Fig. 8a,b. A family of four curves are shown plotted vs linear time in Fig. 8a. The same four curves are plotted vs logarithmic time in Fig. 8b. The logarithmic time plots show that after a short initial time the curve becomes a straight line. This behavior is typical of the logarithmic rate law and is closely supported by data (see Fig. 6). As an example consider the typical device aging data plotted in Fig. 9a. In Fig. 9b the same data is plotted versus four theoretical values of A in the rate law. The best fit appears to be A=4.25 ppm and B=0.12/hr. The aging rate at the end of one year for this crystal can be calculated from the derivative of the rate law,



MRDC41082.4AR

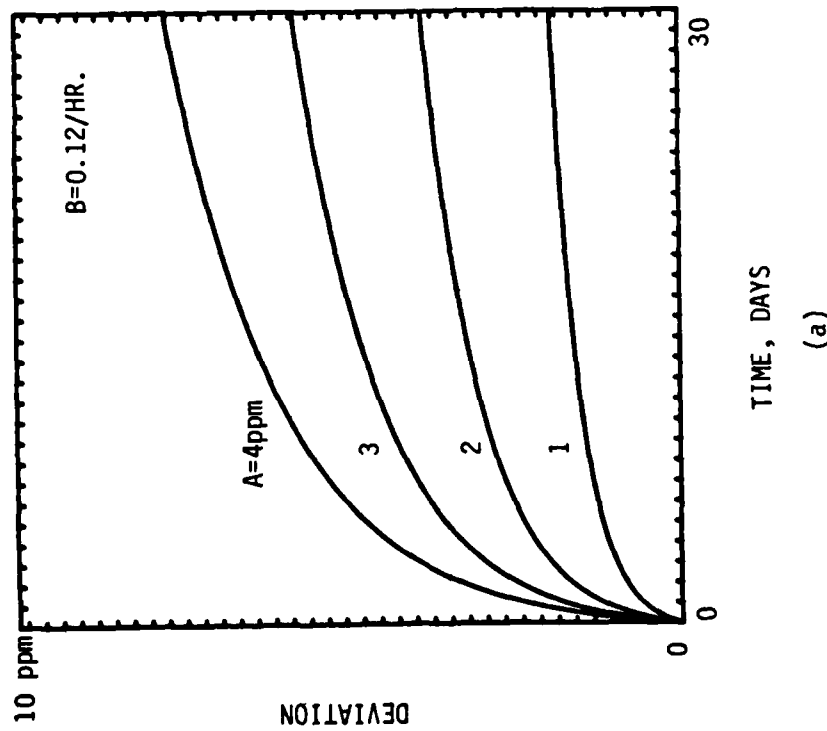
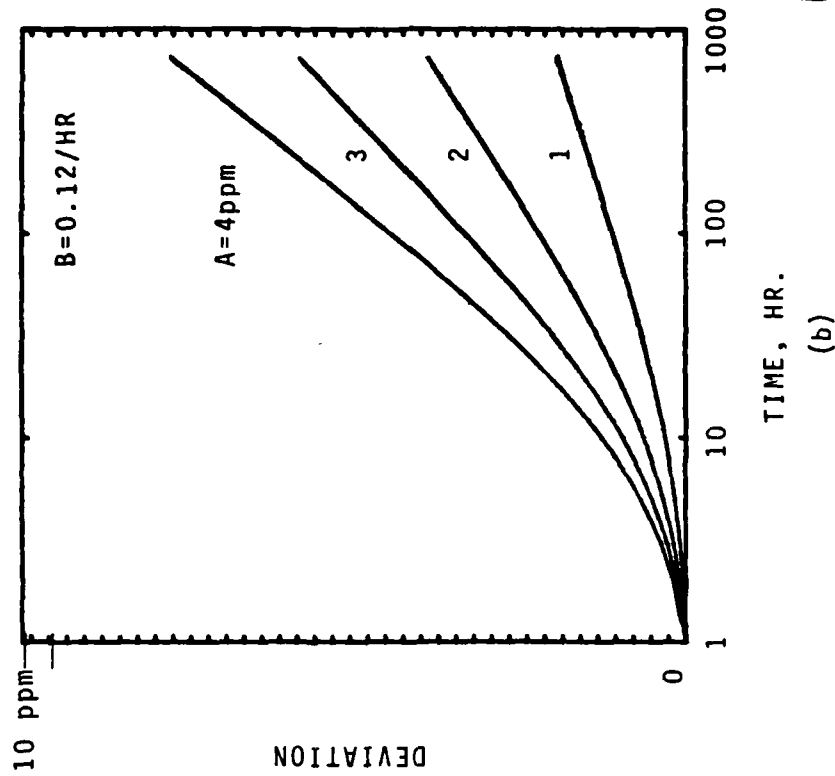
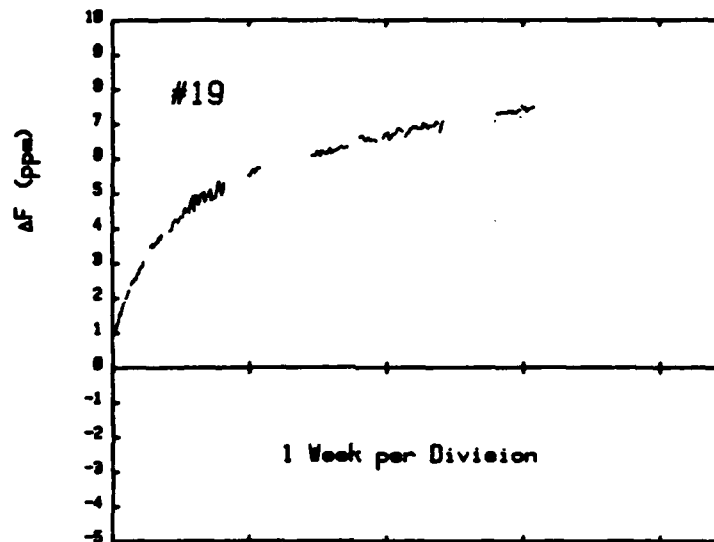


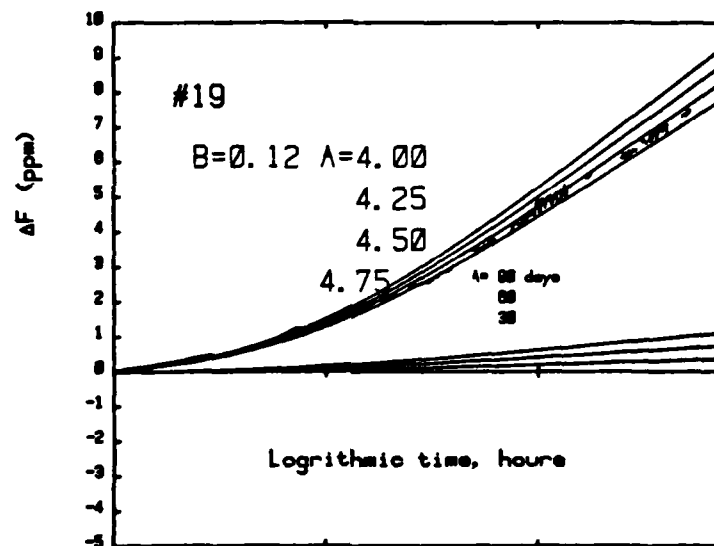
Fig. 8. Theoretically plotted frequency changes based on the logarithmic rate law plotted as a function of (a) linear time and (b) logarithmic time with the constant A as a parameter.



MRDC41082.4AR



(A)



(B)

```

327: for T=0 to 30*24*60*60 by 5000; dso T ← T is in seconds.
328: 4.25+A;.12→E
329: plt log(T/3600+1), A1α(BT/3600+1)
330: next T; nēn
331: stp
*13267

```

Fig. 9. (a) Typical absolute aging data vs linear time for a SAW resonator. The same data is plotted (b) vs logarithmic time and compared to rate-law models with different A parameters.



$$R = \frac{AB \log(e)}{BT + 1}$$

Substituting for A and B, the aging rate at the end of one year is 0.000211 ppm/hour or 1.844 ppm/year. Alternatively the time required to achieve a given aging rate can be expressed as,

$$T = \left( \frac{AB \log(e)}{R} - 1 \right) / B$$

where R is the rate and T is the required time. Substituting the appropriate data for the experimental crystal shown, the time required to reach an aging rate of 1 ppm/year is 1.8448 years.

For large times the logarithmic law can be approximated by

$$\frac{\Delta F}{F} \sim A \log(T)$$

where the controlling parameter is A. The rate of aging using this approximation is simply,

$$R = A \log(e) / T$$

These simple relations can be used to determine the value of A needed to achieve a given degree of aging after a prescribed time. For example to achieve a 1 ppm/year aging rate after 30 days pre-aging will require

$$A = (12 \log(e))^{-1}$$

Assuming the constant B does not change, this curve is plotted in Fig. 9b. Also shown are pre-aging curves under the same conditions for 60 and 90 days pre-aging. Since a pre-aging time of 30 days or less is desired, it is clear that a total aging after 30 days of less than 0.5 ppm is required.

Having established the particular rate law governing SAW resonator crystal aging a study of differential aging was made. Differential aging in the present study was of interest since it directly contributed to differential



bias stability in SAW sensors using dual crystals to detect acceleration. The objective was to predict under what conditions the differential aging was least. Assuming two resonators with the aging behavior given by,

$$F_1 = F_{10}(1 + A_1 \log(B_1 T + 1))$$

$$F_2 = F_{20}(1 + A_2 \log(B_2 T + 1))$$

the change in their difference frequency is given by

$$\Delta F - \Delta F_0 = \log \frac{(B_1 T + 1)^{F_{10} A_1}}{(B_2 T + 1)^{F_{20} A_2}}$$

where

$$\Delta F_0 = F_{10} - F_{20}$$

Two conditions are likely to occur, namely  $A_1 \neq A_2$ , and  $B_1 \neq B_2$ . These are plotted in Figs. 10 and 11 for hypothetical crystals. When the B constants are not equal a small change occurs initially but after a time large compared to BT the difference does not change. However, in the case where the two crystals have different A constants the differential frequency change continues to increase. This can be seen by considering the difference when  $B_1 = B_2$ ,

$$\Delta F - \Delta F_0 = \log(BT + 1)^{F_{10} A_1 - F_{20} A_2}$$

and if  $F_{10}$  is approximately equal to  $F_{20}$  then,

$$\Delta F - \Delta F_0 = F_{\text{avg}}(A_1 - A_2) \log(BT + 1)$$

where

$$F_{\text{avg}} = \frac{F_1 + F_2}{2}$$

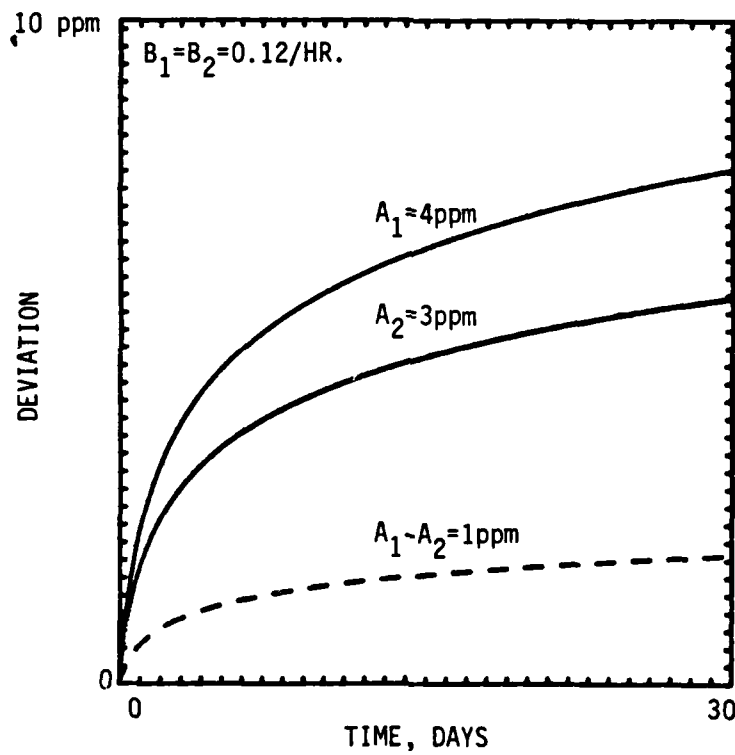


Fig. 10. Theoretical behavior of resonator aging using logarithmic rate law with different A constants but identical B constants plotted vs linear time.

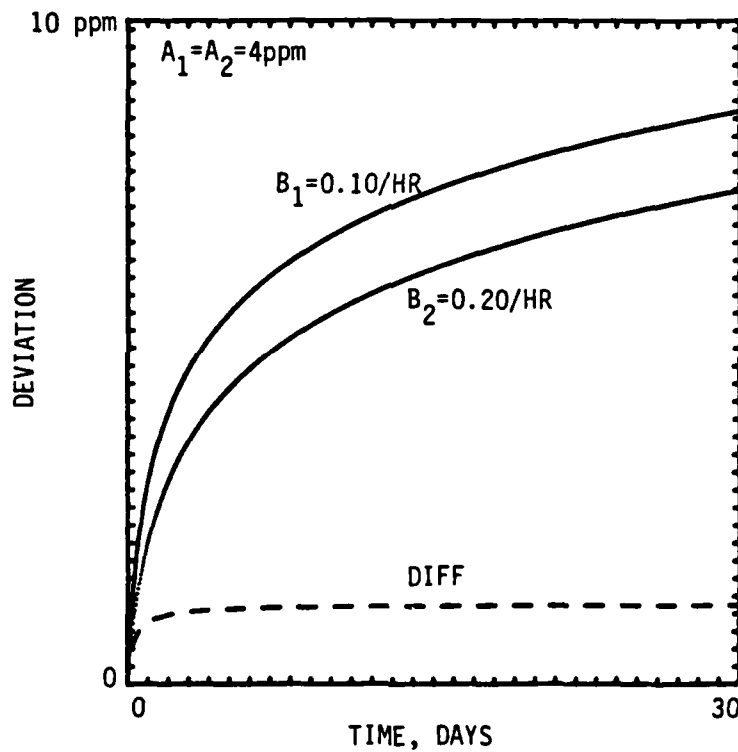


Fig. 11. Theoretical behavior of resonator aging using logarithmic rate law with different B constants but identical A constants plotted vs linear time.



This expression is the same as the original rate law with the A constant replaced by the difference between the two individual crystal A constants. From this type of analysis it is clear that for a high degree of differential bias stability the A constants of the crystals must be closely matched. In fact the desired result plotted on a logarithmic time scale is shown in Fig. 12 and the frequency change with increasing time is zero.

An experimental result which closely confirmed this is shown in the Appendices of this report for the dual crystal pairs #9 & #10, #13 & #14, and #15 & #16. In these cases the individual aging over 30 days was more than 5 ppm, yet the A constants of the two crystals were sufficiently matched that the differential bias stability was less than 0.2 ppm over the same 30 day period. This experimental result is encouraging since it clearly demonstrates that it is possible to fabricate crystals with low differential bias stability due to matched A constants of the logarithmic rate law.

### 3.5 SAW Sensor Electronics and Inertial Errors

An objective of this study was the determination of bias stability errors in SAW acceleration sensors. A SAW acceleration sensor, depicted in Fig. 13, was designed using a dual crystal (two SAW resonators on a single crystal) sensor. The dual resonator concept required two independent oscillators locked to the resonator frequencies. The resonator crystal was mounted such that the frequency difference between the two oscillators was proportional to acceleration. The output from such a sensor is inherently digital, yet quantization errors are zero since the counting processes is continuous. Also because of the stability inherent in crystal controlled oscillators the dynamic range is large.

Oscillator circuitry for dual resonators was designed and constructed using hybrid chip fabrication techniques. The oscillator circuit design was of the negative resistance type with one side of each resonator returned to ground. The negative resistance type of circuit operated on the series resonant frequency of each resonator and required only 3 dB of gain. This was a direct result of using single port resonators. An additional advantage of this

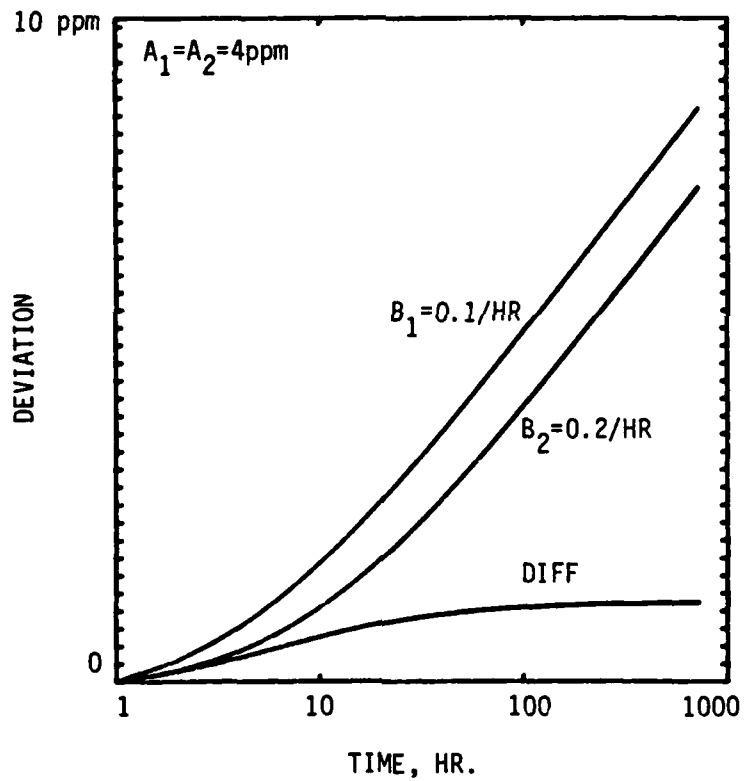


Fig. 12. Theoretical behavior of resonator aging using logarithmic rate law with different B constants but identical A constants plotted vs logarithmic time.

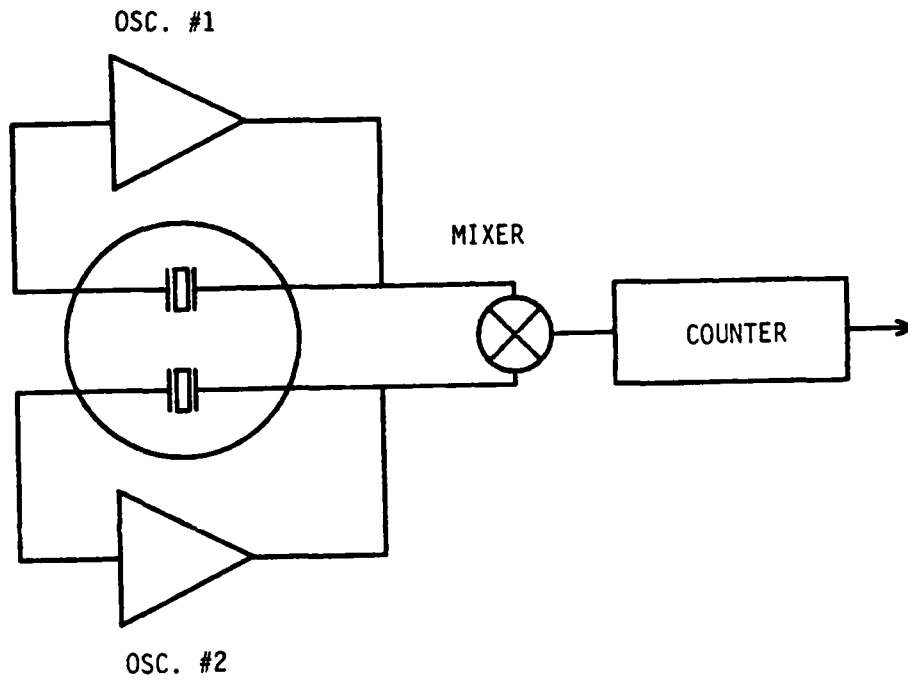


Fig. 13. A SAW acceleration sensor using dual resonator crystal in conjunction with difference frequency measurement system.



design was the minimal crystal loading which resulted in high closed loop Q and overall low power consumption. Typically only 10 mwatt of power at 10 volts supply was required. Also lock-up of the two oscillators was not a problem even though the isolation between them was only 35 dB.

Frequency stability with this type of SAW oscillator was quite good. Shown in Fig. 14 is a typical Allan variance or fractional deviation measured using an HP5390 Stability Analyzer. Short term stability was inversely proportional to time for gate times less than 10 msec. For measurement times greater than 10 second the long term aging and/or temperature induced frequency fluxuations were noticable. In the range 100 msec to 10 second the oscillators show a Flicker noise floor or approximately  $1 \times 10^{-10}$ . These results are only 5 to 10 times worse than the best bulk wave oscillators and are expected to improve.

The SAW dual crystal oscillator frequency stability determines the noise floor or bias stability of the SAW sensor. Directly related to this is the sensor instantaneous dynamic range. The full scale output of the sensor is typically 200 ppm and assuming a noise floor of  $1 \times 10^{-10}$ , the dynamic range is typically  $1 \times 10^6$ .

Associated with this study was an evaluation of integrated noise floors. An important potential application of the SAW sensor is for inertial navigation and guidance. Consider the output of the sensor being a train of pulses whose count per second is proportional to acceleration. To determine velocity, V, from such a sensor the acceleration count must be integrated. This is equivalent to summing the total number of counts and scaling according to the sensor gage factor and count duration.

Shown in Fig. 15 is the actual count output of a SAW sensor when measured by a counter with a 1 second gate time. The difference frequency was 60 kHz which has been subtracted out and only the deviation in the difference frequency ( $\pm 1$  Hz) is shown. Summing the counts results in the velocity count ( $\pm 10$  Hz) as a function of time shown. This curve represents the area under the acceleration-frequency curve. Performing another summation as a function of time results in the curve for displacement ( $\pm 4000$  Hz). The scale factor

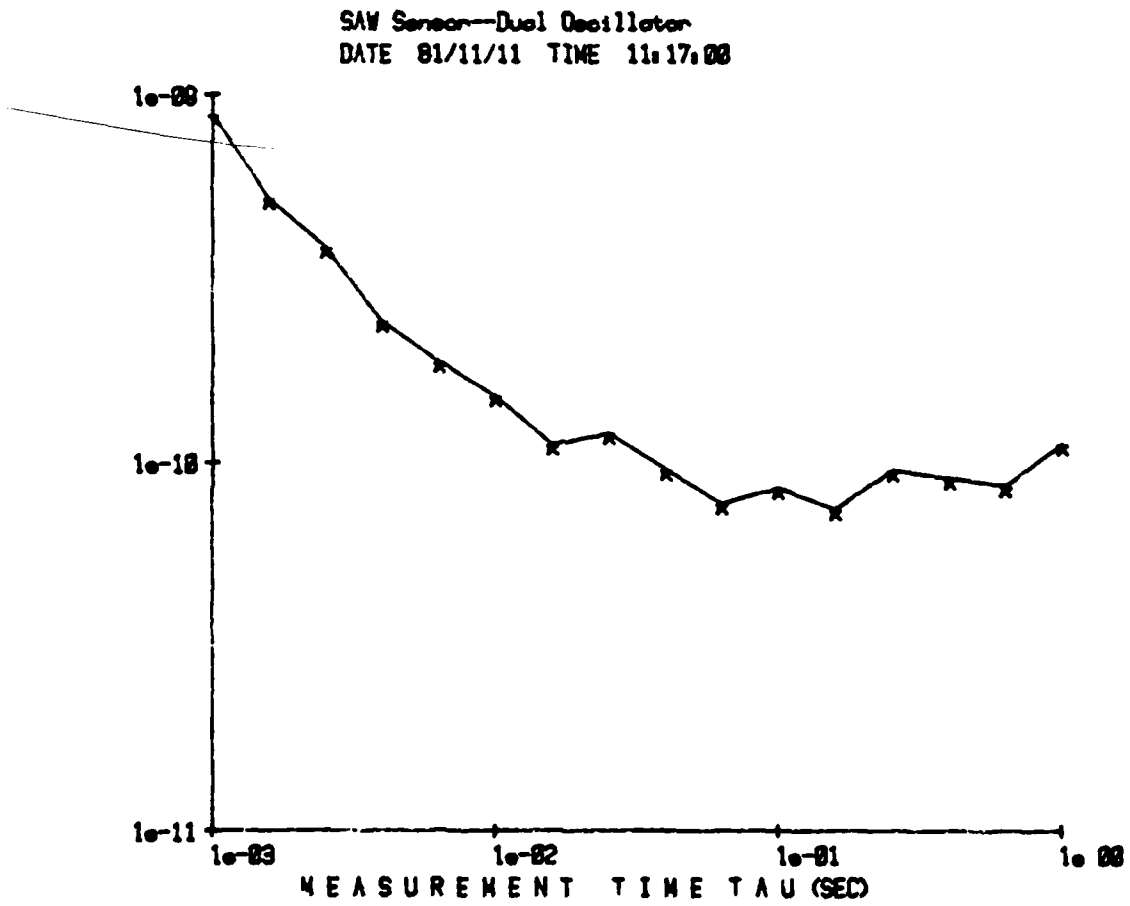


Fig. 14. Allan variance as measured on a typical SAW dual crystal oscillator.

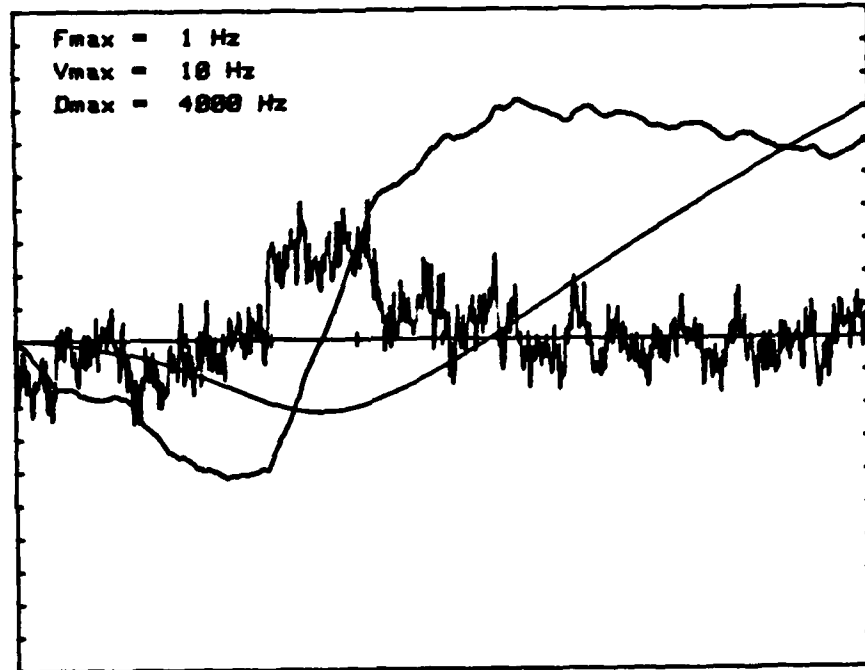


Fig. 15. Measured count output of a SAW dual crystal sensor vs time. Total time was approximately 18 minutes with a 1 second gate time. Also shown is the computed velocity from integrating once as well as the displacement as a result of integrating the counter output twice.



was 200 ppm/g or approximately 769 Hz/m/sec.<sup>2</sup> The integrated velocity error for the 1000 second time period shown was typically less than 0.013 m/sec and the position error typically less than 5.2 meter. As expected the integrated error is closely related to the integration time and this is dependent upon the actual mission time or time for which no other guidance data is available.

Sensor integrated errors for shorter gate and mission times were readily measured. Shown in Fig. 16 is a plot of frequency deviation, velocity error, and displacement error when the gate time is 10 msec for 1000 counts. Theoretically this gives a data output 100 times a second. The actual rate was somewhat slower (0.18 sec) because of dead time in the counter, nevertheless the integrated velocity count was less than 10 Hz and the displacement count less than 1000 Hz after a total integration time of 3 min. This corresponds to a velocity error of less than 0.0023 m/sec and a displacement error of less than 0.042 meters for a 3 min mission time.

Since the mission time was known in these tests the cumulative error per unit time for a SAW inertial sensor can be calculated. In the first test, the mission time was approximately 20 minutes, and the cumulative displacement error was 5.2 meters, giving an error rate of approximately 15.6 meters/hour. In the second test the mission time was 3 minutes and the cumulative position error was 0.042 meters, giving an error rate of approximately 0.84 meters/hour. In perspective these results are quite good. Moderately accurate inertial accelerometers typically have an error rate of 1 nautical per hour or 1851 meters/hour. The SAW sensor error rates are considerably below this value. Thus the SAW accelerometer noise level is such that it can be considered as a very good grade of moderately accurate inertial accelerometer.

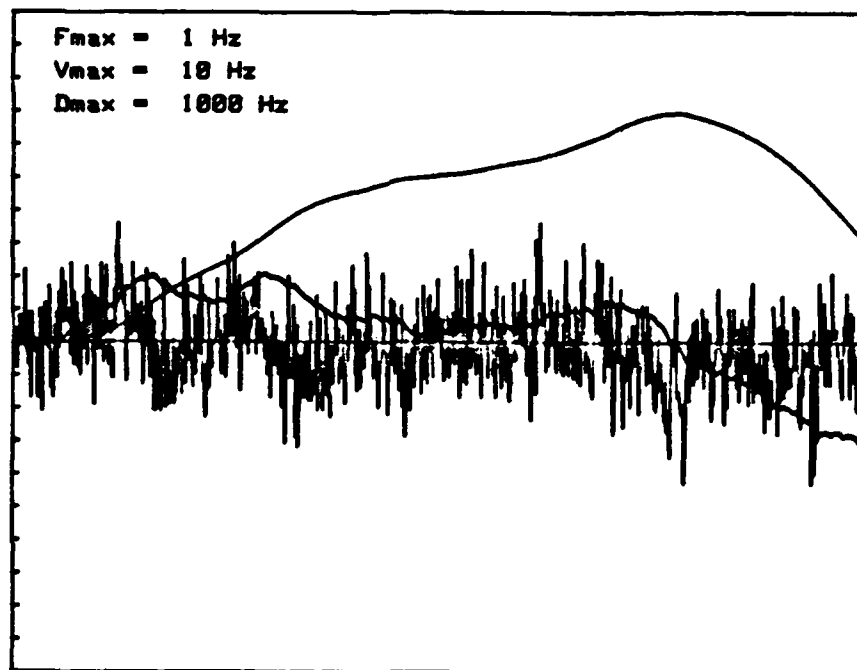


Fig. 16. Measured count output of a SAW dual crystal sensor vs time. Total time was approximately 3 minutes with a 10 msec gate time. Also shown is the computed velocity from integrating once as well as the displacement as a result of integrating the counter output twice.



#### 4.0 FUTURE PLANS

In the second year of this program bias stability, aging, and SAW resonator fabrication related studies will be continued. In order to increase the amount of data available construction of a second 36 crystal oven for monitoring bias stability has already begun. In addition to these areas of study the following tasks will be performed.

Task 1 - Characterize and mathematically model common mode rejection of temperature related frequency shifts in two-resonator differential sensors. Provided the structural and chemical properties of the sensing crystal are homogeneous, common mode rejection will depend upon mounting stresses. This investigation will model these effects and predict their magnitude as a function of crystal mounting and proof mass attachment. The results of this investigation will be coupled with an investigation of stress sensitivity due to g-loading.

Task 2 - Theoretically and experimentally investigate the sensitivity of rotated y-cut quartz surface wave resonators to acceleration effects. The objective of this study shall be to characterize the crystal in terms of second and third order piezo-elastic constants, applied proof mass loading, crystal geometry, and mounting points in order to obtain maximum sensitivity to g-loading while maintaining common mode rejection of temperature induced stress effects.

Task 3 - To study long term bias stability on prototype SAW accelerometers. This work will be an extension of the work performed in the first year, however in this case the two-resonator crystals will be combined with rf circuitry so as to provide a comparison between the effects of crystal frequency shifts and circuit induced frequency shifts. A goal of this task is to include these in the stability model being investigated.



Task 4 - To study the acceleration sensitivity of chemically milled surface wave accelerometer crystals. Experimental structures and fabrication techniques will be evaluated. Theoretical predictions will be compared with experimental results. The goal of this study is to develop crystal structures with improved sensitivity to acceleration while achieving minimal or zero sensitivity to mounting stresses.

Task 5 - To evaluate the overall performance of prototype SAW accelerometers and to calibrate the output in a standard accelerometer calibration test system. These tests will be performed on completed sensors which contain sensing crystals as well as hybrid electronics. Calibration of the sensor will be performed by operating the device under variable levels of vibration and comparing to a known accelerometer standard. Also included with this study will be an evaluation of sensor linearity over the range  $\pm 10$  g and a life test (fatigue) under vibration.



## 5.0 PUBLICATIONS AND PRESENTATIONS

Two papers presenting the technical results of research performed in the course of this program were given during the last year. The first paper entitled "Surface Chemistry Related to SAW Resonator Aging" was presented at the 1980 Ultrasonics Symposium in Boston on November 5-7. This paper described the surface chemistry experiments being performed to determine which factors involving surface chemistry contribute to SAW resonator aging. The second paper entitled "Absolute and Differential Aging of SAW Resonator Pairs" was presented at the Annual Symposium on Frequency Control. In this paper the results of our aging and drive level studies were discussed and compared with the results of other researchers in this area. For the purpose of clarity and background information, pre-prints of these papers have been included as appendices in this report.



## 6.0 REFERENCES

1. R. H. Parvin, Inertial Navigation, D. Van Nostrand, Princeton, N. J., 1962, p. 5.
2. J. M. Slater, "Which Accelerometers for Space Guidance?," *Space/Aeronautics*, October, 1960 p. 227-240.
3. G. M. Siouris, "Survey of Inertial Sensor Technology," *Flugwiss Weltraumforsch*, Vol. 1, No. 5, Sept.-Oct., 1977, p 346-353.
4. W. E. Rosvold and M. L. Stephens, "Cantilever Accelerometer," AFAL-TR-77-152, WPAFB, OH, 1977.
5. P. Chen, R. S. Muller, T. Shiosaki and R. M. White, "Silicon Cantilever Beam Accelerometer Utilizing a PI-FET Capacitive Transducer," presented at the Device Research Conference, Boulder, CO, 1979.
6. J. F. Dias, H. E. Karrer, J. A. Kusters and C. A. Adams, "Frequency/Stress Sensitivity of SAW Resonators," *Electronics Letters*, Vol. 12, No. 22, Oct., 1976, p. 580-582.
7. J. F. Dias and H. E. Karrer, "Stress Effects on Acoustic Surface-Wave Circuits and Applications to Pressure and Force Transducers," presented at the 1975 International Solid-State Circuits Conference.
8. P. Das, C. Lanzl and H. Tiersten, "A Pressure Sensing Acoustic Surface Wave Resonator," *IEEE Ultrasonics Symposium Proceedings*, 1976, p. 306-308.
9. D. F. Weirauch, R. J. Schwartz and R. C. Bennett, "SAW Resonator Frit-Bonded Pressure Transducer," *IEEE Ultrasonics Symposium Proceedings*, 1979, p. 874-877.
10. E. J. Staples and J. Wise, "Surface Acoustic Wave Underwater Sound Sensors," *IEEE Ultrasonics Symposium Proceedings*, 1979, p. 870-874.
11. P. T. Landsberg, "On the Logarithmic Rate Law in Chemisorption and Oxidation," *Journal of Chemical Physics*, Vol. 23, No. 6, p. 1079-1087, June 1955.
12. A. W. Warner, D. B. Fraser and C. D. Stockbridge, "Fundamental Studies of Aging in Quartz Resonators," *IEEE Transactions on Sonics and Ultrasonics*, SU-12, No. 2, p. 52-59.



## 7.0 APPENDICES

7.1 Appendix I - Automatic Aging Measurement Software

This appendix shows the software which has been developed to automatically determine the aging of quartz resonators using the specially designed crystal oven containing a coaxial switching matrix. A total of 36 crystals per oven can be analyzed as a function of time. The data consists of a frequency array, F[36,50], a string array for time, B\$[50,14], and a temperature array, T[50]. After each block of 50 data points has been collected the data arrays are stored on magnetic tape (line 306). Time is stored as a 14 number string in the form [MM;DD;HH:mm:ss] which is read from the real time system clock (line 112). For plotting purposes absolute time is converted to real time (line 10).

The data acquisition is controlled by an interrupt routine (line 181). How often the interrupt occurs is programmed into the real time clock at the beginning of the program (line 34). Upon initiation of the interrupt routine, CYCLE TEST (line 95) is called. This routine sequentially begins the testing procedure for each of the 36 crystals. For each crystal tested the frequency of zero phase (in impedance) is determined on the automatic network analyzer. The temperature is measured in the oven and this is also stored.

The program operates from special function keys which have been previously defined. These keys allow interactive operation of the program functions. After each function is complete the program asks for selection of another key by the operator. All of the plotting routines for impedance or aging data versus time are located at the end of the program listing.

```

0: "AUTOMATIC SAW AGING PROCAM.....EJS...7-13-80":
1: "Software for 36 Xtal test w/J.WISE's CVENS, trk0;file 1; Aging #5":
2:
3: trk 0;ldk 2
4: dim F[36,50],E$[50,14],T[50]
5: dim A$[14],A[0:12],C$[14],D$[14],E$[14],G$[32],H$[36,2],X[500],Y[500]
6: 30→A[4]→A[6]→A[9]→A[11];28→A[2]
7: 0→A[0];31→A[1]→A[3]→A[5]→A[7]→A[8]→A[10]→A[12]
8:
9: dsp "SELECT KEY FUNCTION";stp ;jmp 0
10: "abstime A$":0→T
11: for K=0 to val(A$[1,2])-1;T+A[K]*24*3600→T;next K
12: T+86400*val(A$[4,5])→T
13: T+3600*val(A$[7,8])+60*val(A$[10,11])+val(A$[13,14])→T
14: ret T
15:
16: "PLOT TEMPEFATURE DURING WARM-UP":fxd 2;wrt 9,"P";red 9,A$
17: scl 0,1000,20,80;axe 0,20,100,1;axe 1000,80,100,1;plt 10,70,-1;lbl A$
18: for I=1 to 1000
19: cll 'MEASURE TEMPEFATURE'
20: plt I,X;dsp "temperature=",X
21: next I;per
22: dsp "SELECT KEY FUNCTION";stp ;jmp 0
23:
24: "PERIODIC DATA ACQUISITION":0→T;ent "PFINTOUT?(YES or NC)",A$
25: if A$="YES";1→T
26: cll 'INTERRUPT SET-UP'
27: wrt 9,"Unit 1 Go"
28: cll 'DISPLAY TIME'
29: dsp "SELECT KEY FUNCTION";stp ;jmp 0
30:
31: "DISPLAY TIME":
32: wrt 9,"Request time";red 9,A$;dsp A$;jmp 0
33:
34: "INTERRUPT SET-UP":
35: wrt 9,"A";wrt 9,"E"
36: wrt 9,"Unit 1= Cutput 1"
37: ent "Period (min)?",P;P*60000→P
38: fxd 0;wrt 9,"Unit 1 Period",P,"/"
39: oni 9,"INTERRUPT";eir 9
40: ret
41:
42: "MEASURE TEMPEFATURE":rem 722;wrt 722,"H1R6F4M3";wrt 709,"C00E"
43: wait 2000
44: red 722,R;wrt 722,"F1H1P2M3";wrt 709,"03E";wait 100
45: red 722,S;lcl 722
46: 5041.6/(ln(R)+7.15)-314.052→T;-3.9526e-7→C;3.9747e-5→E;1.2737e-8→A
47: C+BT+AT^2→V;S+V→X;C-X→C
48: -B/2A+√(B^2-4AC)/2A→X
49: ret
50:
*17505

```

```

51:
52: "PPINT DATA APPRAYS":ent "Starting device #",N
53: N→A;N+1→B;N+2→C;N+3→D;N+4→E;N+5→F
54: fmt 38x,"CRYSTAL FREQUENCIES";wrt 701
55: fmt 14x,72"-";wrt 701
56: fmt 4x,"TIME",12x,"#",f.0,10x,"#",f.0,10x,"#",f.0,10x,z
57: wrt 701,A,B,C
58: fmt "#",f.0,10x,"#",f.0,10x,"#",f.0,/
59: wrt 701,D,E,F
60: fmt 86"-",./;wrt 701
61: for I=1 to r0;if I=36;dsp "change paper";beep;stp
62: fmt c14,6f12.6;if I=72;dsp "change paper";beep;stp
63: if I=r0;jmp 3
64: wrt 701,B$(I),F[A,I],F[B,I],F[C,I],F[D,I],F[E,I],F[F,I]
65: next I
66: dsp "SELECT KEY FUNCTION";stp ;jmp 0
67:
68:
69: "INITIALIZE FREQ/DATA APPAYS":
70: ent "NEW or OLD data array to start?",A$
71: if A$="CLD";gto "INITIALIZE FROM FILES"
72: ent "FILE TO START STORING DATA?",W
73: 2→r0
74: for I=1 to 36
75: fxd 0;dsp "enter ch#",I," frequency";ent "",F
76: F/le6→F[I,r0-1];next I
77: dsp "SELECT KEY FUNCTION";stp ;jmp 0
78:
79: "INITIALIZE FROM FILES":
80: ent "FILE # FOR OLD DATA START?",W
81: rew;trk 1;fdf w;ldf w,F[*],B$,T[*]
82: for I=1 to 50
83: if F[1,I]=0;I+1→r0;jmp 2
84: next I
85: if I=51;prt "FULL FILE";c11 'FULL FILE'
86: ent "PRINTOUT STARTING FREQ's??",A$
87: if A$#"YES";jmp 6
88: fxd 0;prt "STARTING INFO:";prt "-----"
89: prt "r0= ",r0;spc
90: for I=1 to 36
91: fxd 0;prt "I= ",I;fxd 6;prt F[I,r0-2]+F[I,r0-1];prt B$[r0-1];spc
92: next I
93: dsp "SELECT KEY FUNCTION";beep;stp ;jmp 0
94:
95: "CYCLE TEST":
96: for J=1 to 36
97: "SET TEST TO CHANNEL 1":rem 720;wrt 720,"1"
98: "SET PROCESSOR TO C1&C2 A/R":rem 716;wrt 716,"C1I4C2I4E"
99: "SELECT CRYSTAL TO TEST1":fmt f.0,f.0,"E"
100: wrt 709,29+J-6*int((J-1)/6),40+int((J-1)/6)
*16768

```

```

101:
102: "INITIALIZE FREQUENCY":F[J,r0-1]*1e6→F
103: cll 'DETERMINE ZERO PHASE FREQUENCY';F/1e6→F[J,r0]
104: "CLEAR SCANNER":wrt 709,"C"
105: next J
106: cll 'MEASURE TEMPERATURE';X→T[r0]
107: cll 'READ TIME'
108: if T=1;spc ;spc
109: r0+1→r0;wrt 709,"C"
110: ret
111:
112: "FEAD TIME":
113: wrt 9,"Request time"
114: red 9,A$;A$→B$[r0]
115: ret
116:
117: "FULL FILE":W+1→W;prt "START NEW FILE";spc ;prt "FILE #=",W
118: for I=1 to 36;F[I,50]→F[I,1];next I
119: for I=2 to 50;for J=1 to 36;0→F[J,I];next J;next I
120: for I=1 to 50;" "→B$[I];0→T[I];next I
121: 2→r0;ret
122:
123: "SELECT RESONATOR TO TEST":
124: ent "enter # to test 1-36",N
125: wrt 709,"C"
126: fmt 1,2f.0,"E";wrt 709.1,N+29-6*int((N-1)/6),40+int((N-1)/6);wait 1000
127: fxd 0;dsp "Dev#",N,":SELECT KEY FUNCTION";stp ;jmp 0
128:
129: "DETERMINE ZERO PHASE FREQUENCY":
130: F/1e9→X
131: "SET INSTRUMENTS TO REMOTE":rem 716;rem 719;rem 718;wait 1000
132: "SYNTHESIZER SET-UP":fmt 1,"/",f.0,"(", "40$", "00%", "500C"
133: "SOURCE CONVERTER SET-UP":fmt 2,"F3M4W5S5T108V99EFA",f.0,"E"
134: "SOURCE/CONVERTER FREQUENCY SET":fmt 3,"FA",f.0,"E"
135: "SYNTHESIZER + FREQ INCREMENT":fmt 4,"/",f.0,"A"
136: "SYNTHESIZER - FREQ INCREMENT":fmt 5,"/",f.0,"B"
137: "SYNTHESIZER FREQUENCY SET":fmt 6,"/",f.0,"("
138:
139: "SETTING UP SYSTEM":dsp "Setting up system";beep
140: "SET UP SYNTHESIZER":wrt 718.1,f(X)
141: "SET UP SOURCE/CONVERTER":wrt 719.2,F/1e6-1;wait 1000
142: wrt 719.2,F/1e6+3;wait 1000
143: "ZERO OUT Co REACTANCE":dsp "Zeroing out Co";beep
144: "F + 1MHz→SYNTHESIZER & SOURCE":(F+1e6)/1e9→X
145: wrt 718.1,f(X);wrt 719.3,(F+1e6)/1e6-1;wait 1000
146: wrt 719.3,(F+1e6)/1e6+2;wait 1000
147: "SET-UP CH 1 FOR MAG":wrt 716,"C1M2S5EC1D2E";wait 1500
148: "SET-UP CH1 ZERO FET LOSS":wrt 716,"C1D4EC1D2E";wait 1500
149: "SET-UP DISPLAY PROCESSOR":wrt 716,"C2M3S8EC2D2E";wait 1500
150: "ZERO PHASE OFFSET":wrt 716,"C2D4EC2D2E";wait 2000
*1991

```

```

151: "READ AMP & PHASE":fmt ;red 716,A,B
152: "CHECK IF PHASE =0":if E#0;jmp -2
153: dsp "phase set =",B;beep;wait 2000
154: dsp "Resetting start frequency";beep
155: "RESET START FREQUENCY":wrt 719.2,F/1e6-2;wait 1000;wrt 719.2,F/1e6+2
156: F/1e9+X;wrt 718.6,'f(X)';wait 1000
157: red 719,A;if abs(A-F)>5e5;jmp -2
158:
159: "EVALUATE PHASE SLOPE":dsp "Evaluating phase slope"
160: "SET F1->SYNTHESIZER":F*2e-6/1e9+X;wrt 718.5,'f(X)';wait 1500
161: "READ PHASE P1":red 716,A,B;c11 'Z-parm phase'(A,B,r1)
162: "SET F2->SYNTHESIZER":2X+X;wrt 718.4,'f(X)';wait 1500
163: "READ PHASE P2":red 716,A,B;c11 'Z-parm phase'(A,B,r2)
164: if r2=r1;gto "RESET START FREQUENCY"
165: "CALC. PHASE SLOPE":(r2-r1)/(F*4e-6)+S
166: fxd 2;dsp "phase slope =",1000S," deg/kHz";wait 2000
167: if S<0;gto "DETERMINE ZERO PHASE FREQUENCY"
168:
169: "ITERATE TO ZERO PHASE":dsp "Iterating to zero phase"
170: "SET UP DO LOOP":for I=1 to 20
171: "SET NEW FREQUENCY":F/1e9+X;wrt 718.6,'f(X)';wait 1000
172: "READ AMPLITUDE AND PHASE":red 716,A,B;c11 'Z-parm phase'(A,B,G)
173: "CHECK IF PHASE= 0":if G=0;jmp 3
174: "CALC. NEW FREQUENCY":F-G/S+F
175: "END DO LOOP":next I
176: fxd 6;dsp "F=",F/1e6,"MHz ", "Phase= ",G,"degrees";wait 1000
177: if T=1;prt "F=",F/1e6;prt "Phase=",G;spc
178: lcl 7
179: ret
180:
181: "INTERPUPT":beep
182: c11 'CYCLE TEST'
183: if r0=51;c11 'RECOPD DATA'
184: eir 9
185: iret
186:
187: "f(X)":
188: 1->E;abs(X)->Y;0->Z
189: Z+Eint(Y)->Z
190: 10(Y-int(Y))->Y
191: 10E->E
192: if Y#0;jmp -3
193: ret Z
194:
195: "PLOT DATA FILES":ent "First file to plot?",P
196: ent "Last file to plot?",C
197: ent "Multiple xtals to plot (YES/NO)?",A$
198: ent "Multiple duals to plot (YES/NO)?",C$
199: ent "Multiple diff' to plot (YES/NO)?",E$
200: if A$="YES";gto "MULTIPLE XTAL PLOTS"
*19256

```

```

201: if C$="YES";gto "MULTIPLE DUAL CRYSTAL PLOTS"
202: if E$="YES";gto "MULTIPLE DIFF CRYSTAL PLOTS"
203: "NEW XTAL":
204: ent "crystal#(or Temp=0) to plot?",X;if X=0;c11 "PLOT TEMPERATURE"
205: ent "PLOT SET-UP(YES or NO)?",A$;if A$="NO";gto "PLOT"
206: c11 "PLOT SET-UP"
207:
208: "PLOT":dsp "change pen color?";beep;stp ;if E$="LIN";lim 0,B-A,R,M
209: if E$="LOG";lim 0,lcg((B-A)/(60*C)+1),R,M
210: for U=P to Q;trk 1;fdf U;ldf U,F[*],B$,T[*]
211: for I=J to 50;if B$[I]="";pen;gto 216
212: B$[I]+A$;'abstime A$'+Y
213: if E$="LIN";plt Y-A,(F[X,I]-r(X+4))le6/r(X+4)
214: if E$="LOG";plt log((Y-A)/(60*C)+1),(F[X,I]-r(X+4))le6/r(X+4)
215: dsp "I=",I
216: next I;pen
217: dsp "File=",U
218: next U;lim
219: ent "PLOT LABELINC(YES or NO)?",A$;if A$="YES";l+R;c11 "PLOT LABELING"
220: ent "ANOTHER XTAL (YES/NO) ?",A$
221: if A$="YES";gto "NEW XTAL"
222: dsp "SELECT KEY FUNCTION";beep;stp ;jmp 0
223:
224: "PLOT LABELINC":if E$="LOG";c11 "LOG PLOT LABELING";ret
225: csiz 3,2
226: if X=0;plt 0,R+(M-R)/2,-1;cplt -6,0;csiz 8,5,1,90;cplt -15/2,0
227: if X=0;lbl "Temperature (C)";csiz 8,5,1;gto 234
228: plt (B-A)/2,0,-1;cplt -10,-3
229: lbl "1 Week per Division"
230: plt 0,R+(M-R)/2,-1;cplt -6,0
231: csiz 3,2,1,90;cplt -4,0
232: wrt 705,"UC99,2,6,2,-6,-4,0,-99"
233: lbl "F (ppm)";csiz 4,2
234: plt .2(B-A)/2,M,-1;cplt 0,-2;if X=0;cplt 0,1
235: if flg8;ret
236: ent "plot label?",G$
237: lbl G$
238: ret
239:
240: "PLOT SET-UP":trk 1;fdf P;ldf P,F[*],B$,T[*]
241: if flg7;gto 265
242: l+J;prt "STAF T TIME="
243: if B$[1]="";prt B$[2];2+J;spc ;jmp 2
244: prt B$[1];spc
245: 50+r0;trk 1;fdf C;ldf C,F[*],B$,T[*]
246: prt "STOP TIME="
247: if B$[r0]="";r0-1+r0;jmp 0
248: prt B$[r0]+E$;spc ;spc ;trk 1;fdf P;ldf P,F[*],B$,T[*]
249:
250: ent "CHANGE STAF T TIME(YES/NO)?",A$
*30929

```

```

251: if A$="YES";ent "ENTER NEW TIME(MM:DD:HH:MM:SS)",C$
252: if A$="NO";B$[J]→C$
253: C$→A$; 'abstime A$'→A
254: ent "CHANGE STOP TIME(YES/NO)?",A$
255: if A$="YES";ent "ENTER NEW TIME(MM:DD:HH:MM:SS)",D$
256: if A$="NO";E$→D$
257: D$→A$; 'abstime A$'→B
258: sfg 7
259:
260: ent "maximum + deviation?",M
261: ent "minimum - deviation?",R
262: ent "Y-tic interval?",D
263: ent "LIN or LOG (T+1)?",E$;ent "Time Units(min)?",C
264: dsp "set up plotter";beep;stp
265:
266: pclr;wrt 705,"VS3"
267: if flg1;wrt 705,"IP1100,7700,3600,9700";cfg 1;gto 273
268: if flg2;wrt 705,"IP4600,7700,7100,9700";cfg 2;gto 273
269: if flg3;wrt 705,"IP1100,4700,3600,6700";cfg 3;gto 273
270: if flg4;wrt 705,"IP4600,4700,7100,6700";cfg 4;gto 273
271: if flg5;wrt 705,"IP1100,1700,3600,3700";cfg 5;gto 273
272: if flg6;wrt 705,"IP4600,1700,7100,3700";cfg 6
273: if E$="LCC";gto "LOG SET-UP"
274: scl 0,E-A,R,M
275: wrt 705,"TL1,1";xax 0,60*C,0,E-A
276: wrt 705,"TL0,1";xax M,60*C,0,E-A
277: if X=0;fxd 1;csiz 5,5;jmp 2
278: fxd 0;csiz 2,2
279: yax E-A,D,R,M;wrt 705,"TL1,0";xax R,C*60,0,E-A;yax 0,D,R,M,1
280: "DETERMINE REFERENCE FREQUENCIES":
281: for I=1 to 36;F[I,J]→r(I+4);next I
282: ret
283:
284: "LCC SET-UP":
285: scl 0,log((B-A)/(60*C)+1),R,M
286: wrt 705,"TL1,1";xax 0,1,0,log((B-A)/(60*C)+1)
287: wrt 705,"TL0,1";xax M,1,0,log((B-A)/(60*C)+1)
288: fxd 0;csiz 2,2
289: yax log((B-A)/(60*C)+1),D,F,M
290: wrt 705,"TL1,0";xax R,1,0,log((B-A)/(60*C)+1);yax 0,D,F,M,1
291: gto "DETERMINE REFERENCE FREQUENCIES"
292:
293:
294: "PLCT TEMPERATURE":ent "REF TEMP???",r99
295: ent "PLCT SET-UP (YES/NO)?",A$;if A$="YES";c11 "PLCT SET-UP"
296: for U=P to Q;trk 1;fdf U;ldf U,F[*],B$,T[*]
297: dsp "change pen color?";beep;stp
298: for I=J to 50;if B$[I]="";pen;jmp 3
299: B$[I]→A$; 'abstime A$'→Y
300: plt Y-A,T[I]-r99
*4907

```

```

301: next I;pen
302: next U
303: ent "PLCT LABELING(YES or NO)?",A$;if A$="YES";gto "PLCT LABELING"
304: gto 204
305:
306: "RECORD DATA":
307: if W=1;rew
308: trk 1;fdf w;rcf W,F[*],B$,T[*]
309: W+1→W
310: for I=1 to 36
311: F[I,50]→F[I,1]
312: for J=2 to 50
313: 0→F[I,J]
314: next J
315: next I
316: T[50]→T[1];B$[50]→E$[1]
317: for I=2 to 50
318: 0→T[I];""→E$[I]
319: next I
320: 2→r0
321: ret
322:
323: "TEFMINATE PROGRAM":
324: wrt 9,"Abort timers"
325: fxd 0;prt "STORING DATA";prt "ON FILE# ",W;spc
326: trk 1;fdf w;rcf W,F[*],B$,T[*]
327: rew
328: wait 5000
329: dsp "REMOVE TAPE FROM CALCULATOR";beep;stp ;jmp 0
330:
331: "cxdiv":p3^2+p4^2+p7;(p1p3+p2p4)/p7+p5;(p2p3-p1p4)/p7+p6;ret
332:
333: "Z-param phase":
334: tn^(p1/20)→p4
335: p4cos(p2)→C;p4sin(p2)→D
336: cll 'cxdiv'(1+C,D,1-C,-D,A,E)
337: atn(B/A)→p3
338: ret
339:
340: "LOG PLCT LABELING":csiz 3,2
341: plt log((B-A)/(60*C)+1)/2,0,-1;cplt -11,-3
342: lbl "Logarithmic time, hours"
343: plt 0,R+(M-R)/2,-1;cplt -6,0
344: csiz 3,2,1,90;cplt -4,0
345: wrt 705,"UC99,2,6,2,-6,-4,0,-99"
346: lbl "F (ppm)";csiz 4,2
347: plt .1*log((B-A)/(60*C)+1),M,-1;cplt 0,-2
348: if flg1 or flg2 or flg3 or flg4 or flg5 or flg6 or flg8;ret
349: ent "plot label?",C$
350: lbl G$
*7756

```

```

351: ret
352:
353: "MULTIPLE XTAL PLOTS":
354: ent "PLCT SET-UP (YES/NO)?",A$
355: if A$="YES";c11 "PLOT SET-UP"
356: if E$="LOG";lim 0,log((B-A)/(60*C)+1),R,M;jmp 2
357: lim 0,B-A,R,M
358: ent "Number of xtals to plot",N
359: for I=1 to N;ent "Xtal # ?",H$(I);next I
360: for U=P to Q;trk 1;ldf U,F[*],B$,T[*]
361: for Z=1 to N
362: val(H$(Z))>X
363: for I=J to 50;if B$(I)="" ;pen;gto 368
364: B$(I)>A$;'abstime A$>Y
365: if E$="LIN";plt Y-A,(F[X,I]-r(X+4))le6/r(X+4)
366: if E$="LOG";plt log((Y-A)/(60*C)+1),(F[X,I]-r(X+4))le6/r(X+4)
367: dsp "I=",I
368: next I;pen
369: next Z
370: next U
371: lim
372: ent "PLOT LABELING (YES/NO)?",A$;if A$="YES";l>R;c11 "PLOT LABELING"
373: dsp "SELECT KEY FUNCTION";beep;stp ;jmp 0
374:
375: "MULTIPLE DUAL CRYSTAL PLOTS":
376: cfg 7;sfg 1;sfg 2;sfg 3;sfg 4;sfg 5;sfg 6;sfg 8
377: ent "Number of xtals to plct(12 max)",N
378: for I=1 to N;ent "Xtal # ?",H$(I);next I
379: for Z=1 to N by 2
380: pen# 4;c11 "PLOT SET-UP"
381: if E$="LOG";lim 0,log((B-A)/(60*C)+1),R,N;jmp 2
382: lim 0,B-A,R,M
383: pen# 3
384: for U=P to Q;trk 1;ldf U,F[*],B$,T[*]
385: for G=Z to Z+1;val(H$(G))>X
386: for I=J to 50;if B$(I)="" ;pen;gto 391
387: B$(I)>A$;'abstime A$>Y
388: if E$="LIN";plt Y-A,(F[X,I]-r(X+4))le6/r(X+4)
389: if E$="LOG";plt log((Y-A)/(60*C)+1),(F[X,I]-r(X+4))le6/r(X+4)
390: dsp "I=",I
391: next I;pen
392: next G
393: next U
394: lim
395: pen# 4
396: c11 "PLOT LABELING"
397: fxd 0;lbl "#",val(H$(Z))," & #",val(H$(Z+1))
398: next Z
399: dsp "SELECT KEY FUNCTION";beep;stp ;jmp 0
400:
*4480

```

```

401: "MULTIPLE DIFF CRYSTAL PLCTS":
402: cfg 7;sfg 1;sfg 2;sfg 3;sfg 4;sfg 5;sfg 6;sfg 8
403: ent "Number of xtals to plot(12 max)",N
404: for I=1 to N;ent "Xtal # ?",H$(I);next I
405: for Z=1 to N by 2
406: pen# 4;c11 'PLOT SET-UP'
407: if E$="LOG";lim 0,log((B-A)/(60*C)+1),R,M;jmp 2
408: lim 0,B-A,R,M
409: pen# 3
410: for U=P to Q;trk 1;ldf U,F[*],B$,T[*]
411: val(H$(Z))>X
412: for I=J to 50;if B$(I)="" ;pen;qto 420
413: B$(I)+A$;'abstime A$>Y
414: (F[X,I]-r(X+4)-F[X+1,I]+r(X+5))le6/((r(X+4)+r(X+5))/2)>F
415: if E$="LOG";gto 418
416: plt Y-A,F
417: gto 419
418: plt log((Y-A)/(60*C)+1),F
419: dsp "I=",I
420: next I;pen
421: next U
422: lim
423: pen# 4
424: c11 'PLOT LABELING'
425: fxd 0;lbl "#",val(H$(Z))," & #",val(H$(Z+1))
426: next Z
427: dsp "SELECT KEY FUNCTIONN";beep;stp ;jmp 0
428:
429: "MULTIPLE DUAL XTAL PCLAR PLOT S-PARM":
430: cfg 7;sfg 1;sfg 2;sfg 3;sfg 4;sfg 5;sfg 6;sfg 8
431: ent "Number of Xtals to plot(max 12)?",N
432: for I=1 to N;ent "xtal #?",H$(I);next I
433: ent "File for reference frequencies?",U
434: trk 1;ldf U,F[*],B$,T[*]
435: dsp "Set up Analyzer";beep;stp
436:
437: for B=1 to N by 2
438: pen# 4;c11 'Polar Plot Set-up'
439: pen# 3
440: for G=B to B+1;val(H$(C))>X;wrt 709,"C"
441: if G=B+1;pen# 2
442: fmt 1,2f.0,"E";wrt 709.1,X+29-6*int((X-1)/6),40+int((X-1)/6);wait 1000
443: F[X,1]*le6>F;F/le9>X;rem 716;rem 719;rem 718;wait 1000
444: fmt 1,"/",f.0,"(", "40$", "CO%", "500C"
445: fmt 2,"R3M4W5S5T1O8V99EFA",f.0,"E"
446: fmt 3,"FA",f.0,"E";fmt 4,"/",f.0,"A";fmt 5,"/",f.0,"E"
447: fmt 6,"/",f.0,"("
448: wrt 719.2,F/le6-1;wait 1000;wrt 719.2,F/le6+3;wait 1000
449: (F+le6)/le9>X;wrt 718.1,'f(X)';wrt 719.3,F/le6;wait 1000
450: wrt 719.3,(F+le6)/le6+2;wait 1000
*24330

```

```

451: wrt 716,"C1M5S2EC1D2E";wait 1500
452: wrt 716,"C1D4EC1D2E";wait 1500
453: wrt 716,"C2M6S2EC2D2E";wait 1500
454: wrt 716,"C2D4EC2D2E";wait 2000
455: fmt ;red 716,A,T;if T#0;jmp -1
456: cll "Zero Phase slope"
457: wrt 719.2,F/1e6-2;wait 1000;wrt 719.2,F/1e6+2
458: F/1e9+X;wrt 718.6,"f(X)";wait 1000
459: red 719,A;if abs(A-F)>5e5;jmp -2
460: wrt 719,"W4E"
461: wrt 718,"/","41$","08%"
462: wrt 714,"EF";wrt 714,"P3";wait 3000
463: for I=1 to 250;red 714,X[I];red 714,Y[I];next I;lcl 714
464: for I=1 to 250;plt X[I]/250,Y[I]/250
465: next I;pen
466:
467: csiz 3
468: if G=B;plt -1.24,.9,-1;fxd 0;lbl "#",val(H$(G))
469: if G=B+1;plt -1.24,.9,-1;cplt 0,-1;fxd 0;lbl "#",val(H$(G))
470: next G
471: next B
472: pen# 0
473: dsp "finished";beep;stp
474:
475:
476: "Polar Plot Set-up":
477: if flg7;gto 479
478: dsp "set up plotter";beep;stp ;sfg 7
479: pclr;wrt 705,"VS3"
480: if flg1;wrt 705,"IP1100,7700,3600,9700";cfg 1;gto 486
481: if flg2;wrt 705,"IP4600,7700,7100,9700";cfg 2;gto 486
482: if flg3;wrt 705,"IP1100,4700,3600,6700";cfg 3;gto 486
483: if flg4;wrt 705,"IP4600,4700,7100,6700";cfg 4;gto 486
484: if flg5;wrt 705,"IP1100,1700,3600,3700";cfg 5;gto 486
485: if flg6;wrt 705,"IP4600,1700,7100,3700";cfg 6
486: scl -1.25,1.25,-1,1;csiz 2
487: xax 0,.1,-1,1;yax 0,.1,-1,1;rad
488: for I=0 to 2π by π/100;plt cos(I),sin(I);next I
489: pen
490: ret
491:
492: "Zero Phase slope":
493: wrt 718,"/","41$","08%";wrt 719,"W4E";l+Z
494: wrt 716,"C2M3S8EC3M2E"
495: fmt ;red 716,A,A,A
496: wrt 719,"FC01E";wait 200;fmt ;red 716,A,Y[1],A
497: wrt 719,"FC99E";wait 200;fmt ;red 716,A,Y[2],A
498: if abs(Y[1]-Y[2])<.2;gto 501
499: if Y[1]>Y[2];fmt "C30",f3.0,"E";Z-1+Z;wrt 716,Z;gto 495
500: if Y[1]<Y[2];fmt "C30",f3.0,"E";Z+1+Z;wrt 716,Z;gto 495
501: wrt 719,"FC50E";wait 200;wrt 716,"C2D2D4EC2D2E"
502: wrt 716,"C2M6S2E";wrt 718,"/","40$","00%";wait 1000
503: ret
*7452

```



7.2 Appendix II - Impedance Characterization

This appendix shows example plots of the impedance of a typical group of 36 SAW resonators. The impedance data is plotted as scattering parameters (Smith Chart transformation). These are automatically measured and plotted using the measurement software presented in Appendix I (program line 429). For each measurement the analyzer automatically nulls out the parasitic capacitance of the test fixture as well as the resonator. This results in resonance characteristics nominally symmetric about zero phase as shown in the following figures. Typically the SAW resonators possess a series resistance of 50 ohms.

MRDC41082.4AR

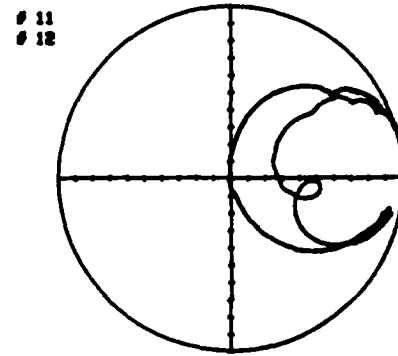
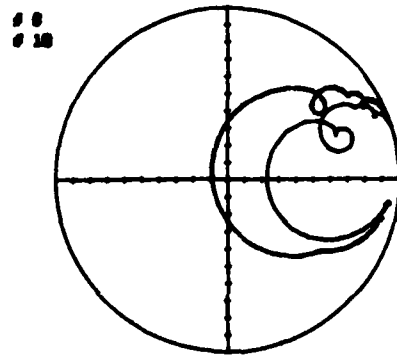
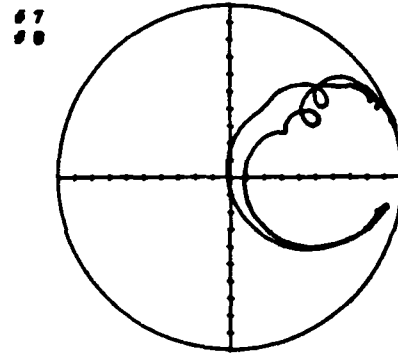
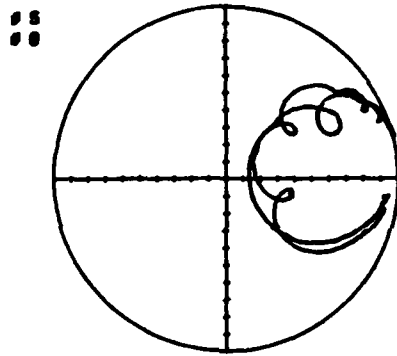
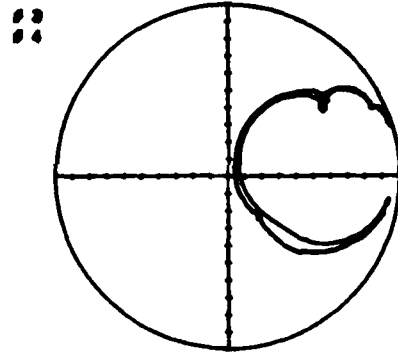
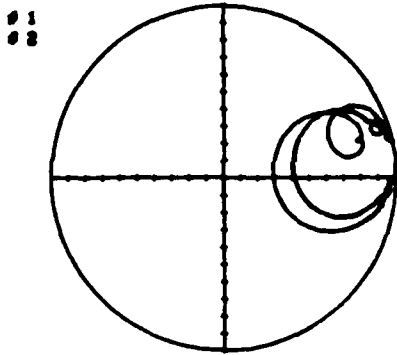
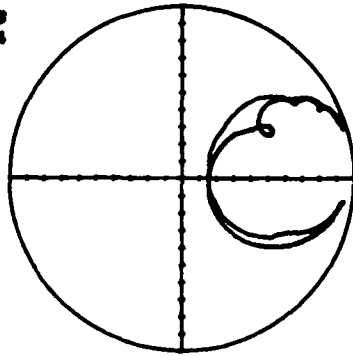


Fig. AII-1 Complex input scattering parameters for crystals #1 through 12.

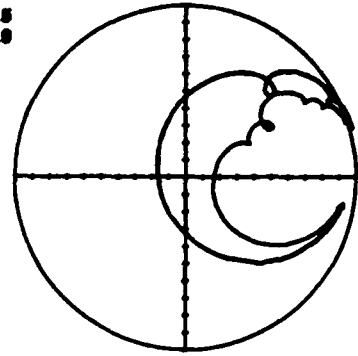


MRDC41082.4AR

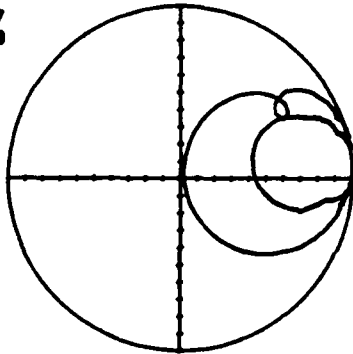
# 13  
# 14



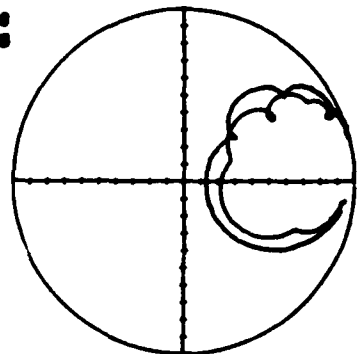
# 15  
# 16



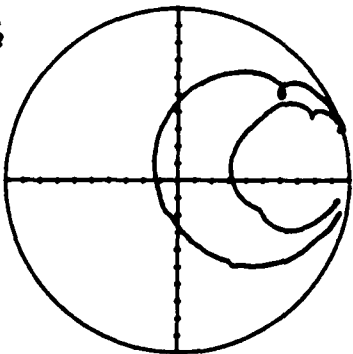
# 17  
# 18



# 19  
# 20



# 21  
# 22



# 23  
# 24

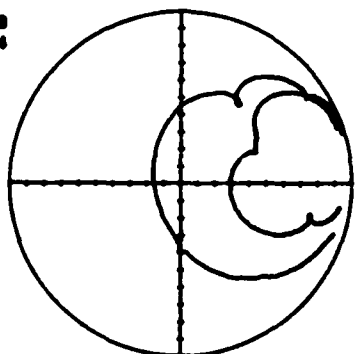
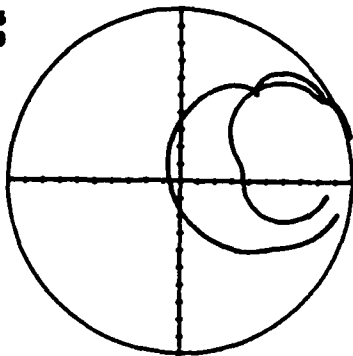


Fig. AII-2 Complex input scattering parameters for crystals #13 through #24.

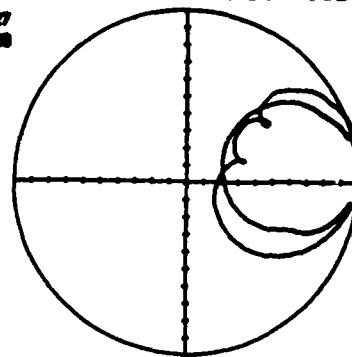


MRDC41082.4AR

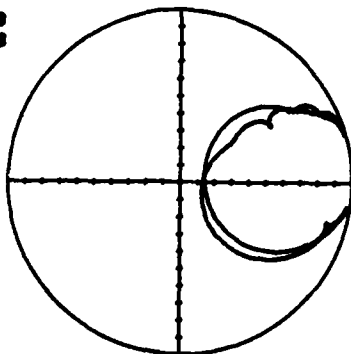
# 25  
# 26



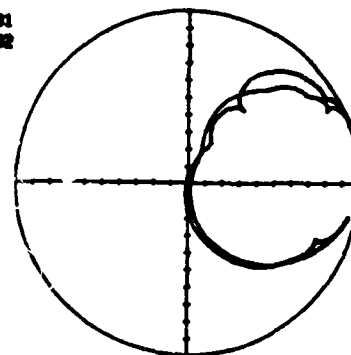
# 27  
# 28



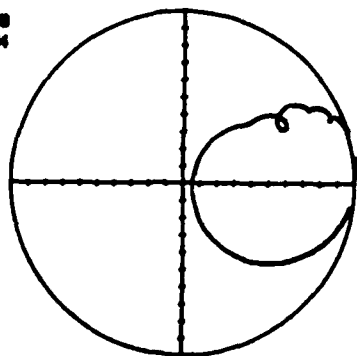
# 29  
# 30



# 31  
# 32



# 33  
# 34



# 35  
# 36

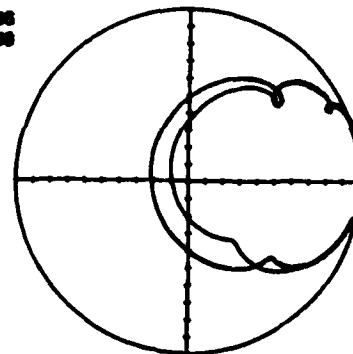


Fig. AII-3 Complex input scattering parameters for crystals #25 through #36.



7.3 Appendix III - Absolute Aging Results

This appendix shows typical data output for absolute aging of a group of 36 SAW resonators. The data is plotted as a linear function of time for all 36 crystals (program line 353). The aging data in this case has been plotted as 18 plots, two resonators per plot. This indicates that dual resonator crystals were tested. The absolute aging is also plotted as a function of logarithmic time in the latter three figures of this appendix. This type of plot clearly shows the logarithmic straight line behavior indicative of chemisorption or oxidation.



MRDC41082.4AR

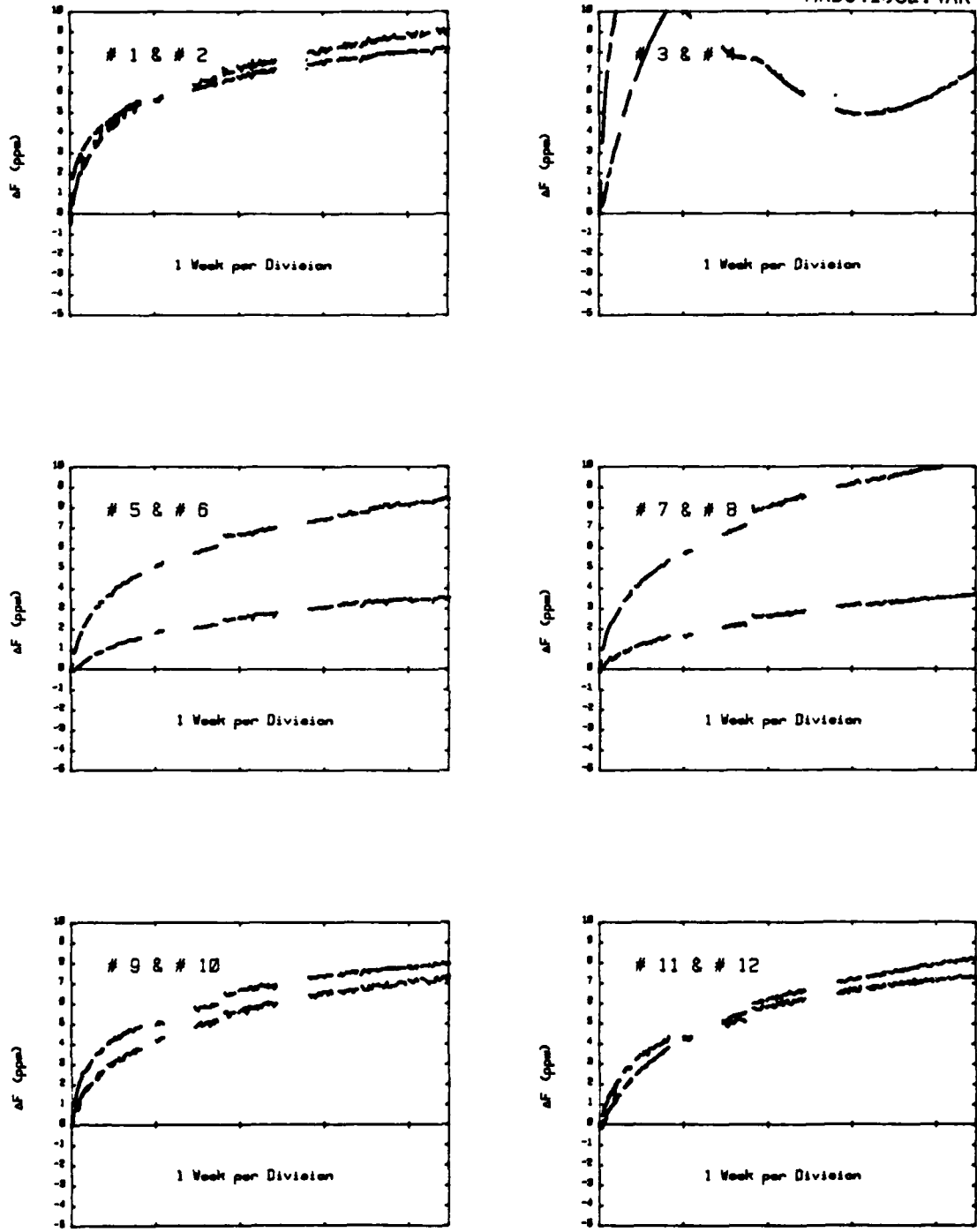


Fig. AIII-1 Absolute aging plotted vs linear time for crystals #1 through #12.



MRDC41082.4AR

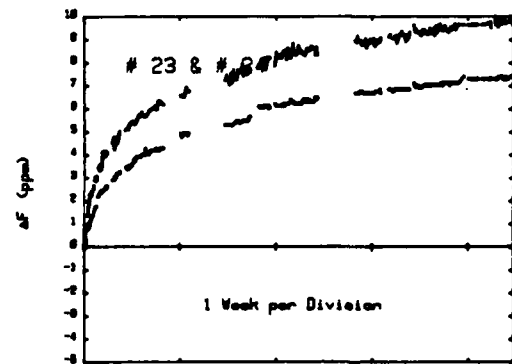
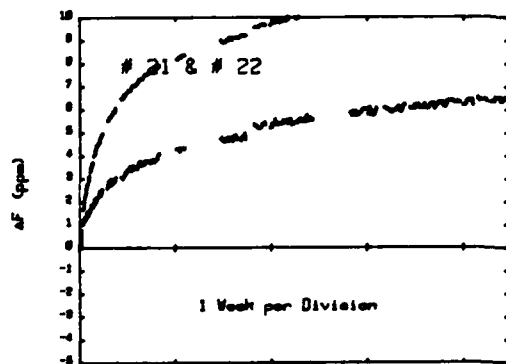
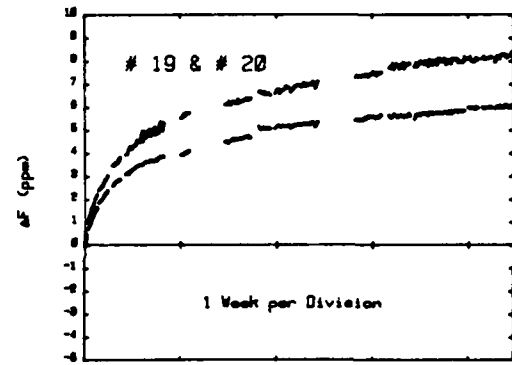
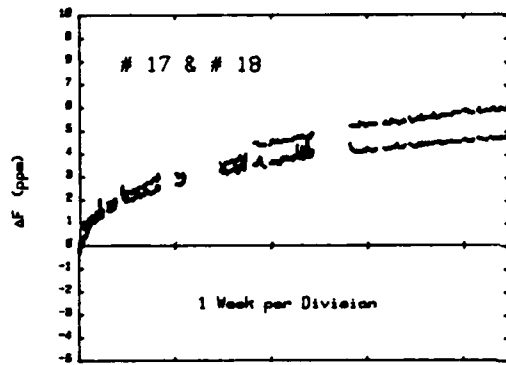
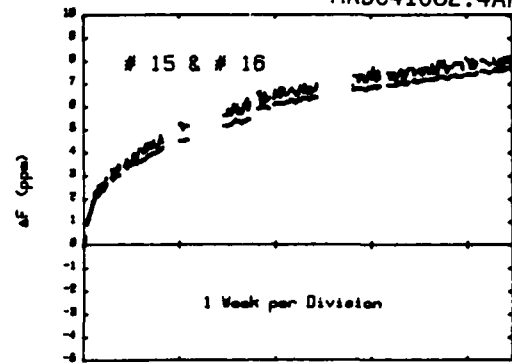
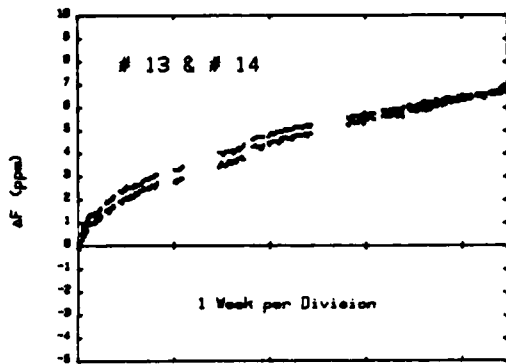


Fig. AIII-2 Absolute aging plotted vs linear time for crystals #13 through #24.



MRDC41082.4AR

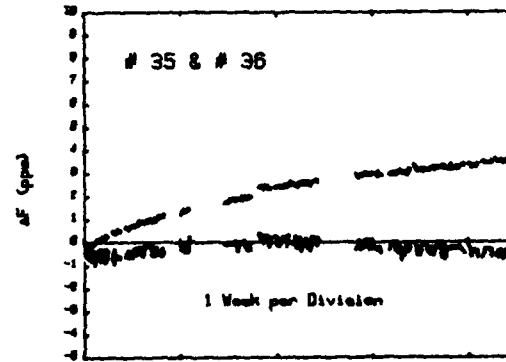
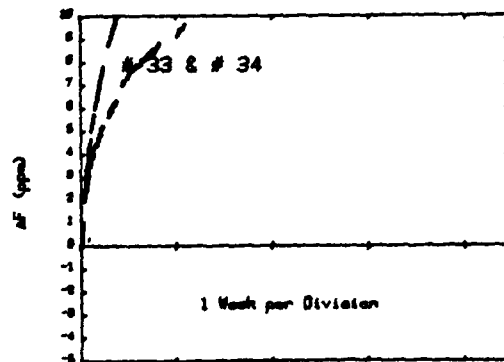
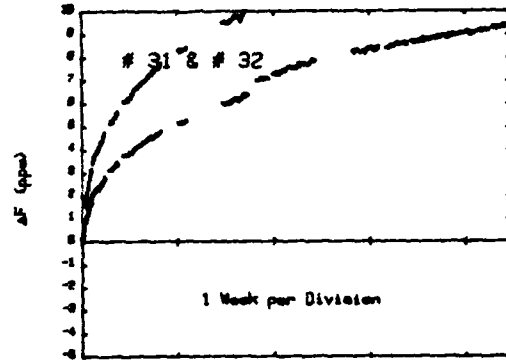
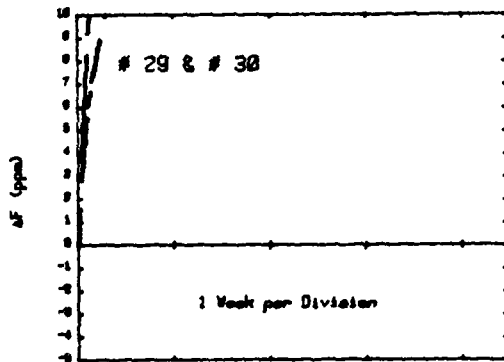
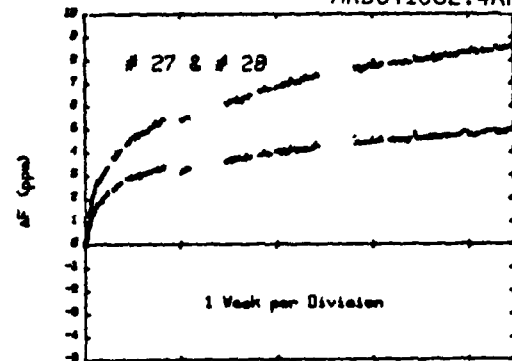
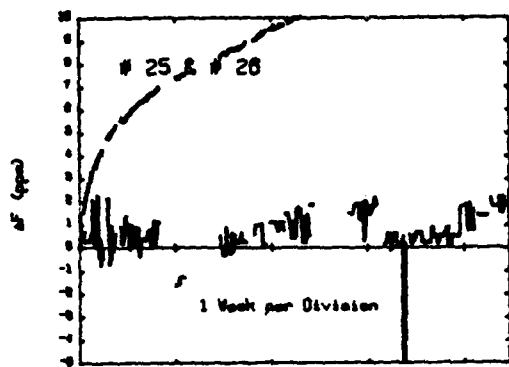


Fig. AIII-3 Absolute aging plotted vs linear time for crystal #25 through #36.



MRDC41082.4AR

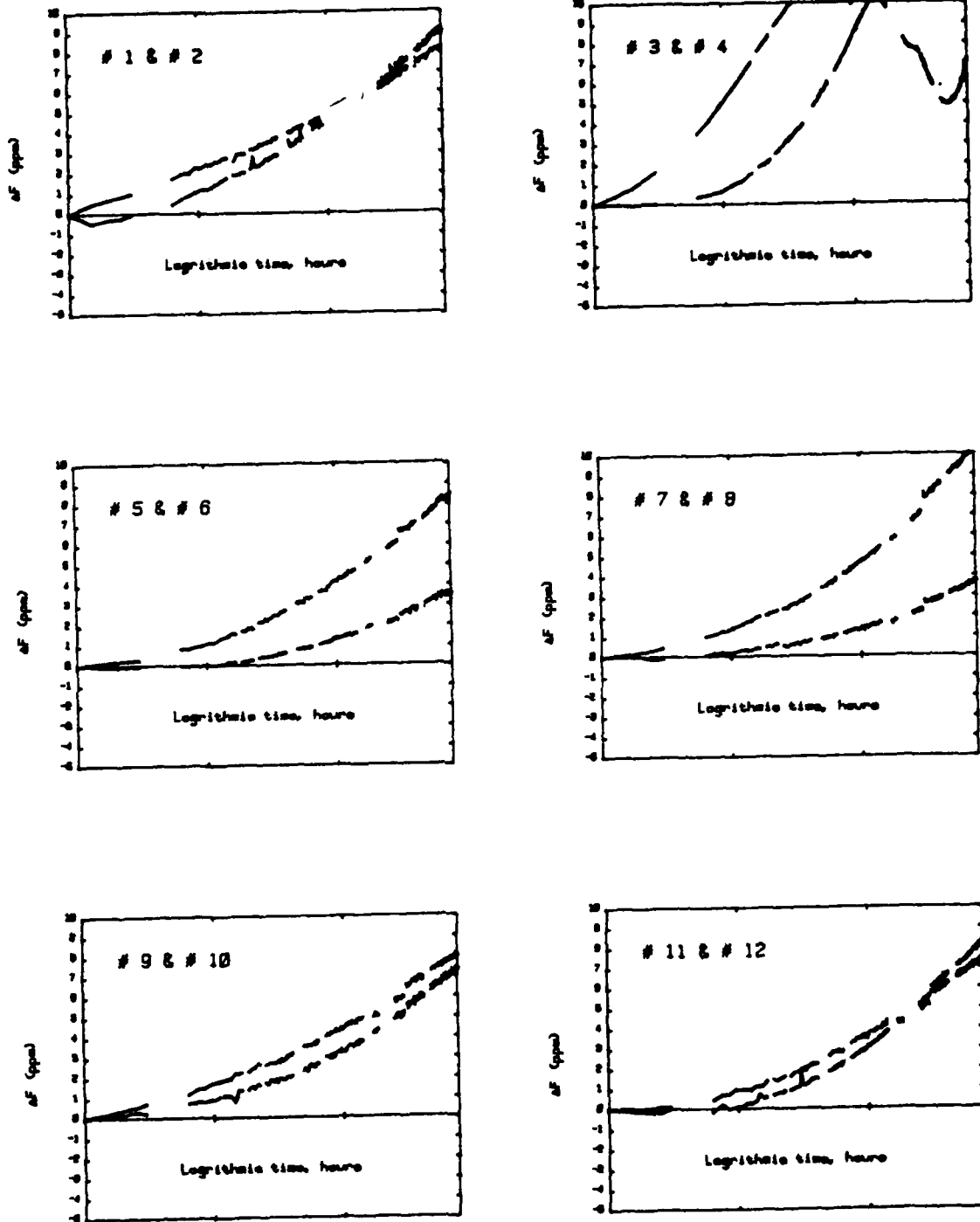


Fig. AIII-4 Absolute aging plotted vs logarithmic time for crystals #1 through #12.



MRDC41082.4AR

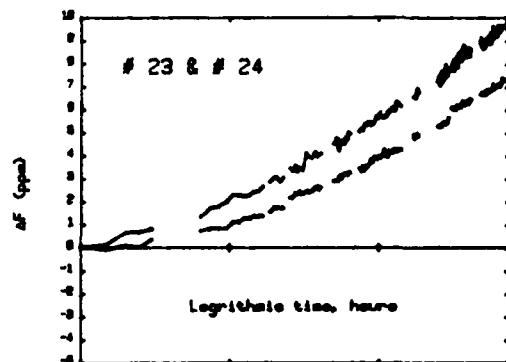
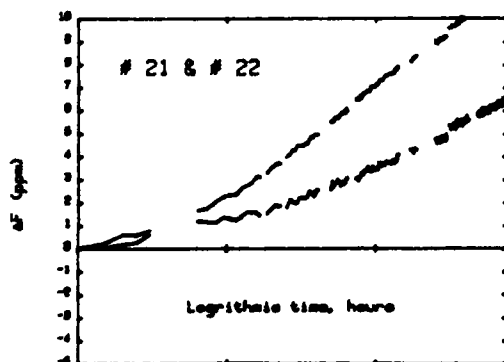
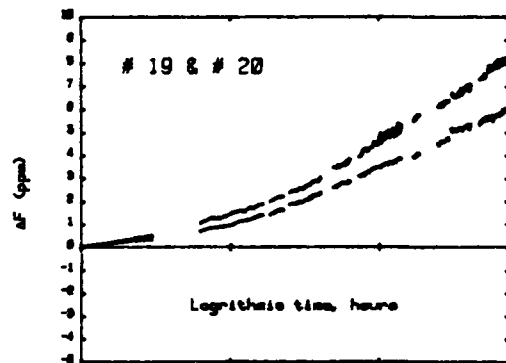
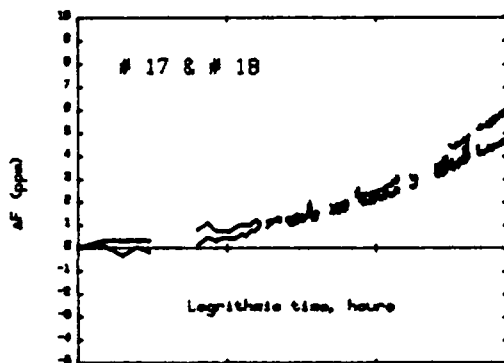
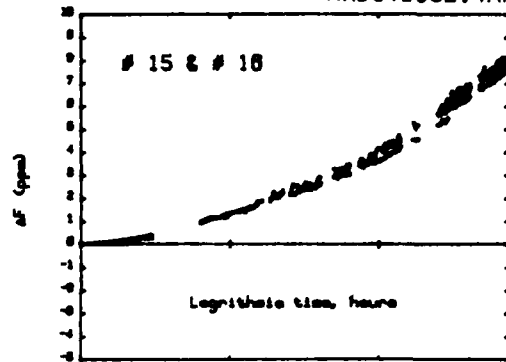
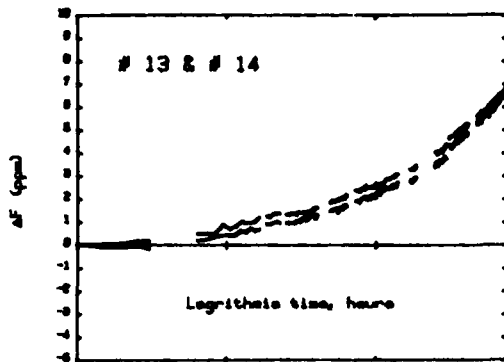


Fig. AIII-5 Absolute aging plotted vs logarithmic time for crystals #13 through #24.



MRDC41082.4AR

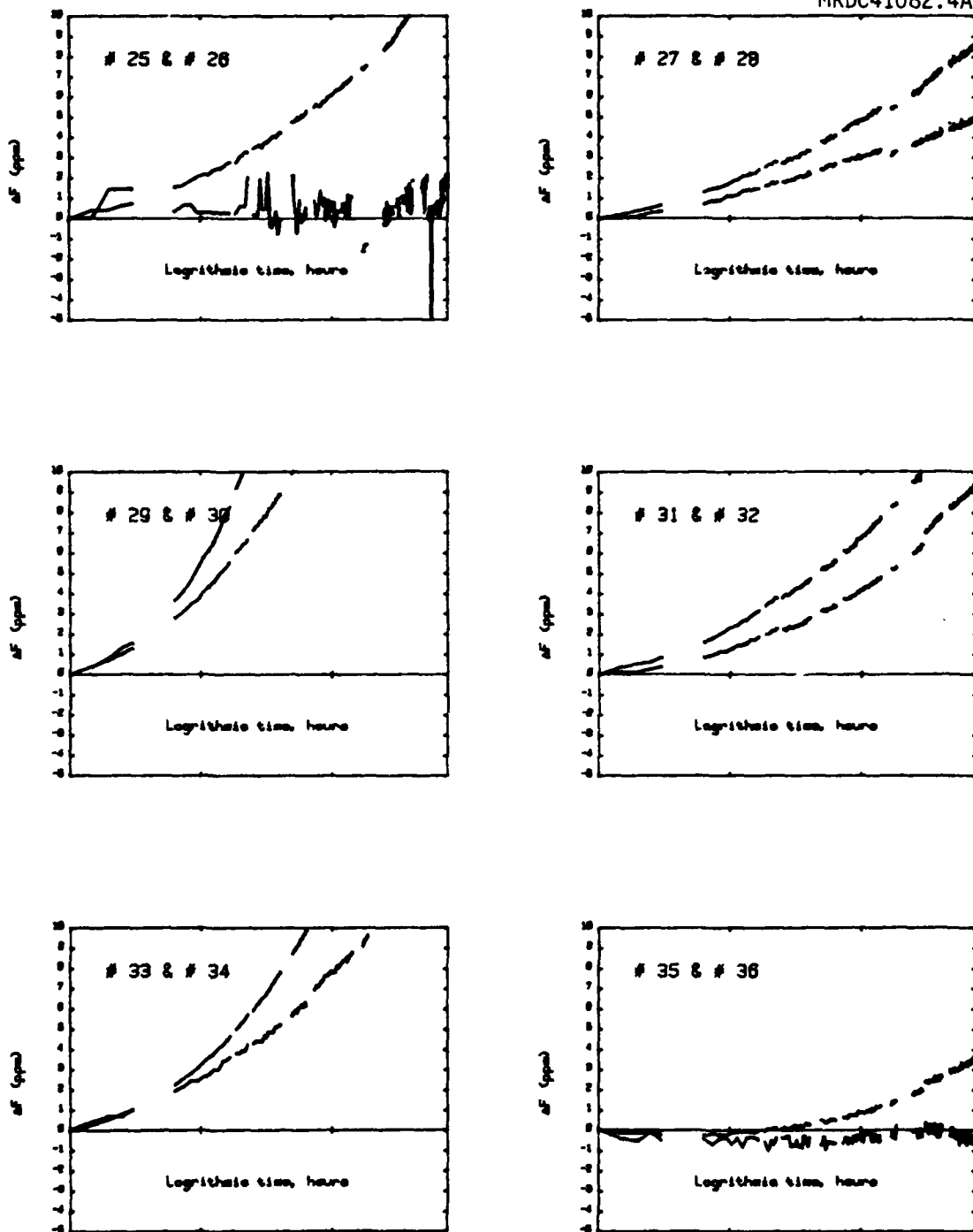


Fig. AIII-6 Absolute aging plotted vs logarithmic time for crystals #25 through #36.



7.4 Appendix IV - Differential Aging Results

This appendix shows differential aging evaluated for the group of 36 crystals discussed in the previous appendices. The data is first plotted as a linear function of time in the first three figures and as a logarithmic function of time in the latter three figures. Analysis of differential aging (program line 401) indicates that it is possible to obtain excellent differential bias stability even though absolute stability in each crystal may not be possible.



MRDC41082.4AR

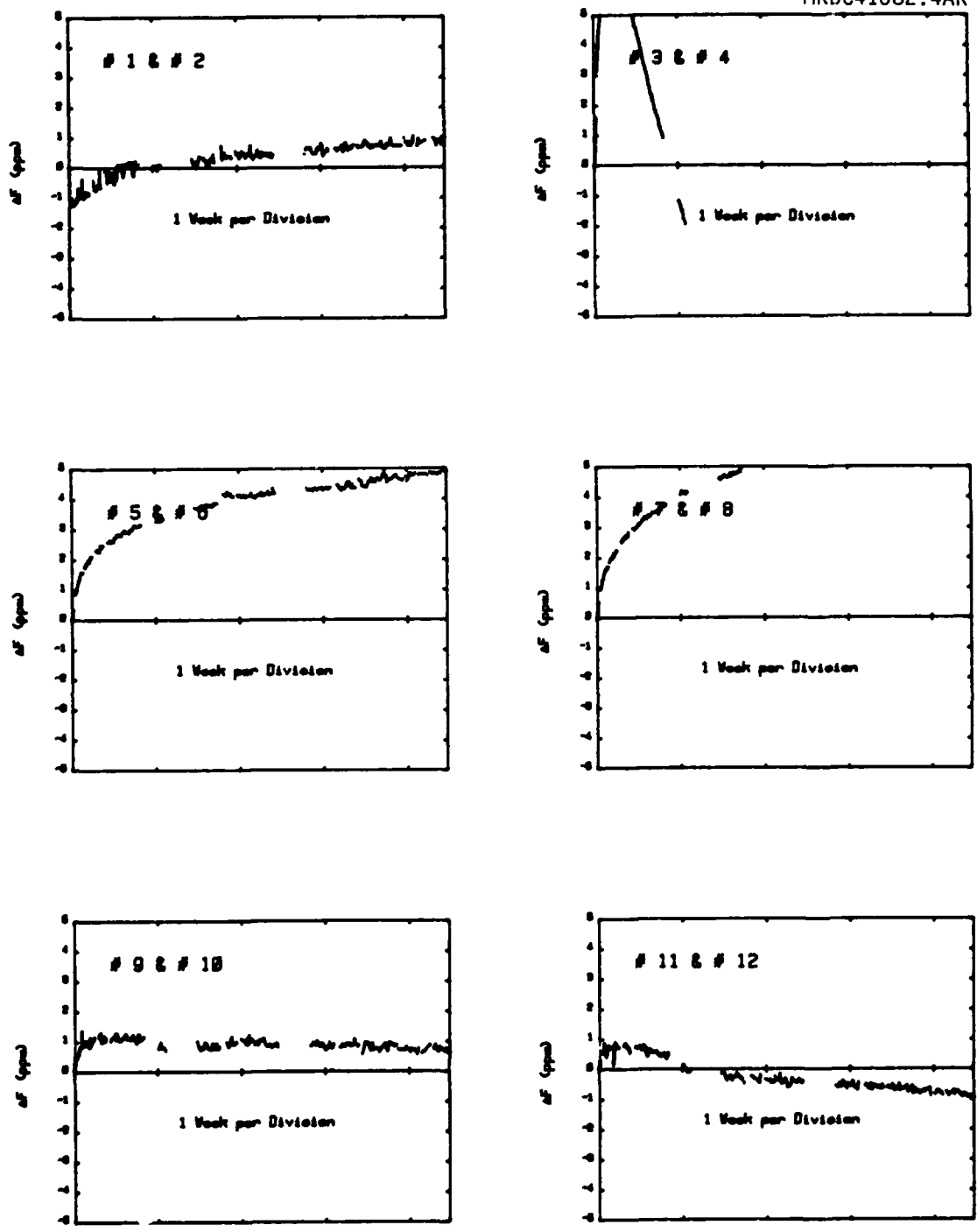


Fig. AIV-1 Differential aging plotted vs linear time for crystals #1 through #12.



MRDC41082.4AR

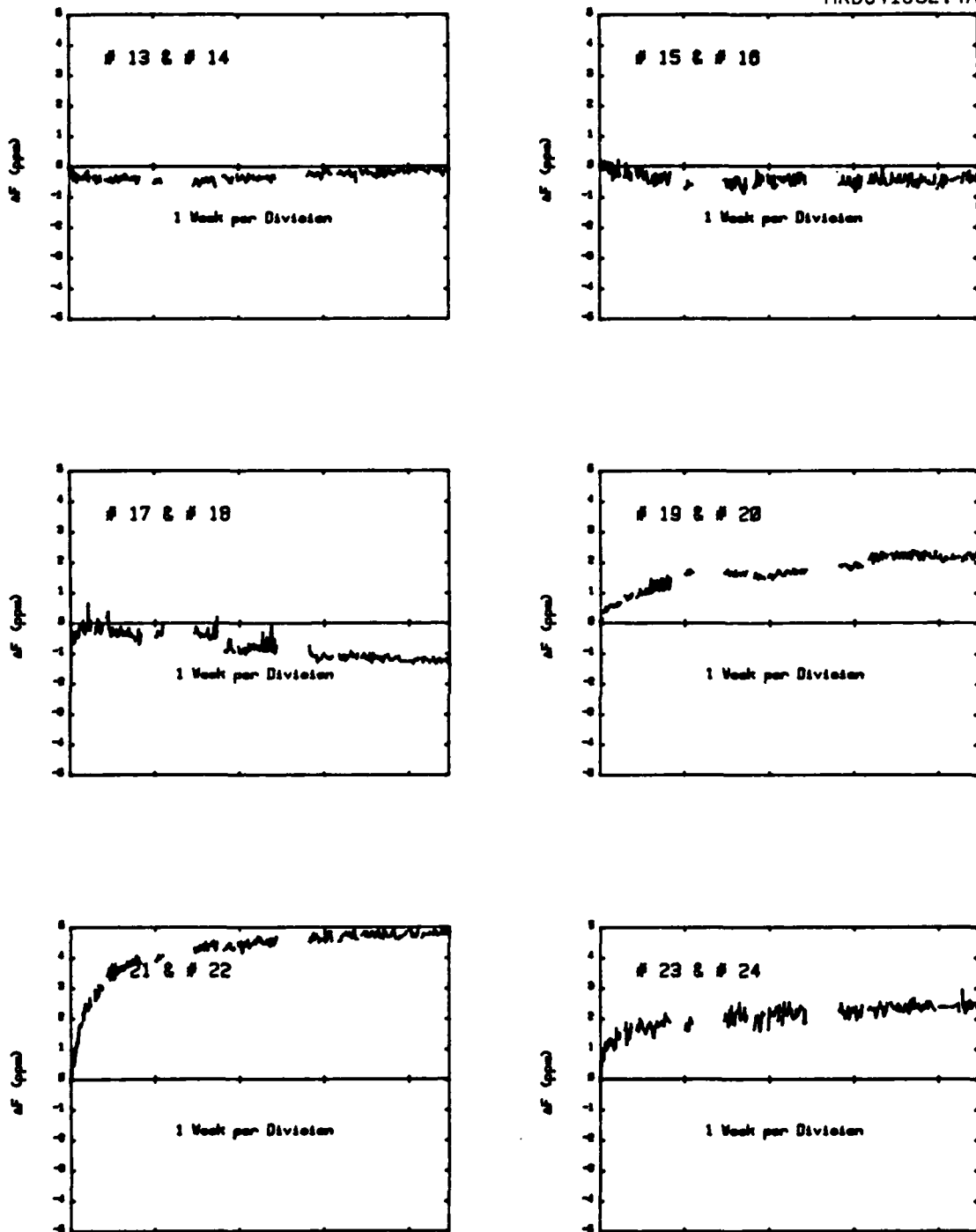


Fig. AIV-2 Differential aging plotted vs linear time for Crystals #13 through #24.



MRDC41082.4AR

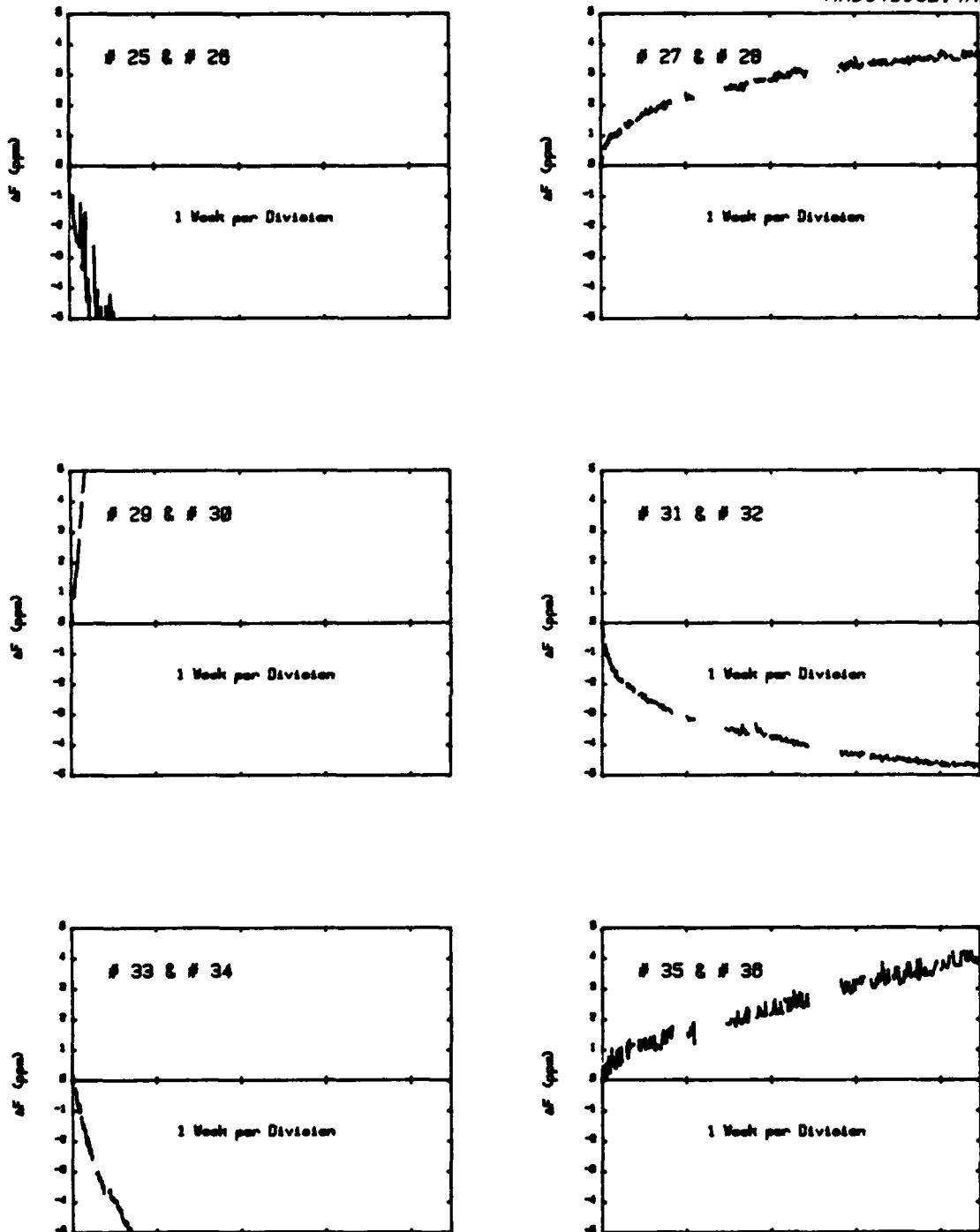


Fig. AIV-3 Differential aging plotted vs linear time for crystals #25 through #36.



MRDC41082.4AR

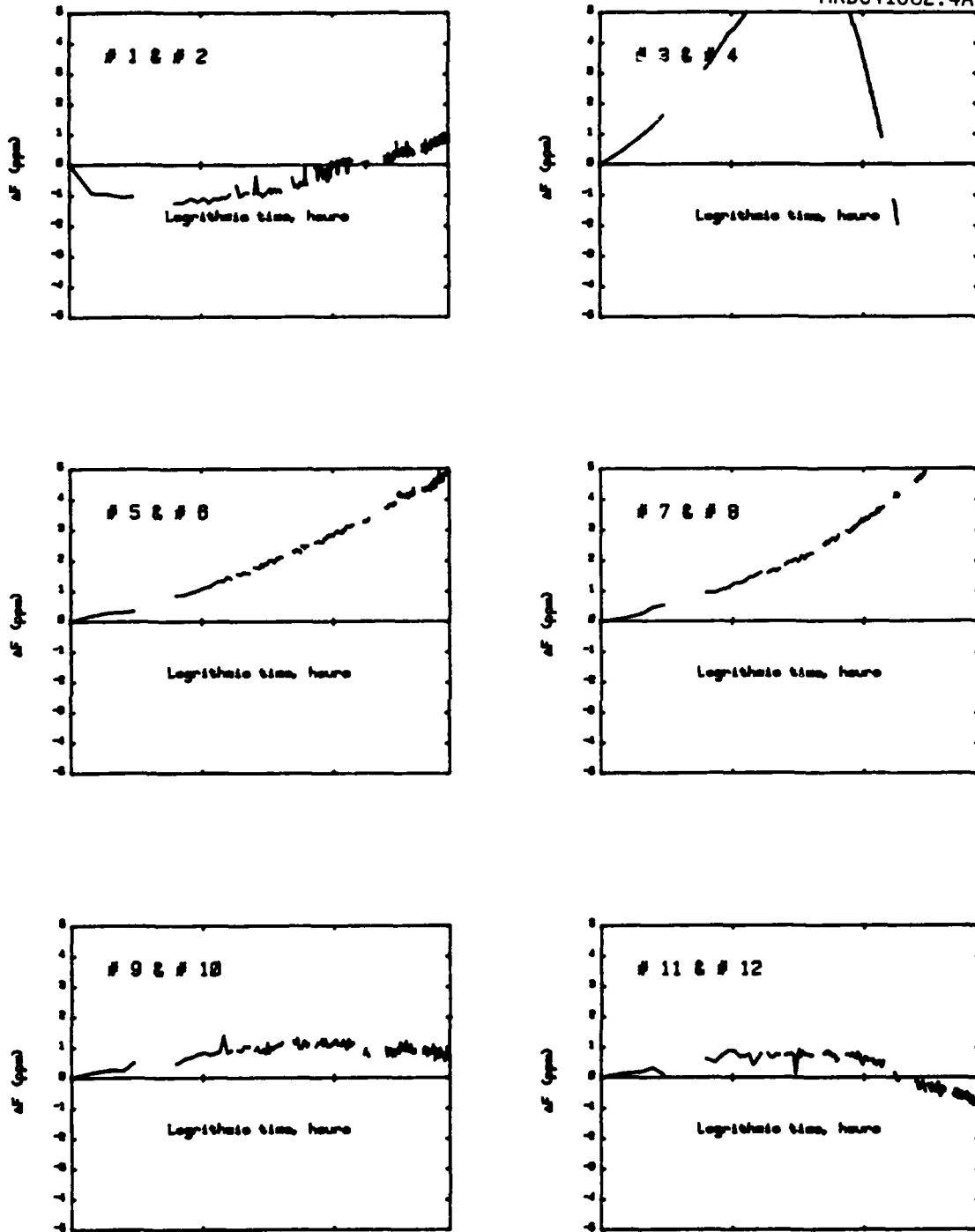


Fig. AIV-4 Differential aging plotted vs logarithmic time for crystals #1 through #12.



MRDC41082.4AR

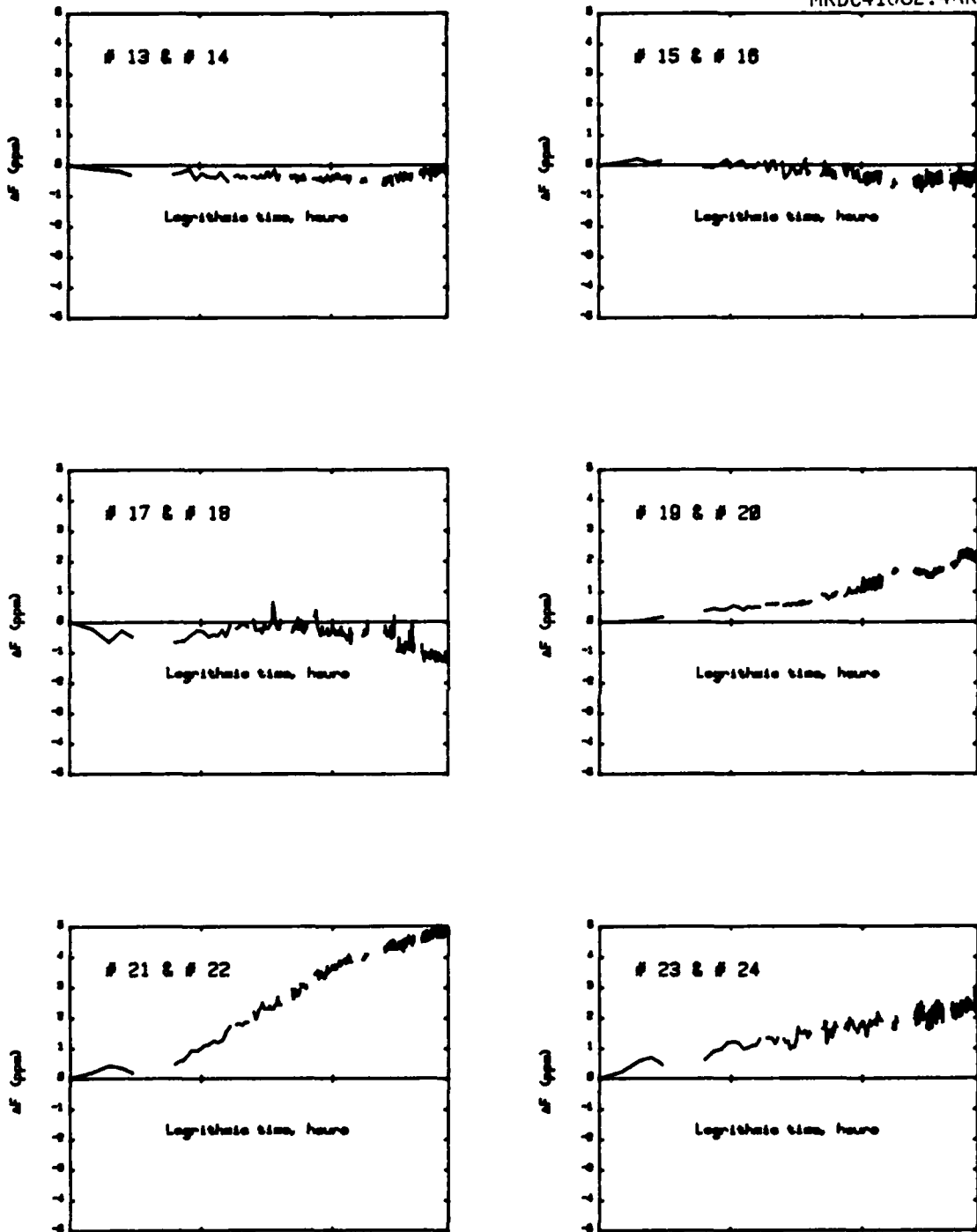


Fig. AIV-5 Differential aging plotted vs logarithmic time for crystals #13 through #24.



MRDC41082.4AR

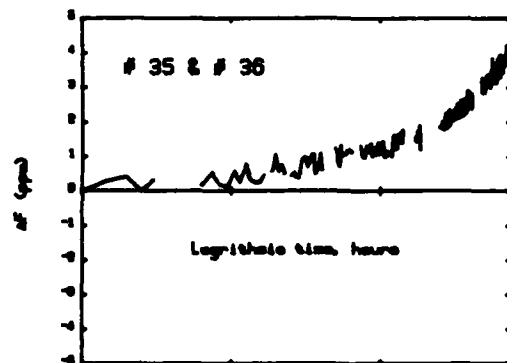
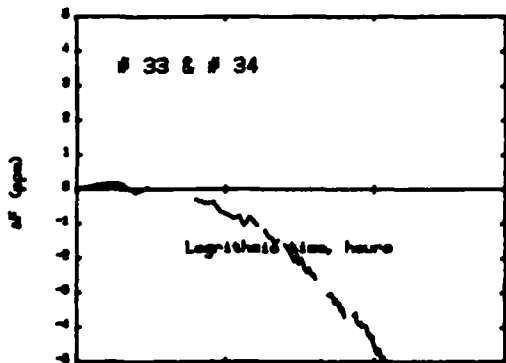
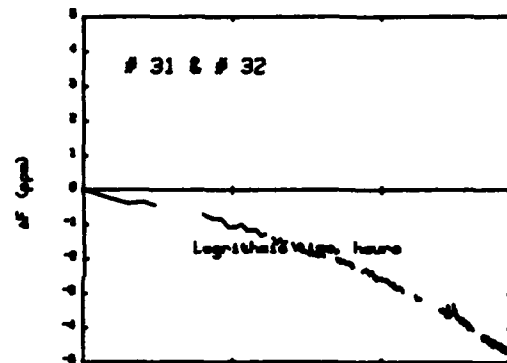
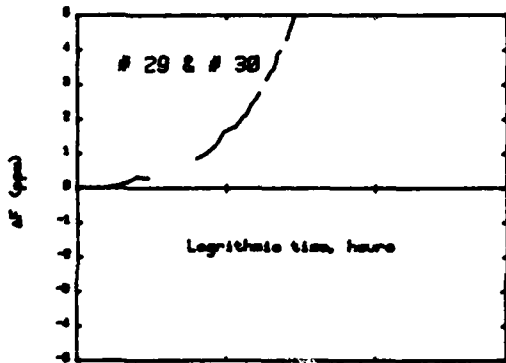
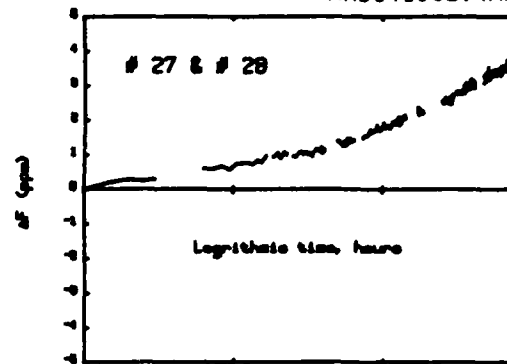
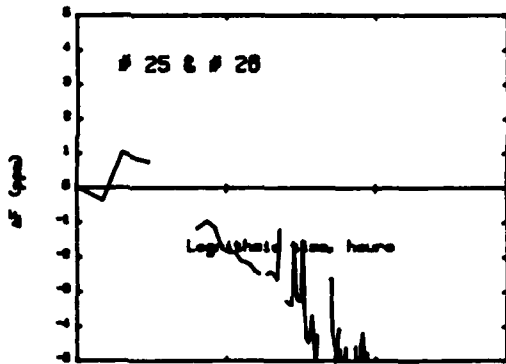


Fig. AIV-6 Differential aging plotted vs logarithmic time for crystals #25 through #36.



7.5 Appendix V - Preprints of Publications

In this appendix preprints of two papers on absolute and differential aging in SAW resonators are shown. These papers discuss research carried out under contractual support from DARPA.

## SURFACE CHEMISTRY RELATED TO SAW RESONATOR AGING

J. S. Schoenwald, A. B. Marker, W. W. Ho, J. Wise and E. J. Staples

Rockwell International Corporation  
Thousand Oaks, California 91360

### Abstract

The electrical characteristics of surface acoustic wave devices depend critically on the physical and chemical properties of the device surface as well as on the interaction between the propagating wave in the substrate with its surrounding gaseous medium. The gas-surface interactions were carried out in a dual chamber vacuum apparatus with a SAW resonator isolated in each chamber. One resonator, kept continually under vacuum, acted as a reference, while the second resonator was exposed to a variety of gases under controlled conditions. The nature of the chemical changes occurring on the surface were confirmed by examining the device surface by x-ray photoelectron spectroscopy. Experiments have been performed to study the physical and chemical absorption of reactive and non-reactive gases. These experiments are needed to understand and model the aging mechanisms of SAW resonators. Typical results will be presented.

### 1. Introduction

The electrical characteristics of surface acoustic wave (SAW) devices depend critically on the physical and chemical properties of the device surface as well as on the interaction between the propagating wave in the substrate with its surrounding gaseous medium. These effects, which previous researchers have dealt with only in terms of maximizing oscillator and filter performance<sup>1,2</sup> were studied in this investigation to establish their relationship to such gas-surface phenomena as surface oxidation, adsorption, and the interaction of the electroded metallic surfaces and the substrate with reactive and non-reactive gases.

An elementary theory of kinetic rate processes is then derived for the case of chemisorption, which appears to be the predominant effect observed in the fabrication and aging studies discussed in this paper. From the resulting derivation we obtain insight concerning the molecular process at the device surface and how it brings about a shift in frequency over time.

The results of several pre-aging studies conducted under varying conditions is presented in order to show the connection between aging and the presence of reactive gases and moisture both during the fabrication process and after hermetic sealing.

### 2. Gas-Surface Interaction Studies

The gas-surface interaction studies were carried out in a dual chamber vacuum apparatus with a SAW resonator isolated in each chamber. The resonators were matched devices (to within 0.5%) operating at 300 MHz. One resonator, kept continually under vacuum, acted as a reference, while the second resonator was exposed to a variety of gases under controlled conditions. The nature of the chemical changes occurring on the SAW surface were confirmed by examining the device surface by x-ray photoelectron spectroscopy (ESCA or XPS). The SAW resonator devices were fabricated by first defining the device pattern by conventional photolithography techniques on ST-quartz and then forming grooves in the reflector portions of the device via plasma etching. The transducer is masked during the plasma etching process. The aluminum metalization pattern of the reflector arrays mask the substrate and etching of the quartz substrate takes place only in the gaps between the metallized stripes. The resonant frequency and Q of the resonators were measured with a HP8505A dual channel network analyzer, a HP8660C frequency synthesizer and a HP5345A frequency counter. The long term frequency stability of the resonators were found to be better than 1 ppm with a Q of about 10,000. The measurement accuracy of the frequency difference between the two resonators was found to be about 100 Hz.

### 3. Results for Non-reactive Gases

The propagation of surface acoustic waves along the boundary between the quartz surface and a gas results in the generation of bulk longitudinal waves in the gas. This, in turn, causes an increase in the attenuation along the direction of propagation, with a consequent decrease in the Q of the resonator. It is noteworthy that the shift in frequency as a function of gas pressure is always positive for the gases studied, as shown in Figure 1. As can be seen, at a given gas density, the diatomic molecules (N<sub>2</sub>, O<sub>2</sub>) give approximately 5 times the shift as that due to the rare gases. The effect is totally reversible, indicating no significant chemisorption of the gases. Since different frequency shifts are observed for various gases at a fixed pressure, the measured effect cannot be caused by mechanical distortion or compression of the surface of the device. Hence, it can be concluded that the perturbation

of the resonant frequency is due primarily to the coupling of the surface waves to compression longitudinal sound waves in the gases. Although there is no existing theory for quantitatively describing this phenomena, it is expected that the magnitude of the shift is related to the compressibility and velocity of the gas present. It is therefore reasonable to expect that diatomic gases will have a larger effect than the rare gases.

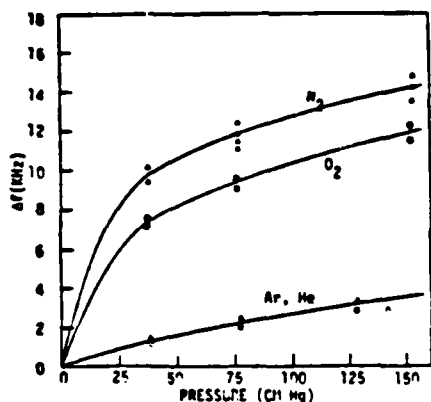


Figure 1 - Frequency Shift of St-Quartz Resonators as a Function of Gas Loading at 300 MHz.

These results indicate that great care must be exercised in vacuum or noble gas encapsulation of SAW devices since air leakage can result in frequency shifts as large as 30 ppm.

The attenuation of the surface acoustic waves caused by the emission of compressional waves in the gases was also determined by measuring the changes in the quality factor  $Q$  of the SAW resonators as a function of gas density. Typical results of the attenuation measurements for nitrogen gas are shown in Figure 2 as a function of gas pressure. The data is linear in pressure and has a value for the slope of  $2.05 \times 10^{-6}$  db/cm-MHz-mmHg. Similar data were obtained for  $O_2$  which showed a slope of  $2.14 \times 10^{-6}$  db/cm-MHz-mmHg. The measurements showed good agreement for repeated cycling of the gases. Since oxidation of fresh aluminum surfaces is expected to occur in the presence of oxygen, the absence of any non-reversible effect demonstrates that the surface is in the form of  $Al_2O_3$  and no further surface reaction is taking place.

There are several existing theories describing the attenuation loss in propagating surface waves along the boundary of a solid substrate and a gas. These are the approximation approach developed by Artz and co-workers,<sup>4</sup> the continuum mechanical approach originally proposed by Campbell and Jones<sup>5</sup> and the perturbation formulation by Tiersten and Sinha.<sup>6</sup> The first two approaches have been used by Slobodnik<sup>7</sup> for comparison with experimental data obtained with various monatomic gas loading on Y-cut and Z-propagating  $LiNbO_3$  surfaces. He found

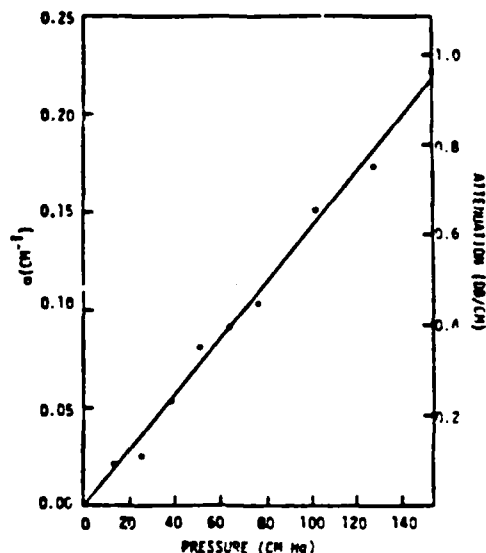


Figure 2 - Surface Wave Attenuation as a Function of  $N_2$  Gas Loading for St-Quartz SAW Resonator at 300 MHz.

that the theoretical calculations bracketed the experimental results with the approximate theory giving consistently higher values for the attenuation. When these same calculations are scaled to the case for  $O_2$  and  $N_2$  loading on ST-quartz at 300 MHz, the correct pressure dependence is obtained but the absolute magnitudes are, respectively, 20% and 50% lower than the experimental values observed in the present investigation.

The more recent theory of Tiersten and Sinha,<sup>5</sup> include the previously neglected effect of gas viscosity which significantly increases the attenuation. The result of their calculation for air loading on ST-quartz at 300 MHz is, however, still about 30% lower than the present results.

#### 4. Results for Reactive Gases

Experiments were carried out to study the adsorption and chemisorption of gases on the SAW resonator surface. Since extensive previous work has been carried out in this laboratory on the gas-surface chemistry of HCl gas and  $Al_2O_3$  surfaces,<sup>8</sup> this system was chosen for the initial experiment. The test resonator surface was exposed to known concentrations of HCl with  $N_2$  as the carrier gas in the measurement system. The changes in the electrical properties of the resonator were measured in situ as a function of exposure time. The resonator surface was chemically characterized by XPS before and after the exposure.

Upon exposure of the test SAW device to HCl gas, the resonant frequency shifts rapidly towards a lower frequency. This trend then continues as a

function of time at a constantly decreasing rate. When the system is evacuated, the frequency immediately returns to a steady state value which is significantly lower than the initial vacuum resonant frequency for the device before exposure. Upon a second exposure of the device, the resonant frequency again decreases and shows the general behavior as that during the first exposure. However, upon evacuation, the vacuum resonant frequency is again shifted to a lower value from that before the exposure.

The data from a typical run (1% HCl in N<sub>2</sub>, 25 cm total pressure) are shown in Figure 3, in which the background shift to higher frequency caused by the N<sub>2</sub> gas loading is corrected for via the data shown previously in Figure 1. As can be seen, the irreversible shift in the vacuum resonant frequency also decreases with each successive cycling of the gas. When the concentration of HCl gas is varied, it was found that the measured effect scales linearly with HCl concentration.

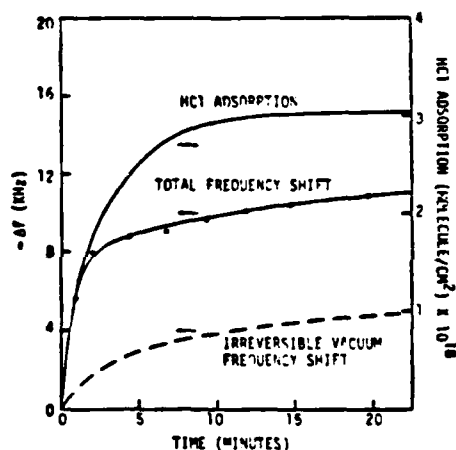


Figure 3 - Resonant Vacuum Frequency Shift as a Function of Exposure Time for 1% HCl Concentration in Nitrogen Gas at 25 cm Hg N<sub>2</sub> at Room Temperature (296K). Also Shown is HCl Adsorption Rate on Al<sub>2</sub>O<sub>3</sub> Surfaces as Determined by Wet Chemistry Analysis (note that Δf is negative).

XPS analysis of the SAW resonator before and after HCl exposure showed a chlorine uptake and a loss of oxygen from the Al<sub>2</sub>O<sub>3</sub>. The ratio of the chlorine uptake to oxygen loss was 2 to 1, indicating that the Al<sub>2</sub>O<sub>3</sub> was being chemically converted to AlCl<sub>3</sub>. Further confirmation that the chemisorption was occurring on the Al<sub>2</sub>O<sub>3</sub> rather than on the quartz surface was provided by additional XPS studies made on a blank quartz substrate before and after exposure to HCl gas under identical conditions. The results showed no significant Cl<sup>-</sup> present.

The electrical measurements together with the XPS findings demonstrate that both reversible adsorption and irreversible chemisorption of HCl was occurring on the Al<sub>2</sub>O<sub>3</sub> surface. The observed time dependence of the data given in Figure 3 indicate that when fresh Al<sub>2</sub>O<sub>3</sub> surfaces are exposed to HCl, an initial gas-surface reaction occurs which forms a chloride coating. This process is then followed by adsorption of gaseous HCl onto bound chloride ions until equilibrium is reached between the vapor pressure of the adsorbed HCl coating and the gas phase HCl concentration. At this point, the surface HCl concentration saturates and no further adsorption occurs. Upon evacuation to vacuum, desorption of a surface takes place and the shift in the vacuum frequency of the resonator is a measure of the net chemisorption on the surface.

In order to quantitatively relate the electrical measurements to the surface chemistry, the data are compared to the results from a previous study undertaken in this laboratory to determine the surface absorption efficiency (the ratio of reactive collisions to the total number of gas-surface collisions) of HCl gas onto alumina particles. In this prior work, total adsorbed Cl<sup>-</sup> on Al<sub>2</sub>O<sub>3</sub> particles were measured as a function of both HCl concentration and exposure time with a wet chemical analysis technique. The data were found to be in agreement with the expression

$$d[\text{HCl}]_s/dt = \gamma V A [\text{HCl}]_0 / 4 \quad (1)$$

where V is the mean kinetic velocity of the HCl gas molecule, A is the Al<sub>2</sub>O<sub>3</sub> surface area, [HCl]<sub>0</sub> is the vapor phase concentration and [HCl]<sub>s</sub> is the total adsorbed HCl on the surface. The observed HCl adsorption as a function of time from this previous work is scaled to the experimental conditions of the present study and the excellent agreement in the general shape of the curves seen in Figure 3 demonstrates that the present experimental method can be used for quantitative real-time measurement of the adsorption processes.

The sensitivity of the measurement method can be evaluated by a direct comparison of the data given in Figure 3. The result shows that the frequency shift is related to the absolute HCl adsorption via the calibration factor,  $3 \times 10^{17}$  molecules/cm<sup>2</sup> = 1 kHz, corresponding to a sensitivity for HCl adsorption at the level of 3 to 5 monolayers on the device.

Similar experiments were conducted to determine the frequency shift caused by exposure of the SAW resonator to water vapor under atmospheric conditions. Measurements were made with a SAW resonator having a clean surface as well as one which has been previously exposed to HCl gas. It was found that the lowering of the SAW frequency was totally reversible for the former case, whereas a large irreversible vacuum frequency off-set was observed for the latter case. The magnitude of the shifts were considerably larger than that found for HCl and the time scale for the effect was approximately a factor of two shorter. The results from a typi-

cal run at 75% relative humidity are shown in Figure 4. The total observed shift was about 40 kHz and the observed vacuum offset before and after exposure was 14 kHz. This sensitivity to water vapor is most likely caused by H<sub>2</sub>O deposition over the entire device surface, rather than reacting specifically with the aluminum as is the case for HCl. The experimental results obtained for the clean surface indicate that no chemisorption is taking place for water vapor on the quartz or the oxide-coated aluminum surfaces. The observed chemisorption for the device previously exposed to HCl vapor can be attributed to the highly deliquescent nature of AlCl<sub>3</sub> which readily forms AlCl<sub>3</sub>·6H<sub>2</sub>O in the presence of water vapor.

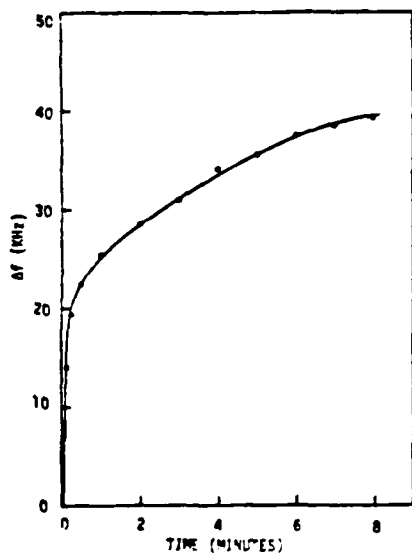


Figure 4 - Resonant Frequency Shift as a Function of Exposure Time for 75% Relative Humidity in Air at Atmospheric Pressure and Room Temperature (296K).

### 5. Rate Theory of Kinetic Processes

Parker has pointed out that frequency aging effects due to chemisorption and oxidation, behave according to the logarithmic rate relation<sup>7</sup>

$$\Delta f/f = A \log(Bt + 1) \quad (2)$$

where A and B are fit parameters. Equation (2) is a specific statement of the more generalized Elovich equation, which describes catalytic oxidation and chemisorption of various gases on a variety of metal and metal oxide surfaces.<sup>8</sup>

We will now derive the general form of the Elovich equation in order to appreciate the physical basis of the parameters A and B in (2). We begin by first presenting the more general form of (2):

$$bq(t) = \log(1 + t/t_0) \quad (3)$$

q is the number of particles chemisorbed per unit area at time t after the beginning of the experiment. t<sub>0</sub> is a time constant depending on the physical conditions and b is a constant appropriate to the quantity being measured.

Suppose that at the time t = 0 we have a surface with adsorption sites in contact with a gas. The nature of these sites, and their mode generation, is not specified by the theory, nor is the amount of gas already adsorbed on the surface at time t = 0 of importance. The sites may be due to the properties of that part of the surface which has not yet been covered by adsorbed molecules, they may be produced by the action of the already adsorbed molecules on the surface, and they might even be offered by adsorbed molecules themselves. At this time let there be s<sub>0</sub> sites per unit area, and let there be s sites per unit area at an arbitrary time t. Let there be N impacts by gas molecules with the surface, expressed per unit area and per unit time. Let a be the effective contact area between a molecule and the surface upon collision, so that a\*s is the fraction of impacts that could be effective in trapping a molecule. One may expect a to be roughly of the order of a molecular cross section. The probability that a molecule sticks upon impact is proportional to a\*s, i.e.,

$$p = Cas \quad (4)$$

where C is a constant. The number of molecules sticking per unit area per unit time is

$$dq/dt = CasN \quad (5)$$

Let b be the effective area over which sites become invalidated by the adsorption of a single molecule. b is not necessarily of the same order as a, since it is the area covered by an adsorbed molecule (which is of the order of a) reduced by the area of a new site generated on top of the adsorbed molecule. This is reasonable to expect since it is likely that a surface of adsorbed molecules are likely to offer new sites to further adsorption. The number of sites invalidated per unit area per unit time is therefore

$$-ds/dt = CNas*bs \quad (6)$$

Integration yields

$$s_0/s = 1 + CNabs_0t \quad (7)$$

Solving for s, inserting in (5) and solving for q yields



As mentioned earlier, there is strong evidence that this shift is due to the presence of water vapor and oxygen or other reactive gases in the package due to lack of hermeticity or process control. Out-gassing of moisture diffused in the quartz lattice may be a significant factor. The correspondence between high device Q, low aging, and very small shifts in frequency due to temperature retrace seem to be coupled to the rate at which reactive chemical processes occur at the crystal surface, and these in turn are related to the partial pressures of the gasses in the crystal enclosure. Further evidence in support of this phenomenon will be presented later in this paper.

The dependence of aging on environmental moisture and other gasses that might contribute by reaction or oxidation at the crystal surface was studied by preparing a set of samples in the usual manner, with the following exception. A 24 hr high vacuum bakeout at 150 degrees C preceded resistance weld sealing under high vacuum. The glove box enclosing the chamber was purged of moisture to the extent that the dew point was -40 degrees C. In an environment relatively free of moisture, nonreversible aging effects, such as those discussed earlier in which resonators were exposed to moisture after prior exposure to HCl, it is expected that aging rates should be considerably lower. Figure 7a shows the results for a set of six crystals sealed under high vacuum after a 24 hour bakeout in high vacuum. The long term fluctuations are caused by 24 hour cyclic fluctuations in the oven temperature, as can be seen in Figure 7b (later remedied), and the short term fluctuations are due to the relative shift of the turning point for this set of devices (50 degrees C) from the oven temperature (73 degrees). It can readily be seen, however, that within two days, crystal aging subsides below 0.5 ppm/day after temperature fluctuation effects are normalized out. This is an order of magnitude improvement over aging rates for previous devices.

Further confirmation of device sensitivity to ambient atmospheric conditions was revealed during the frequency fine tuning procedure. The resonant frequency of a device is tracked with an HP8660C

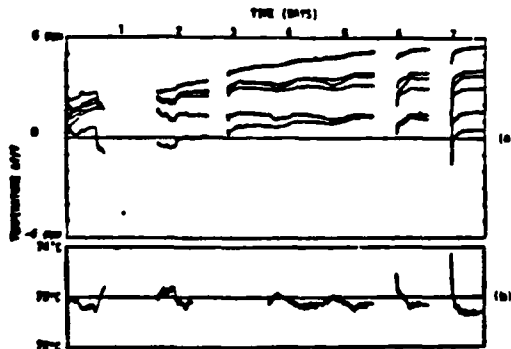


Figure 7 - Low Aging Rate Saw Resonators.

synthesized signal generator, an HP8405A and a dual directional coupler. A thermocouple beneath the T0-5 header monitored temperature. After fine tuning the device frequency in the plasma etcher, the chamber was repressurized via an air inlet valve. Immediate re-evacuation of the chamber, followed by a suitable time delay to relax temperature fluctuations during pressure changes, resulted in a nonreversible shift up in frequency by 30-40 kHz for resonators operating at 375 MHz. This result is consistent with that obtained for 300 MHz resonators exposed to moisture after exposure to reactive gases. No epoxy or other mounting material was used; instead, the devices were strapped to the header using gold wire. Therefore, contamination from mounting material was not a factor. The probable cause of this effect is the removal of at least part of the oxidized or chemisorbed layer from the aluminized portions of the device during plasma etching in  $CF_4$ , which thins the metal film (raising velocity and therefore frequency), followed by reoxidation in the presence of atmospheric humidity (further raising frequency).

A frequency shift of this magnitude (100 ppm) is catastrophic in a device where the Q is typically greater than 10,000. Clearly, the presence of moisture and reactive gases at the crystal surface during the course of fabrication and sealing plays a demonstrated role in the absolute frequency and long term stability of SAW resonators. Environmental conditions, certainly in the final stages of fabricating a tuned sealed device, should be carefully controlled.

Batch handling of crystals through the entire fabrication cycle except the final tuning provides additional evidence that uniformity of the environmental history for all devices results in uniformity of long term stability. Figure 8 shows aging results for a group of crystals we have recently begun to investigate. The entire group was processed as a single wafer section and segmented into chips only after the initial plasma etch and just prior to mounting. No extraordinary procedures were undertaken, such as long term high vacuum backout. Only in the final tuning and sealing steps were crystals treated individually, but the procedure for each was relatively uniform. The resultant aging rates are very tightly clustered. Low initial aging rates was not the objective in this study. Rather, we were concerned with the variation that might be expected in a very uniformly treated set of samples, and we observe that, in fact, the aging is quite uniform.

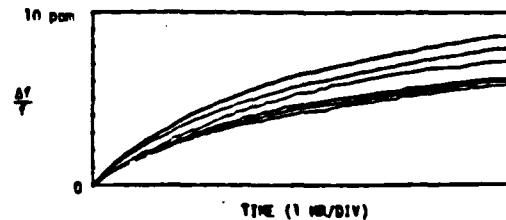


Figure 8 - Preaging of Six Crystals Subjected to Very Uniform Process Conditions.

A comparison with the aging Equation (1) for  $A = 3$  ppm and  $1.5 < B < 3.5$  plotted in Figure 9 shows how closely the aging data in Figure 8 follows a logarithmic rate dependence with  $t_0 = 1/B = 20-30$  minutes being the time constant characteristic of the chemisorptive process occurring at the electrode surface.

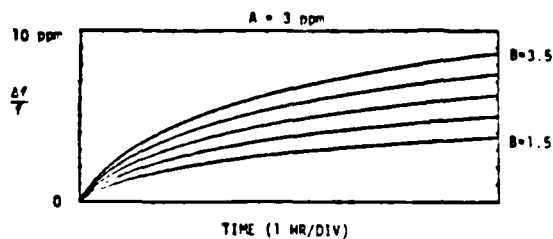


Figure 9 -  $A \ln(Bt + 1)$  Plotted for Values of A, B that Model Aging Results Shown in Figure 8.

### 7. Conclusions

We have presented results of the effects of non-reactive and reactive gases on the frequency and attenuation of SAW resonators. For non-reactive gases it has been determined that the effect of the gas is totally reversible upon return of the SAW resonator to a condition of high vacuum. If complete oxidation of the aluminum electrodes has preceded measurement, the effect of oxygen is also completely reversible. As an example of reactive gas effects, exposure of a SAW resonator to HCl gas which had previously been exposed to oxygen to allow electrode oxidation resulted in a nonreversible frequency shift down. Subsequent exposure to moisture in air results in a nonreversible shift up. The initial exposure to HCl converts  $Al_2O_3$  to  $AlCl_3$ . Moisture then combines to form  $AlCl_3 \cdot 6H_2O$ . X-ray photoelectron spectroscopy (XPS) was used to confirm the presence of the various compounds mentioned. Comparison with blank substrates of quartz indicate that no chemical process occurs in which chlorine is taken up, from which we conclude that the aluminum is the catalytic surface promoting the chemisorptive reaction. Wet chemistry analysis indicates that the observed frequency shifts result from the chemisorptive formation of 3 to 5 monolayers on the device.

We have presented an elementary theory of kinetic rate processes as applied to chemisorption. This results in a molecular level model that predicts the logarithmic aging rate behavior of the SAW resonators.

We have presented the results of SAW resonator pre-aging studies under various conditions and have shown the connection between environmental control of the fabrication process and device stability after fabrication. The effects of moisture, catalytic oxidation and reactive gases can be measured and quantified. It is shown that steps can be taken to reduce the effect of these aging mechanisms on the long term stability of SAW resonators.

### References

1. P. Carr, A. J. Slobodnik, Jr., and J. C. Sethares, Intern. Microwave Symposium Digest, 354 (1969).
2. A. J. Slobodnik, Jr., "Surface Acoustic Waves and SAW Materials," Proc. IEEE, vol. 64, pp. 581-595 (1976).
3. R. M. Artz, E. Saltzmann, and K. Dransfeld, "Elastic Surface Waves in Quartz at 316 MHz," Appl. Phys. Letts., vol. 10, pp. 165-167 (1967).
4. J. J. Campbell and W. R. Jones, "Propagation of Surface Waves at the Boundary Between a Piezoelectric Crystal and a Fluid Medium," IEEE Trans. Sonics and Ultrasonics, vol. SU-17, pp. 71-76 (1970).
5. H. F. Tiersten and B. K. Sinha, "A Perturbation Analysis of the Attenuation and Dispersion of Surface Waves," J. Appl. Phys., vol. 49, pp. 87-95 (1978).
6. W. Ho, A. B. Harker, and J. J. Ratto, "Formation and Growth of Acid Aerosols from Gaseous HCl in the Presence of Water Vapor and  $Al_2O_3$  Particles," accepted for publication in Atmospheric Environment.
7. T. E. Parker, "Analysis of Aging on SAW Oscillators," Proceedings, 34th Annual Symposium on Frequency Control, U.S. Army Electronics Command, Ft. Monmouth, N.J., pp. 292-297 (1980).
8. S. Yu Elovich and G. M. Zhabrova, "Mechanism of the Catalytic Hydrogenation of Ethylene in Nickel," J. Phys. Chem. (USSR) 13, pp. 1761-1786 (1939) (in Russian).
9. S.J. Dolochycki, E. J. Staples, J. Wise, J. S. Schoenwald and T. C. Lim, "Hybrid SAW Oscillator Fabrication and Packaging," Proceedings 33 Annual Symposium on Frequency Control, U.S. Army Electronics Command, Fort Monmouth, N.J., pp 374-378 (1979).

## ABSOLUTE AND DIFFERENTIAL AGING OF SAW RESONATOR PAIRS\*

J. S. Schoenwald, J. Wise and E. J. Staples

Rockwell International Corporation  
Thousand Oaks, California 91360

### Summary

This paper examines the absolute and differential aging of SAW resonators fabricated as pairs. Low absolute aging rates of individual SAW resonators have been observed after hermetic sealing and temperature stabilization inside 70°C pre-aging ovens. Typical drift rates fall below 0.5 ppm/day within 48 hours and 0.1-0.5 ppm/wk after 3 weeks. The differential drift rate between pairs was less than 0.25 ppm/day after 48 hours and typically 0.1-0.2 ppm/wk after 3 weeks.

The effect of drive level was studied for devices fabricated using evaporated chromium (50Å)/aluminum (1000Å), rf sputtered aluminum (1000Å) and evaporated aluminum + 4.5% copper alloy. Significant performance degradation occurs at 75°C for power levels above +10 dBm delivered to the crystal at resonance. Comparative studies of frequency dependence on drive level show no significant differences among the three metallization systems described.

Key words (for information retrieval)  
Surface Acoustic Wave (SAW) Resonators, Aging, Drive Level, Fabrication, Electromigration.

### Introduction

Systems requiring long term stability and insensitivity to undesirable effects provide strong motivation for investigating the common mode rejection characteristics of appropriately configured pairs of surface acoustic wave (SAW) resonators.

Low absolute aging of individual SAW resonators depends on device material composition, process controls and cleanliness, packaging environment and hermeticity. Extended pre-aging appears to be necessary to reduce long term drift below 1 ppm/yr with typical aging studies reported in the literature now approaching the two year mark.<sup>1-3</sup> An objective of this study was to isolate as much as possible those factors contributing to the long term instability. By a study of resonator pairs in a common enclosure, effects such as packaging could be eliminated or deduced by evaluating differential aging.

\*Work supported by Defense Advanced Research Projects Agency, Contract No. MDA 903-81-C-0081.

This paper will examine the absolute and differential aging of SAW resonators fabricated as pairs and sealed under vacuum in a common TO-5 enclosure. The design of the fabrication process and control of the process is described. Also, the effects of power level at which the devices are driven and the damage encountered under sustained conditions of high power and elevated temperature are discussed.

### Fabrication Process Design and Control

Reliable device performance requires a fabrication process that is reproducible. Analysis procedures were instituted at appropriate steps in the process to monitor the condition of the SAW substrate as it proceeded from wafer to chip and finally to packaged environment. Figure 1 is a flow chart of the fabrication process. As pilot wafers progress through the fabrication process they are subjected to a variety of surface and bulk analytical measurements to determine the presence of contaminants, interdiffusion of deposited metals, or surface chemical reactions that may have significant consequences for device long term stability after the package is sealed.\* This required vacuum baking prior to sealing, to pump off moisture and accelerate short term surface reactions. Also a small plasma etch chamber for frequency calibration was installed directly in the dry nitrogen glove box containing the resistance weld sealer. After vacuum sealing the packages were bombed with helium and leak tested. Typically better than 90% of all sealed devices indicated leak rates of less than  $1 \times 10^{-10}$  std cc/sec air equivalent.

### Pre-Aging System

An oven was designed for monitoring the aging of 36 SAW resonators simultaneously. By using interchangeable PC boards, either 18 TO-5 packages with resonator pairs or 36 packages containing single resonators could be monitored. Resonator groups of six were connected to a single pole six throw (SP6T) coaxial switch. The six switches were connected to a seventh in a switching matrix arrangement. Figure 2 shows photograph of the oven, containing the PC board into which the TO-5 packages were inserted and the coaxial switches.

The resonators were periodically interrogated through the switches by a network analyzer, frequency synthesizer and counter, all of which were controlled by a desktop computer. The resonant

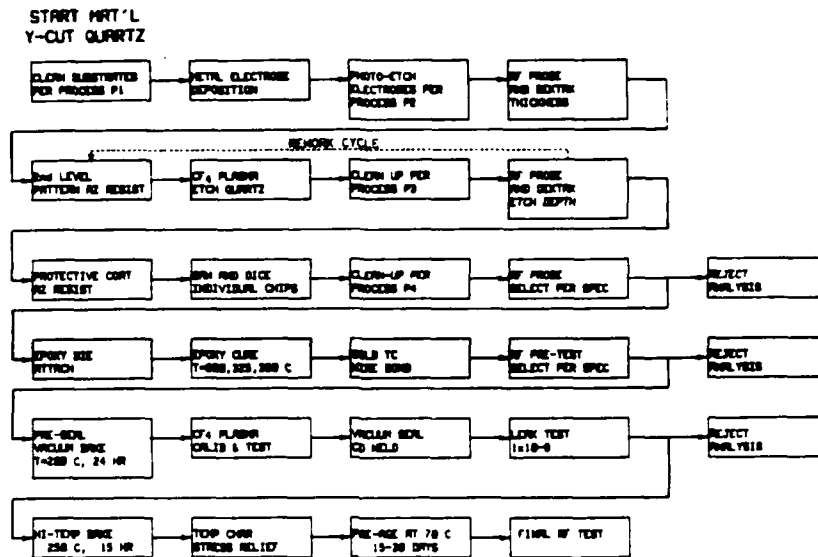


Figure 1 Fabrication process flow chart.



Figure 2 Photograph of oven showing SP6T coaxial switches and PC board for TO-5 crystal enclosures.

frequencies were sequentially measured, the oven temperature recorded, and the time logged from the computer's real time clock. In this manner, the frequency/temperature drift was tracked with time. Software computed the differential drift between packaged pairs of SAW resonators.

#### Absolute and Differential Pre-Aging Results

Pre-aging studies were conducted on two paired resonator configurations and two types of electrode metalizations:

1. Pairs: two separate chips in one package; evaporated Cr/Al electrodes.
2. Dual resonators: two resonators on a common chip; evaporated Cr/Al electrodes.
3. Dual resonators: same as #2 but with evaporated Al + 4.5% Cu alloy electrodes.

Figures 3, 4 and 5 show the absolute and differential aging for each of the three cases indicated. In all cases, frequency drift follows a logarithmic time dependence characteristic of chemisorptive reactions. Small oscillations in the aging were primarily due to fluctuations in oven temperature that occurred with a 24 hour cycle. These frequency variations result from an offset between the oven operating temperature (85°C) and the turning point of the crystals (70°C). In the case of paired Cr/Al crystals the absolute aging rates typically showed between 5 and 20 ppm frequency increases within the first

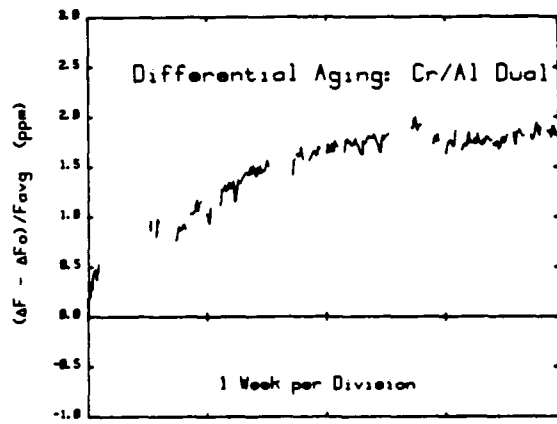
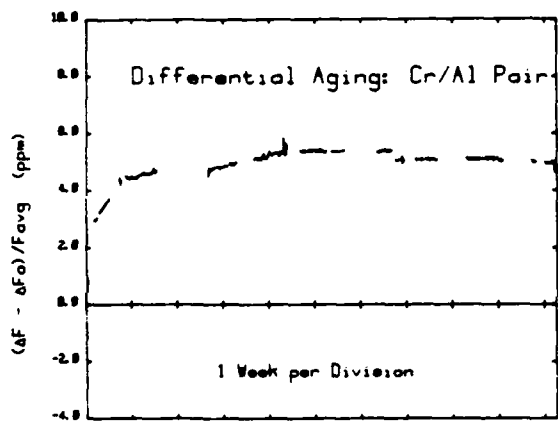
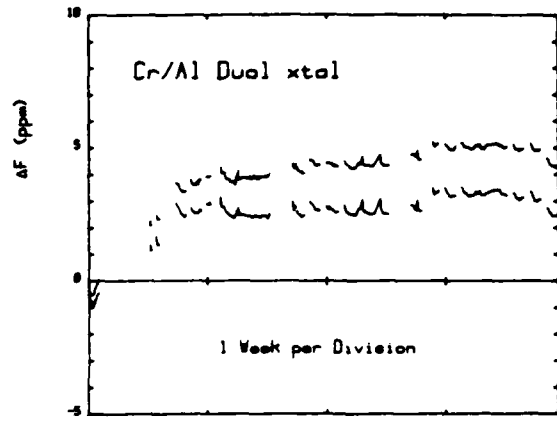
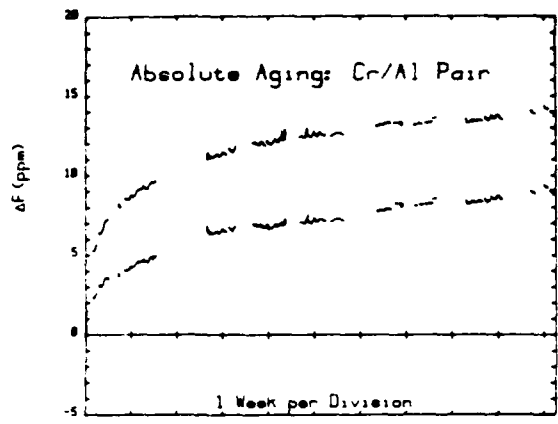


Figure 3 Absolute and differential aging for pairs of Cr/Al resonators sealed in a common package.

Figure 4 Absolute and differential aging for Cr/Al dual resonators.

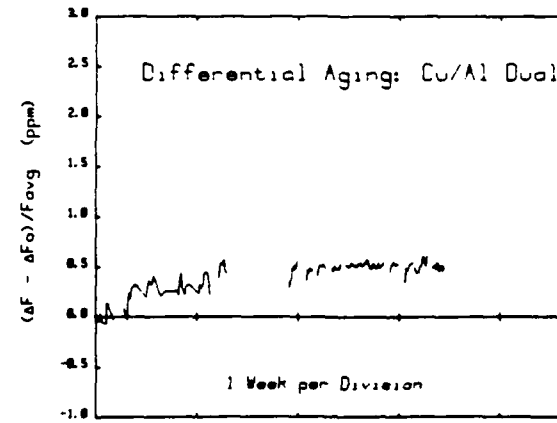
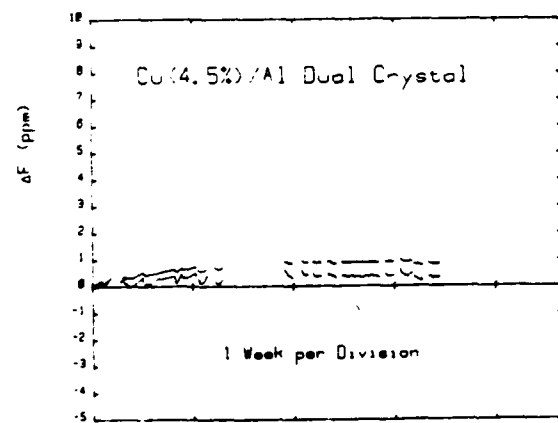


Figure 5 Absolute and differential aging for Cu doped Al dual resonators.

30 days. typical drift rates fell below 0.5 ppm/day within 48 hours and 0.1-0.5 ppm/wk after three weeks. Typical differential drift rates fell below 0.25 ppm/day within 48 hours and typically 0.1-0.2 ppm/wk after three weeks (5-10 ppm/year). Fabricating the devices as dual resonators on the same crystal, Fig. 4, improved the differential aging rates but absolute aging remained high. Replacing the Cr/Al metallization with copper alloyed aluminum remarkably improved the absolute as well as differential aging, Fig. 5. The total pre-aging amounted to less than 2 ppm and drift rates less than 0.1 ppm/mo were obtained after only 3 weeks pre-aging. As expected the differential aging showed a similar improvement. A more accurate assessment of these rates requires either individual oscillator measurements or longer pre-aging times. The former is currently under investigation using a dual oscillator circuit.

#### Drive Level Studies

The effect of rf power delivered to the resonators from a 50 ohm source at the resonant frequency of each device was investigated and compared for three different types of electrodes: (1) evaporated chrome, 50A, and aluminum, 1000A, (2) rf sputtered aluminum and (3) evaporated 4.5% copper-aluminum alloy, 1000A. It has been reported that excessive power levels in SAW resonators result in drive level dependent frequency shifting and degraded performance with time.<sup>5,6</sup>

Figure 6 shows the frequency dependence on drive level for eight resonators from each of the metallization groups described above. From the results of the three types of metallized devices studied it does not appear that one type provides better frequency stability under varying drive levels than any other. This may indicate that the dependence of the device frequency is controlled primarily by thermal heating due to power dissipation in the bulk of the quartz, and not by any property of the metallization.

#### Degradation at High Drive Levels

The equivalent circuit series resonant resistance was typically 45-75 ohms for the 375 MHz SAW resonators studied in this work and a 50 ohm resonator will dissipate all the power delivered to it from a 50 ohm frequency source. At +10 dBm drive level, in excess of 1 Kw/cc is being dissipated in the skin depth of the central region of the electrode pattern. In view of the fact that the Q of these devices ranged from 12,000 to 20,000, and the energy stored in the device is proportional to the product of the Q and the energy dissipated, large stored energy densities are achieved. It comes as no surprise, then, that electromigration effects due to large piezoelectrically induced potentials, severe mechanical distortions and thermal stresses are likely to have a degenerative effect on the structure of the device, and particularly the metal electrodes.

SAW resonators were driven for periods exceeding 15 hours at drive levels of +10 dBm.

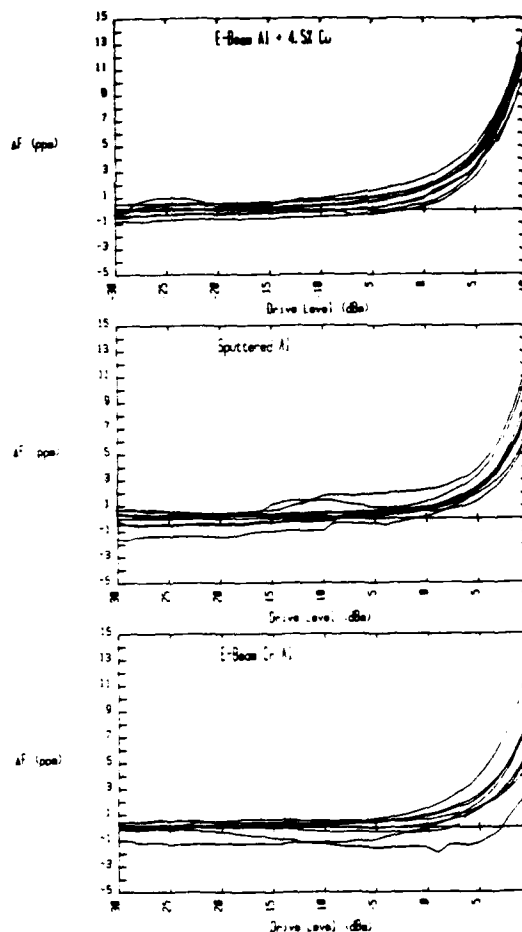


Figure 6 Frequency dependence of drive level for Cr/Al, Cu-doped aluminum, and sputtered aluminum metallized resonators.

Device degradation was found to be closely related to the temperature at which the drive level measurements were made. At room temperature little or no change in the device characteristics occurred. At 75°C, however, significant damage was observed after prolonged active aging at +10 dBm. Figure 7 shows the return loss magnitude and polar response for a SAW resonator fabricated with a Cr/Al electrode pattern before and after 15 hours of active aging at 75°C. The appearance of spurious resonances, a shift in the resonant frequency and an increase in the series resonant resistance indicates damage has occurred either in the acoustic cavity, the interdigital transducer, or both.

Scanning electron micrographs of the transducer region of the SAW resonator, taken afterward confirmed that damage had occurred. Small hillocks, typical of electromigration damage, were

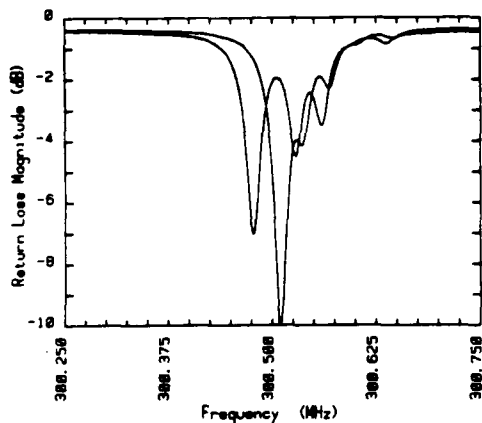
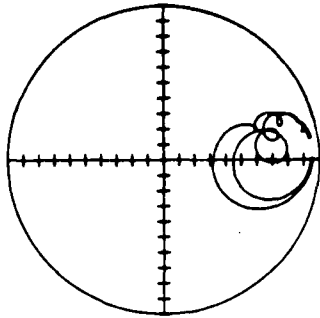


Figure 7 Return loss degradation for +10 dBm drive level at 75°C.

found.<sup>6</sup> In addition, "drag" type effects were noticeable at the edges of the electrodes, as if aluminum had been physically brushed or scraped in the direction of acoustic motion. Neither of these artifacts were present in undamaged devices.

#### Conclusions

The absolute and differential aging of SAW resonators was investigated. A fabrication

process which included techniques for monitoring process conditions resulted in devices with low absolute and differential drift rates after a short period of pre-aging. Absolute aging rates less than 0.1 ppm/mo after only 3 weeks pre-aging at 70°C were demonstrated. Low differential aging rates were obtained using dual resonator crystals. Drive level studies on devices fabricated with different types of aluminum metallizations have not conclusively shown that one type of metallization is superior to another based upon drive level. For the purpose of long term frequency stability however, copper alloyed aluminum appears to be superior to chrome/aluminum metals. Damage due to elevated drive levels for extended periods was found to be more sensitive to operating temperature than the drive level up to +10 dBm.

#### Acknowledgement

The authors would like to thank A. B. Harker for his assistance in surface chemistry analysis.

#### References

1. T. E. Parker, "Analysis of Aging Data on SAW Oscillators, Proceedings, 34th Annual Symposium on Frequency Control, U.S. Army Electronics Command, Ft. Monmouth, N.J., pp. 292-297 (1980).
2. M. Gilden, G. K. Montress, and R. A. Wagner, "Long-Term Aging and Mechanical Stability of 1.4 GHz SAW Oscillators," 1980 Ultrasonics Symposium Proc., IEEE Cat. No. 80CH1602-2, pp. 184-187.
3. W. R. Shreve, "Active Aging of SAW Resonators," 1980 Ultrasonics Symposium Proc., IEEE Cat. No. 80CH1602-2, pp. 188-192.
4. J. S. Schoenwald, A. B. Harker, W. W. Ho, J. Wise, and E. J. Staples, "Surface Chemistry Related to SAW resonator Aging," 1980 Ultrasonics Symposium Proc., IEEE Cat. No. 80CH1602-2, pp. 193-199.
5. J. I. Latham, W. R. Shreve, N. J. Tolar, and P. B. Ghate, "Improved Metallization for Surface Acoustic Wave Devices," *Thin Solid Films*, 64 (1979), pp. 9-15.
6. W. J. Tanski, M. Block, and A. Vulcan, "High Performance SAW Resonator Filters for Satellite Use," 1980 Ultrasonics Symposium Proc., IEEE Cat. No. 80CH1602-2, pp. 148-152.